PICOSECOND NONLINEAR OPTICAL PROPERTIES

OF UNDOPED CADMIUM TELLURIDE

By

MARK STEFAN PETROVIC

Bachelor of Science

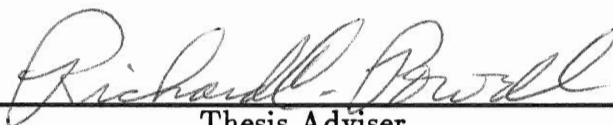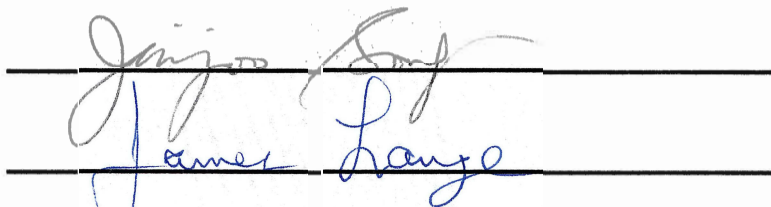Oklahoma State University

Stillwater, Oklahoma

1983

Submitted to the Faculty of the
Graduate College of the
Oklahoma State University
in partial fulfillment of
the requirements for
the Degree of
DOCTOR OF PHILOSOPHY
May, 1991
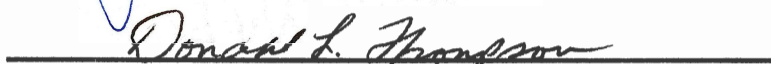
PICOSECOND NONLINEAR OPTICAL PROPERTIES
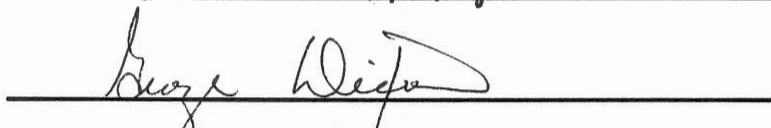## OF UNDOPED CADMIUM TELLURIDE

Thesis Approved:

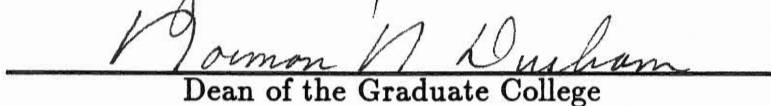_Richard C. Powell_
Thesis Adviser

Jinjoo Song

James Lange

Donald L. Thompson

George Dixon

Norman N. Durham
Dean of the Graduate College

ACKNOWLEDGMENTS

No number, no volume, of pages in this work can register the singular pleasure I take in writing this one where I might mention those individuals who have helped make possible this degree and dissertation.

To my thesis advisor, Prof. Richard C. Powell, for the opportunity to work in his laboratory and learn the research physicist's trade. I could not want for a mentor of more help or better humour. To my committee members, Profs. G.S. Dixon, J.N. Lange, J.J. Song, and D.L. Thompson, for abiding my requests and questions. To Dr. Andrzej Suchocki of the Polish Academy of Science in Warsaw, who taught me the details of careful laboratory work, and for countless hours of stimulating discussion. If ever I plumbed fully the depths of his patience, he never showed it. To Dr. George C. Valley of Hughes Research Laboratories, Malibu, California, who explained his work to me many times.

To the two people who will always remain the youngest I know, my parents, Alexander M. and Frances M. Petrovic, in whose acknowledgment words utterly fail. Their contribution began some thirty years ago, with the finest, most treasured of gifts - a sense of congenital optimism, a tool of the hardest steel which I cannot repay but only hope to pass on. To my brothers and sisters, Fran, Alex, Teresa, Chris, and Anastasia for their unflappable surety that I could do this work.

To Mr. Albert E. Lederman of Woodside, New York, whose support and paternal encouragement helped me maintain a healthy perspective on the experience. To Drs. Edward G. Behrens, Guy D. Gilliland, Mahendra Jani, Bahaeddin Jassemnejad, W. Scott McCullough, Gregory J. Quarles, and Roger J. Reeves, and office mates, Messrs. Roger R. Petrin, Keith Ver Steeg, and Bahman Taheri for many insightful discussions and laboratory assistances. To Ms. Carol

J. Wicksted, who never buckled under the weight of my wailings. To Mr. and Mrs. Don Fristoe, for their unfailing moral support over these past four years.

To our two beautiful daughters, Amelia Leisl and Lydia Tess, whose happiness upon seeing me come through the door in the evening was my Lourdes-come-to-Stillwater. And finally, to my wife, Velina, who stood down the wind with me. I cannot imagine what this would have been like without her sense of humor, companionship, and devotion. The world must know that I would surely do it all again with her.

TABLE OF CONTENTS

LIST OF TABLES

LIST OF FIGURES

ix

CHAPTER I

INTRODUCTION

It is generally accepted that modern communications systems will rely heavily not on transistors alone but also on light-matter interactions in all-optical or opto-electronic information processing. The intense optical electric fields made available with the development of the laser in the early 1960's has permitted workers to push the study of nonlinear optical interactions as well as devices based on such processes so that a dual goal may be achieved: a better understanding of the basic physics of nonlinear optical interactions in materials and an incorporation of these effects into modern optical information processing systems. Nonlinear optical effects such as CW and pulsed four-wave mixing, two-beam coupling, frequency-doubling, and holographic information storage are phenomena which are likely to form part of the foundation necessary to realize high-speed switching and computing.

It is the purpose of this work to present the results of certain studies of fast nonlinear optical effects, effects which may find use in optical information processing, in the II-VI semiconducting compound cadmium telluride (CdTe). Single-crystal CdTe was chosen as an object of study because of its relatively fast response time, large electrooptic coefficient, and large two-photon absorption coefficient in the near-infrared spectral region, where many high-gain lasers operate. Each of these attributes marks CdTe as a candidate for use in modern optical information processing.

Summary of the Thesis

This Thesis reports the results of several picosecond, near-infrared non-linear optical studies performed on the II-VI unintentionally-doped semiconductor cadmium telluride (CdTe).

Chapter II presents the results of a series of experiments performed to determine the Pulse-Probe Degenerate Four-wave Mixing (PP DFWM) response of CdTe under picosecond, near-infrared laser excitation. It is found that the nonlinear response of the material can be described by the free-carrier optical nonlinearity. From these measurements we deduce the ambipolar diffusion coefficient and free-carrier lifetime under several hundred megawatt per square centimeter picosecond excitation. The results of thin-grating, two-beam scattering are presented, from which the laser-induced refractive index changes are deduced. An investigation of band-edge enhancement of the PP response is also presented, which shows that in this particular sample for the conditions of excitation investigated no significant enhancement to the absolute scattering efficiency vs. excitation wavelength is obtained.

Chapter III presents the results of the first observation of picosecond photorefractive two-beam coupling in a material (undoped CdTe) lacking appreciable linear absorption. Additionally, results of polarization rotation by scalar gratings are also presented.

Chapter IV presents the results of a series of measurements made of second harmonic generation in a transmission geometry in various thicknesses of CdTe. It is found that the second harmonic light originates in the material bulk rather than at the exit surface, and that no significant enhancement to the conversion efficiency is obtained by varying the sample thickness, down to a thickness of roughly six times the second harmonic generation coherence length. Results are presented for both 1064 nm and 921 nm excitation.

CHAPTER II

PULSE-PROBE DEGENERATE FOUR-WAVE MIXING

Introduction

Interest in the nonlinear optical properties of some III-V [5] and II-VI semiconductors has undergone a recent resurgence with the realization that these materials can be used effectively in optical processing. Of the II-VI compounds, renewed interest has been taken in CdTe owing to its relatively high electro-optic coefficient in the near infrared [6]. In addition, its nonlinear response to two-photon absorption (TPA) in the infrared is of interest because the material is transparent in this spectral region. We have used the laser-induced grating technique of picosecond pulse-probe (PP) degenerate four-wave mixing and two-beam self scattering (SS) to determine the nonlinear optical responses of CdTe due to free carriers. The ambipolar diffusion coefficient D_a, free carrier lifetime τ_{fc}, and laser-induced change in refractive index Δn were found for samples of CdTe having different conductivity types.

Dynamic holographic gratings were first observed in semiconductors by Woerdman, $et\ al$ [7] in Si and first studied in CdTe by Kremenitskii, $et\ al$ [8]. Two in-phase laser beams are crossed inside the sample to form an interference pattern in the shape of a sine wave. Through one or two-photon absorption, this creates an initial distribution of free carriers with the same spatial distribution as the light interference pattern. The nonlinear optical properties associated with a free carrier population density cause this spatial distribution to act as a refractive index grating. A third beam incident on this grating is diffracted in a well-defined direction and can be detected by a photodiode. The strength of this scattered beam is then monitored as a function of time delay between the

3

pulses writing the grating and the probe pulse reading the grating. The write beam crossing angle, 2θ, is used as a variable parameter since it determines the wavelength of the laser-induced grating.

Because of its high TPA coefficient in the infrared, dynamic gratings can be created in CdTe using pump photons of energy less than that of the band gap energy, E_g. Since the linear optical absorption coefficient of CdTe at 1.064 μm is approximately 0.8 cm^{-1}, the laser-induced grating created by TPA will extend throughout the entire thickness of the sample. The method therefore constitutes a nondestructive way to determine bulk material properties.

The samples used in this work were prepared by Eagle-Picher Laboratories. Stoichiometric quantities of 6-9's pure Cd and Te were loaded into a graphite crucible and the vessel was pressurized to 650 psi with argon and held above the melting point of CdTe until complete reaction was assured. The molten CdTe was then quenched to room temperature. Crystal growth was accomplished by the modified Bridgman technique using a Cd overpressure to suppress vaporization and control the desired type and resistivity of the growing crystal.

Theoretical Background

In this section we derive the basic equations for the scattering efficiency of both thin and thick transmission gratings. The approach will be to solve the wave equation in the medium assuming one monochromatic incident wave, and an initially infinite number of scattered waves. Once the difference-differential equation for the various scattered waves is obtained, we will solve it for two limiting cases; one where the scattered waves differ little in phase at the exit plane of the grating, and the other where this phase difference is substantial. The two cases define the *thin* and *thick* grating regimes, respectively. We assume that the incident wave is polarized perpendicular to the plane of incidence, or, the transverse magnetic (TM) case. The transverse electric (TE) case is treated in [1],[2], and [3]. The geometry for the ensuing discussion is shown in Fig. 1.
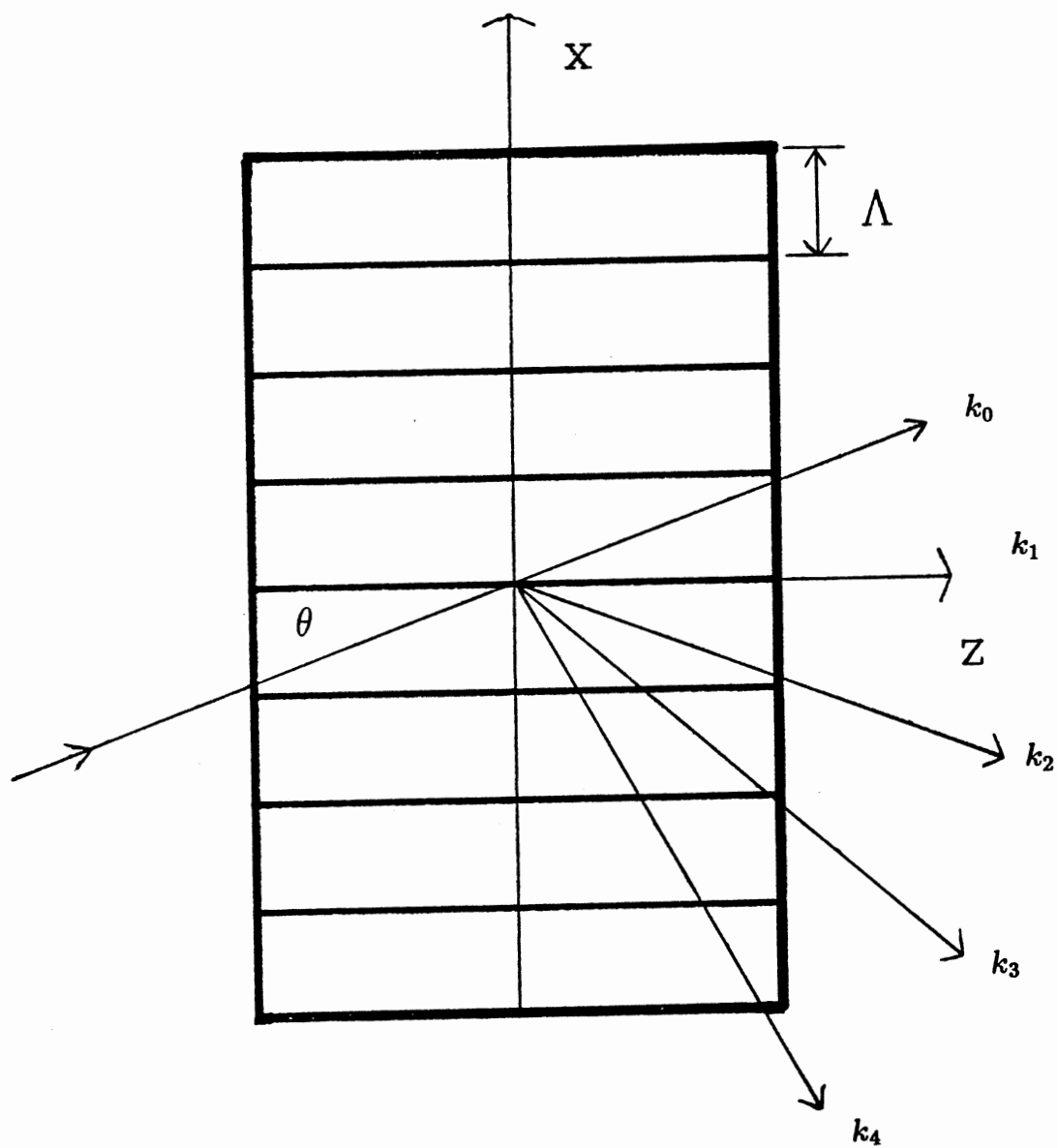
Figure 1. Coupled Wave Theory Geometry, Showing the Incident Wave k_0, and Scattered Waves $k_1, k_2, \ldots$.

We begin by writing the wave equation for the electric field inside the material

$$\nabla^2 E = \mu_0 \epsilon \frac{\partial^2 E}{\partial t^2} + \mu_0 \sigma \frac{\partial E}{\partial t} \tag{II.1}$$

where the permeability μ_0 is taken to be unity, $\epsilon = \epsilon_0(1 + \chi)$ is the permittivity for linear susceptibility χ, and σ is the conductivity. Anticipating the form of the refractive index/absorption coefficient modulation, we assume a total electric field in the material of the form

$$E_{tot} = \sum_{p=-\infty}^{\infty} \phi_p(z) \exp[i(\vec{k}_p \cdot \vec{r} - \omega t)] \tag{II.2}$$

where $\phi_p, \vec{k}_p = n_b \vec{k} + p\vec{k}_g$, and ω are the amplitude, wave vector, and angular frequency, respectively, of the pth scattered wave inside the material. $\vec{k}_g = k_g \hat{x}$ is the wavevector of the refractive index/absorption grating, and corresponds to a *grating wavelength* $\Lambda = 2\pi/k_g$. $\vec{k}$ is the wave vector of the incident wave (i.e., zeroth order) in free space, and n_b is the background refractive index of the material. For compactness of notation, the explicit summation symbol in Eq. (II.2) will be dropped; the sum remains implicit.

Substituting the electric field in Eq. (II.2) into the wave equation in Eq. (II.1) gives

$$\left[2i(k_p)_z \phi' - k_p^2 \phi_p\right] \exp[i(\vec{k}_p \cdot \vec{r}) - \omega t] = -\kappa^2 \phi_p \exp[i(\vec{k}_p \cdot \vec{r} - \omega t] \tag{II.3}$$

where $k_p^2 = (k_p)_x^2 + (k_p)_z^2$, and the prime denotes differentiation with respect to z. Here κ is the complex propagation constant defined as

$$\kappa^2 = \omega^2 n^2 / c^2 + i2\omega n \alpha / c \tag{II.4}$$

where $c^2 = (\mu_0 \epsilon_0)^{-1/2}$, $n^2 = 1 + \chi$ is the square of the refractive index, and $\alpha = \mu_0 c \sigma / 2n$ is the absorption coefficient. En route to Eq. (II.3), we invoked the Slowly Varying Envelope (SVE) approximation, embodied in

$$\phi_p'' \ll 2i(k_p)_z \phi_p', \qquad (\text{II.5})$$

which states that there is only a small absorption loss per unit wavelength and a slow interchange (per wavelength) of energy between the waves. It is also assumed that the variation of ϕ_p with x is small compared to the variation with z.

The refractive index and the absorption coefficient appearing in the expression for κ can be characterized by a background value plus some small deviation from that value. Or,

$$n = n_b + \Delta n \qquad (\text{II.6})$$

$$\alpha = \alpha_0 + \Delta\alpha. \qquad (\text{II.7})$$

The quantities n_b and α_0 are the background refractive index and absorption coefficient, respectively, while Δn and $\Delta\alpha$ represent the maximum deviations of these quantities from the background values. Neglecting terms in second order ($\Delta n \Delta\alpha$, for example) and using Eqs. (II.6) and (II.7) for n and α, respectively, gives

$$\kappa \approx \beta_0^2 + 2i\alpha_0\beta_0 + 2\beta_0(2\pi\Delta n/\lambda + i\Delta\alpha) \qquad (\text{II.8})$$

where $\beta_0 = 2\pi n_b/\lambda$, and λ is the wavelength of the incident wave in free space. If we now use for Δn and $\Delta\alpha$ the forms

$$\Delta n = n_1 \cos(\vec{k}_g \cdot \vec{r} + \delta) \qquad (\text{II.9})$$

$$\Delta\alpha = a_1 \cos(\vec{k}_g \cdot \vec{r} + \delta) \qquad (\text{II.10})$$

where δ is an arbitrary phase, and substitute them into the wave equation of Eq. (II.3) we find, after equating like coefficients of the phases of the fields,

$$\phi'_p = -\frac{i}{\cos\theta}\left(\frac{k_p^2 - \beta_0^2}{2\beta_0} - i\alpha_0\right)\phi_p$$

$$-\frac{1}{2\cos\theta}\left(\frac{2\pi}{\lambda}n_1 + i\alpha_1\right)(\phi_{p-1} - \phi_{p+1}) \tag{II.11}$$

$$= -\frac{ipQ}{2l}(p - 2A)\phi_p - \frac{\alpha_0}{\cos\theta}\phi_p - \frac{\Gamma}{2l}(\phi_{p-1} - \phi_{p+1}) \tag{II.12}$$

where l is the grating thickness along the z direction and

$$Q = k_g^2 l / k n_b \cos\theta \tag{II.13}$$

$$A = -(n_b k / k_g)\sin\theta \tag{II.14}$$

$$\Gamma = \frac{l}{\cos\theta}\left(\frac{2\pi}{\lambda}n_1 + i\alpha_1\right) \tag{II.15}$$

$$\delta = \pi/2. \tag{II.16}$$

In obtaining Eq. (II.11) for the field amplitudes ϕ_p, it is instructive to note that the multiplication of the fields E_p by the grating terms Δn and $\Delta\alpha$ on the right-hand side of the wave equation Eq. (II.3) gives rise to terms of the sort $\exp[i(\vec{k}_p \pm \vec{k}_g) \cdot \vec{r}]$. Observing that such a term is just $\exp[i(\vec{k}_{p\pm 1} \cdot \vec{r})]$, for dummy index p, reveals that the shifting of that index on the associated ϕ_p term by ∓ 1 is the origin of the $p \mp 1$ terms in Eq. (II.11).

The parameter Q in Eq. (II.12) is a measure of the difference in phase of the various partial waves due to their different directions of propagation. A plane wave travelling across the index grating at an angle Θ_p with respect to the z axis travels an optical path of

$$n_b l \sec\Theta_p \approx n_b l(1 + \Theta^2/2), \tag{II.17}$$

and since the angle between adjacent orders is approximately

$$\Theta \approx k_g / k n_b, \tag{II.18}$$

the difference in spatial phase for the wave travelling in the Θ_p direction and a wave travelling parallel to the z axis is

$$n_b k[l \sec \Theta - l] = p^2 Q/2. \tag{II.19}$$

When the phase difference between these two waves becomes large (say $Q \gg 1$), the diffracted light tends to remain in the lower orders because of the large disparity in phase. When the phase difference is very small (say $Q \ll 1$) light can be scattered into and remain in the higher orders during propagation through the material.

We consider the two limiting casess for which analytical solutions to the difference-differential equations can be had: $Q \ll 1$ and $Q \gg 1$. For the case $Q \approx 1$, the solution must be obtained numerically. For $Q \ll 1$, the number of diffracted orders is usually relatively small, say 10 or less; the absolute value of p is therefore also small. However, for moderate angles of incidence A can be quite large, since it is expressed in normalized units of diffraction angles. Therefore, in Eq. (II.12) the term in Qp^2 can be neglected compared to the term in $2AQp$, so that the wave equation becomes

$$\phi_p' + \frac{\Gamma}{2l}(\phi_{p-1} - \phi_{p+1}) = \frac{ipQ}{l \cos \theta} A \phi_p - \frac{\alpha_0}{2 \cos \theta} \phi_p. \tag{II.20}$$

Neglecting losses ($\alpha \approx 0$), Klein *et al.* [4] have shown the solution of Eq. (II.20) for the ϕ_p to be

$$\phi_p = \exp(ipQAz/2l) J_p \left[\frac{2v}{QA} \sin \left(\frac{QAz}{2l} \right) \right], \tag{II.21}$$

subject to

$$\phi_0(z = 0) = 1 \tag{II.22}$$

$$\phi_{p \neq 0}(z = 0) = 0, \tag{II.23}$$

where $v = 2\pi l n_1 / \lambda \cos \theta$ and J_p is the ordinary Bessel function of integer order p. The quantity of interest is the *scattering efficiency* η, defined as the irradiance of the pth diffracted wave at $z = l$ divided by the irradiance of the incident wave

at $z = 0$. Since ϕ_0 is normalized to unity at the grating boundary $z = 0$, η is simply

$$
\begin{aligned}
\eta_p &= |\phi_p(z = l)|^2 \\
&= J_p^2 \left[v \frac{\sin(QA/2)}{QA/2} \right].
\end{aligned}
\tag{II.24}
$$

At normal incidence, $A = 0$ and the intensity reduces to

$$
I_p = J_p^2 (2\pi l n_1 / \lambda \cos \theta).
\tag{II.25}
$$

$Q \ll 1$ constitutes the *thin grating* regime.

We next treat the case $Q \gg 1$, where, from the discussion above, light appears in only one or two of the lower diffraction orders. Assuming, then, only one scattered wave, and for incidence at the Bragg angle, (for which $k_p^2 = \beta_0^2$ in Eq. (II.11)), we obtain from Eq. (II.12)

$$
\phi_0' + \frac{\alpha_0}{\cos \theta} \phi_0 = i \xi \phi_1
\tag{II.26}
$$

$$
\phi_1' + \frac{\alpha_0}{\cos \theta} \phi_1 = i \xi \phi_0
\tag{II.27}
$$

where

$$
\xi = \Gamma / 2l.
\tag{II.28}
$$

The arbitrary phase factor δ in Eqs. (II.9) and (II.10), has been set to zero. Assuming solutions of the form

$$
\phi_0 = r_1 \exp(\gamma_1 z) + r_2 \exp(\gamma_2 z)
\tag{II.29}
$$

$$
\phi_1 = s_1 \exp(\gamma_1 z) + s_2 \exp(\gamma_2 z),
\tag{II.30}
$$

substituting them into the coupled wave equations of Eqs. (II.26) and (II.27), and setting $z = 0$ (the relations must hold for all z) results in

$$(\cos\theta\gamma_i + \alpha_0)r_i = i\xi s_i \tag{II.31}$$

$$(\cos\theta\gamma_i + \alpha_0)s_i = i\xi r_i. \tag{II.32}$$

Multiplying these two equations together provides an expression quadratic in the γ_i

$$\cos^2\theta\gamma_i^2 + 2\alpha\cos\theta\gamma_i + (\alpha_0^2 - \xi^2) = 0, \tag{II.33}$$

from which follows

$$\gamma_1 = -\frac{1}{\cos\theta}(\alpha_0 + i\xi) \tag{II.34}$$

$$\gamma_2 = -\frac{1}{\cos\theta}(\alpha_0 - i\xi). \tag{II.35}$$

Applying the boundary conditions to the incident and diffracted waves

$$\phi_0(z = 0) = 1 \tag{II.36}$$

$$\phi_1(z = 0) = 0 \tag{II.37}$$

and combining the result with Eqs. (II.31) and (II.32) gives

$$s_1 = -\frac{i\xi}{\cos\theta}\left(\frac{1}{\gamma_1} - \frac{1}{\gamma_2}\right) \tag{II.38}$$

$$= -s_2.$$

Since the scattering efficiency η is again given by

$$\eta = |\phi_1(z = l)|^2, \tag{II.39}$$

we combine Eq. (II.28) for ξ, (II.30) for $\phi_1(z)$, and (II.34) and (II.35) for the γ_i, to give

$$\eta = \exp(-2\alpha_0 l/\cos\theta)\left[\sin^2\left(\frac{\pi d}{\lambda\cos\theta}n_1\right) + \sinh^2\left(\frac{l}{2\cos\theta}\alpha_1\right)\right], \tag{II.40}$$

which is the desired result for *thick gratings* $(Q \gg 1)$.

Experimental Procedure

The resistivity, mobility, infrared transmission, and etch pit density were determined on samples cut from locations near the bottom and top of the ingot. The resistivity and mobility were determined by Hall measurement at room temperature. The resistivity, mobility, and majority carrier dark number density for the n-type sample are 13 Ω cm, 1040 cm^2 V^{-1} s^{-1}, and 4.6 $\times 10^{14}$ cm^{-3}, respectively, and for the p-type sample 5.5 MΩ cm, 90.1 cm^2 V^{-1} s^{-1}, and 1.3 $\times 10^{10}$ cm^{-3}.

Polished, $1 \times 1 \times 0.1$ cm, n- and p-type samples of CdTe were used in this study. The n- and p-type samples were taken from Eagle-Picher Lot Numbers FT84325-01-05 and FT87104-01-05, respectively. The polished surfaces were (111) faces. Room temperature absorption spectra were obtained using a Perkin-Elmer Model 330 Spectrophotometer. In the PP and SS experiments performed at 1.064 μm, the samples were excited and probed with $\tau_p = 18$ ps full-width-half-maximum (FWHM) Gaussian pulses of the $\lambda = 1.064$ μm emission of a YAG:Nd laser operating at a repetition rate of 10 Hz. Incident pulse intensities were in the 24 MW cm^{-2} range. We also have made a preliminary study of band-edge enhancement of the pulse-probe signal in the wavelength range of 880-930 nm in the same material. For this work, a tunable short cavity dye laser, pumped at 532 nm by a frequency-doubled picosecond YAG:Nd laser was used.

Figure 2 depicts schematically the experimental setup used in the PP study. A single, vertically polarized laser pulse was split into three parts, two write beams, and a probe beam. The relative intensities of the two write beams had a ratio of 2:1 and the probe beam intensity was ten times less than the weaker write beam. All three beams were linearly polarized, and the polarization vectors of the write beams were parallel. The write beams were focused down to a 1 mm diameter spot size and directed non-collinearly onto one of the (111) faces of the sample so as to intersect at an angle 2θ, measured *outside* the sample. This angle of intersection is termed the write angle. By mechanical adjustment of a variable
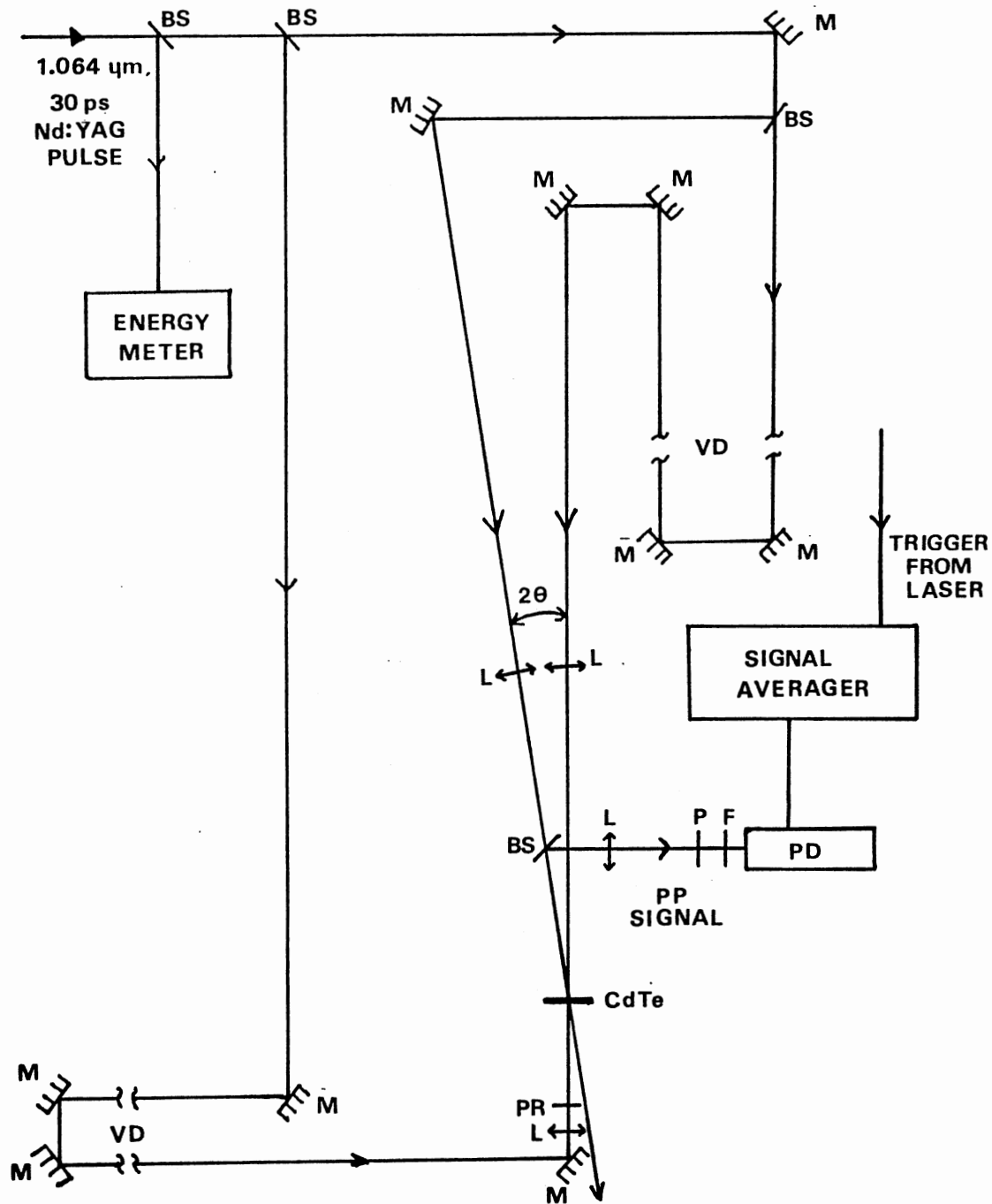
Figure 2. Block Diagram of the Experimental Setup for Pulse-probe and Self-scattering Measurements. M, Mirror; BS, Beam Splitter; VD, Optical Variable Delay Line; P, Polarization Analyzer; PR, Polarization Rotator; L, Lens; F, Filter; PD, Photodiode.

optical delay line through which one of the write beams passed, the optical path difference between the write beams was maintained equal to zero to ensure that the beams arrived at the sample in phase and at the same time.

The probe beam also passed through a variable optical delay line, allowing the time delay between the writing and probing of the grating to be continuously adjusted. This feature of the setup allowed the characterization of the grating decay kinetics. The longest pulse/probe delay realizable with this setup was 2 ns. After passing through the delay line, and having its polarization vector rotated 90° with respect to the write beam polarization, the probe beam was also focused down to a 1 mm diameter spot size and introduced into the sample exactly conjugate to one of the write beams. At each value of time delay the probe beam was realigned to assure best counterpropagation to the appropriate write beam. The rotated polarization of the probe beam, together with its relatively weak intensity, precludes it from interacting with one of the write beams to create additional grating effects in the sample. The PP diffracted beam is also of wavelength 1.064 μm and, according to the Bragg scattering condition, is conjugate to the other write beam. The signal was monitored with an EG&G Photon Devices YAG-100A photodiode. To minimize the background signal levels introduced by scattered light and band edge luminescence, a polarization analyzer and absorbing filter were placed in series before the photodiode to allow passage of only those beams with the same polarization and wavelength as the probe beam. This filtered signal was averaged by an EG&G PAR 4202 Signal Averager, and the resultant intensity read from an oscilloscope driven by the signal averager.

The experimental setup for the SS study is similar to that described above for the PP study with the exception that only two parallel-polarized, equal intensity write beams were used to produce the scattered signal beams. The two in-phase, focused write beams are again directed onto the sample so as to intersect inside at a write angle 2θ. At sufficiently small values of the grating parameter Q, higher scattered orders may be observed. The relative intensities

of these diffracted orders were measured using the photodiode/signal averager setup described above.

Experimental Results

Optical Absorption and Luminescence

Figure 3 shows the results of room temperature optical transmission measurements on the samples studied. The band gap, E_g, in both samples is about 1.4 eV. No pronounced regions of decreased transmission were observed in the energy range 0.48 eV up to the fundamental absorption edge at 1.4 eV, with special attention directed to the region near the laser photon energy of 1.17 eV. It should be noted that the transmission spectra is *not* corrected for Fresnel losses. Using the index of refraction of CdTe at 1.064 μm, and assuming normal incidence leads to a value of the transmission at 1.064 μm of 0.99, corresponding to a linear absorption coefficient of no greater than 0.1 cm^{-1}. Also shown in Fig. 3 is the room temperature luminescence spectra of CdTe under 1.064 μm laser excitation.

The dependence of the band edge luminescence intensity on the laser excitation intensity is shown in Fig. 4. The observed quadratic dependence demonstrates that one of two possible types of two-photon processes is responsible for the excitation process. The first is a sequential two-photon absorption (STPA) process, where there is a real intermediate impurity state between the initial and final electron/hole state; the second a virtual two-photon absorption (VTPA) process, where there is no real intermediate state between the initial and final electron/hole state. Both the lack of appreciable optical absorption at 1.17 eV and the known-high value of the TPA coefficient of CdTe at this excitation wavelength [9] indicate free-carrier populations created via VTPA processes. In addition, the observed charge carrier dynamics described below are consistent with the creation of electron-hole pairs.
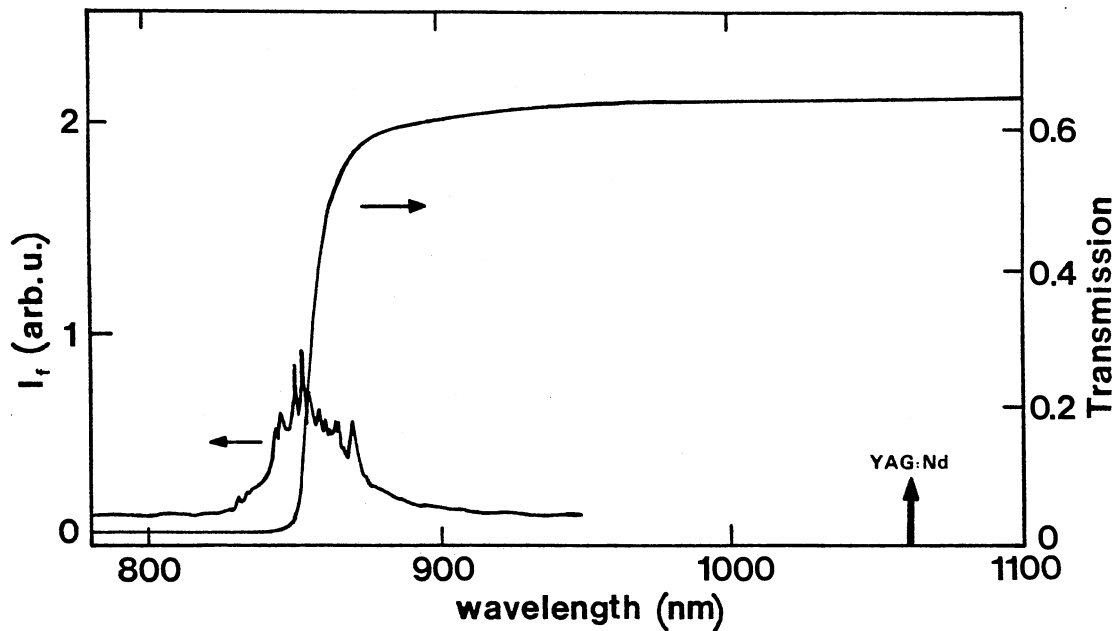
Figure 3. Band Edge Emission and Transmission Spectra of CdTe. The Results are Representative of Both N- and P-type Samples. The Arrow at 1.064 μm Shows the Spectral Position of the Excitation Laser Line.
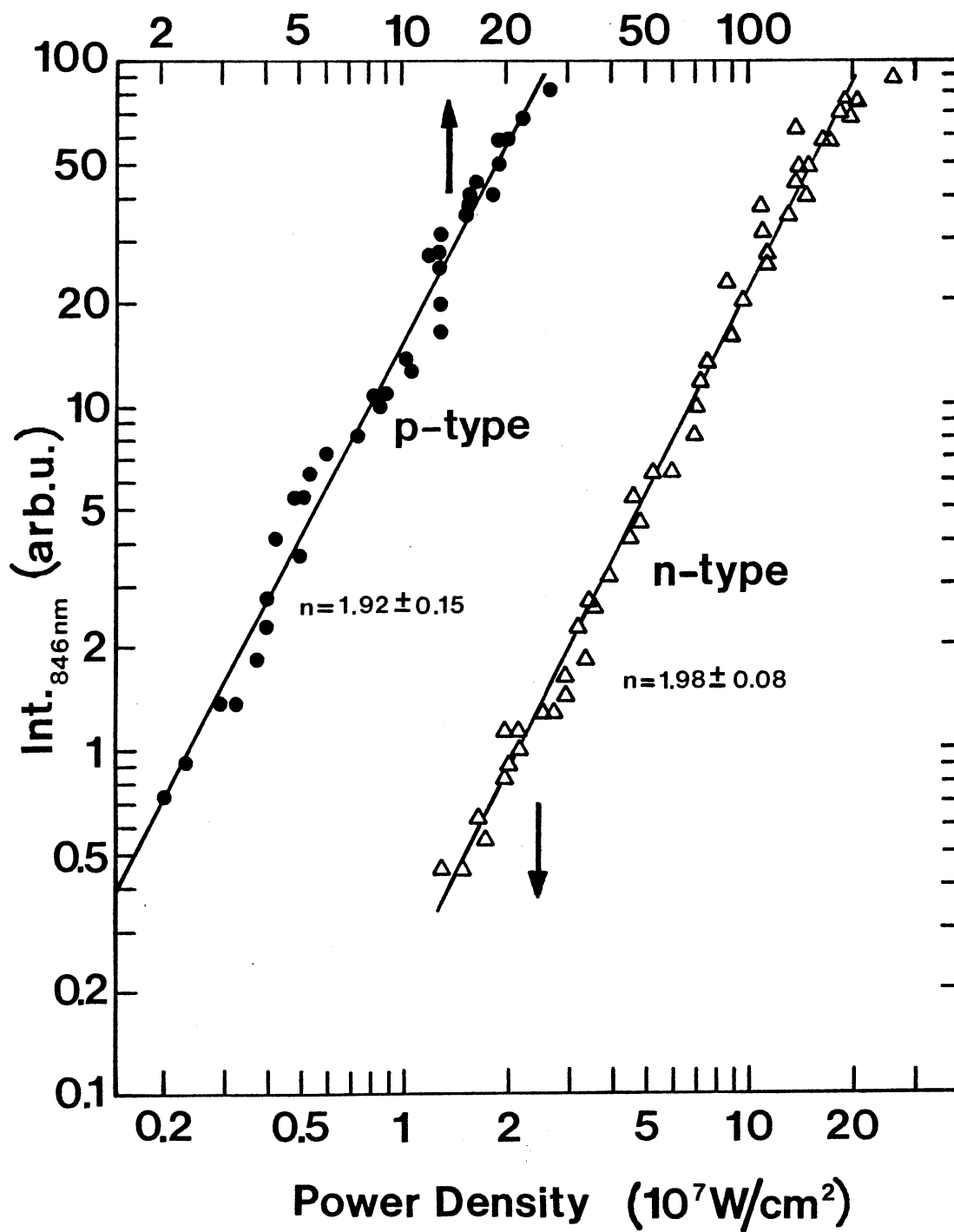
Figure 4. Dependence of the Band Edge Luminescence Intensity on the 1.064 μm Laser Excitation Power Density.

Pulse-Probe Four-wave Mixing

Figure 5 shows the dependence of the PP signal intensity on the laser beam power density I_{exc} for two write beam crossing angles and several probe delay times. For each case it is found that the PP signal I_{sig} is approximately proportional to the 3.7-4.0th power of the laser up to an excitation level at which saturation is reached. Because the scattering efficiency is proportional to Δn^2 for small modulation depths, one expects an I_{exc}^5 power dependence for free-carrrier gratings created through two-photon absorption and for probe beams proportional to I_{exc}. At higher excitation intensities, the signal levels off due to TPA and free-carrier absorption. The PP signal intensities exhibit saturation behavior near $I_{exc} = 3 \times 10^8$ W cm^{-2} for large write beam crossing angles and an order of magnitude lower for small

Figure 6 shows the grating decay kinetics of the p- and n-type samples measured at five different values of 2θ. From the relation between the grating spacing and write beam crossing angle, $\Lambda = \lambda/2\sin\theta$, this set of write angles corresponds to grating spacings ranging from 8.7 to 1.5 μm. Figure 7 shows the laser write beam autocorrelation overlaid on the PP signal rise times, making apparent that the autocorrelation is the origin of the seemingly-finite signal response time. At the largest three write angles, both samples also exhibit single-exponential decays for times after the initial rise. At the two smallest write angles, however, the signal from the n-type sample exhibits kinetics that are clearly not single-exponential. In the n-type sample at 15°, the decay is composed of a two components, one active up to about 1.75 ns, with a rate constant of 2.04×10^9 s^{-1}, and a longer lived component for times after 1.75 ns with a rate constant too small to accurately measure. At 7° the signal again tapers off at a rate that is too small to measure accurately. The p-type sample exhibited no multiple components of decay at 15°.

For optically thin samples, assuming intensity variations are important in only one transverse direction x, and the pulse width is much smaller than the
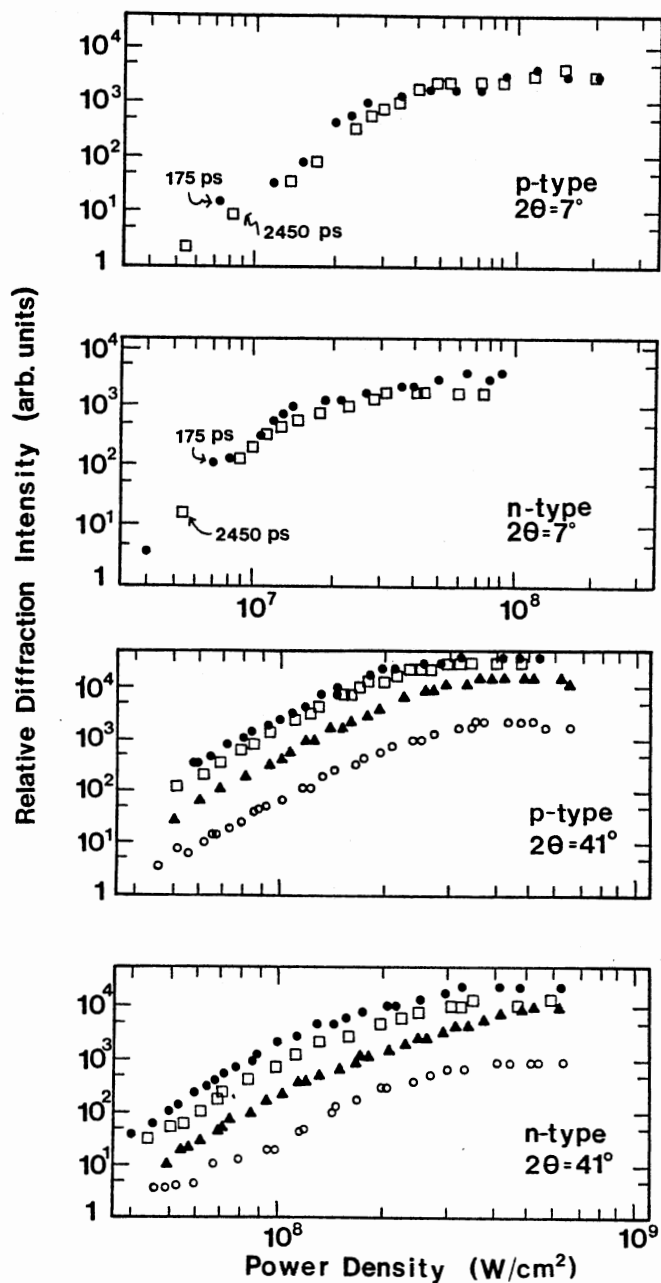
Figure 5. PP Signal Intensity Dependence on Laser Excitation Intensity at Various Times After Grating Creation for N- and P-type CdTe. (a) $2\theta = 7°$; (•) $\Delta t = 175$ ps, (□) $\Delta t = 2450$ ps. (b) $2\theta = 41°$; (•) $\Delta t = 119$ ps, (□) $\Delta t = 189$ ps, ($\triangle$) $\Delta t = 280$ ps, (o) $\Delta t = 455$ ps.
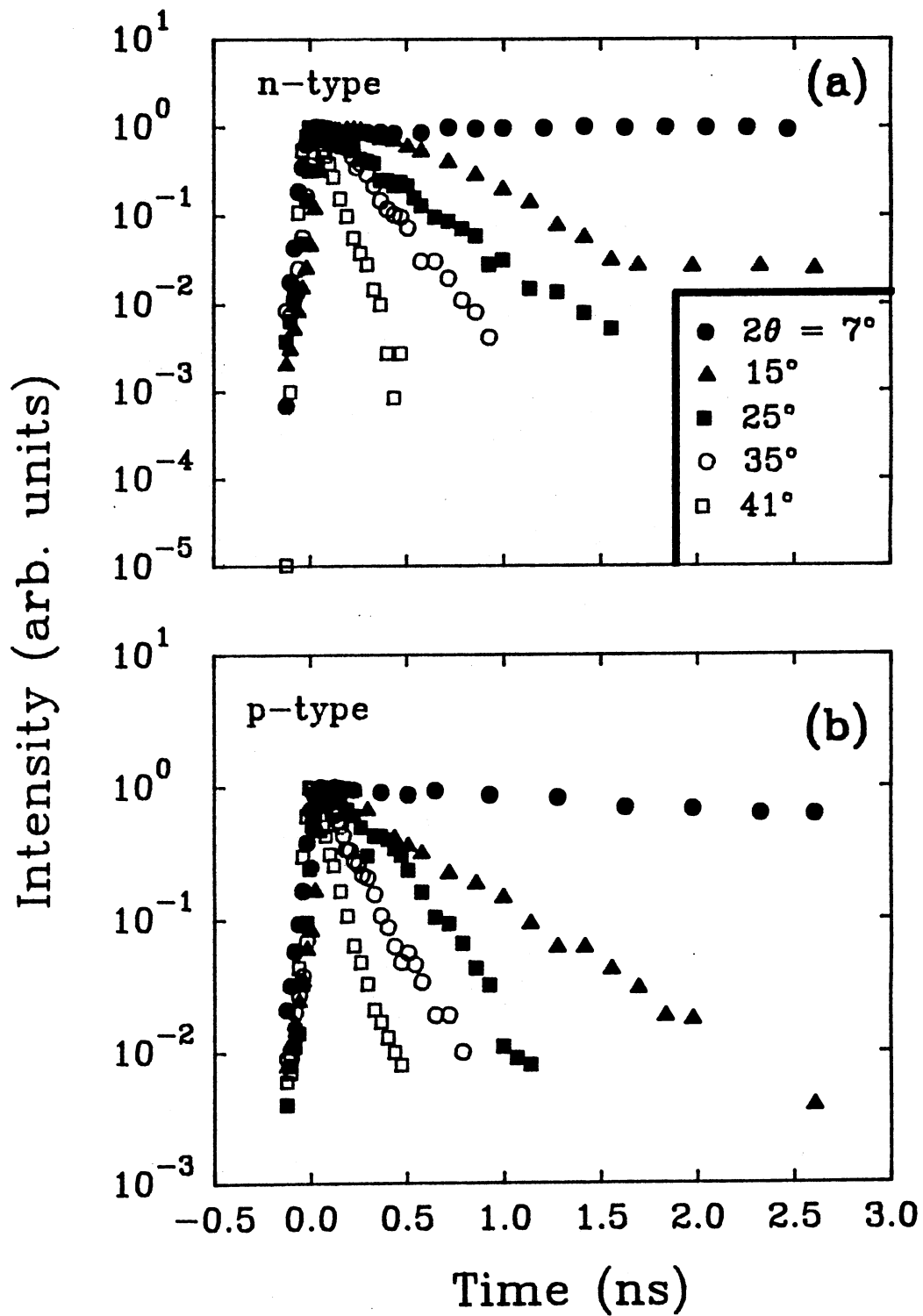
Figure 6. PP Signal Intensity as a Function of Time after Grating Creation for Various Write Beam Crossing Angles. (a) N-type CdTe, (b) P-type CdTe.
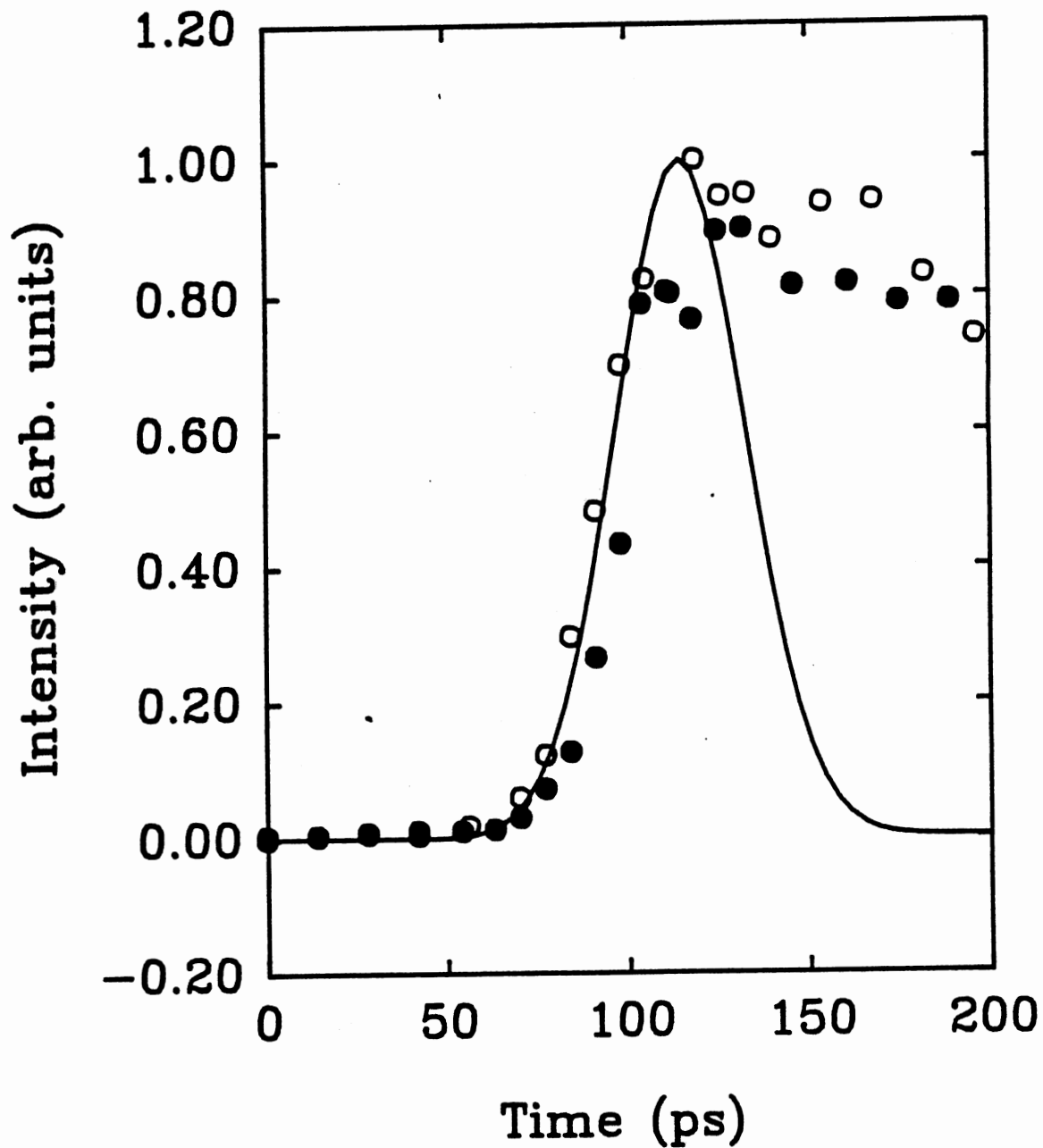
Figure 7. PP DFWM Signal as a Function of Time after Grating Creation for Two Different Crystal Orientations. Open and Closed Circles Denote Measurements Made in Orientations Differing by a 90° Rotation about the Write Beam Bisector. The Solid Line is the Autocorrelation Trace of the Writing Pulses.

carrier lifetime, the spatial and temporal dependence of the free carrier density, N, is given by the one-dimensional diffusion equation

$$\frac{\partial N(x,t)}{\partial t} = \frac{-N(x,t)}{\tau_{fc}} + D_a \frac{\partial^2 N(x,t)}{\partial x^2}. \tag{II.41}$$

Here τ_{fc} is the free carrier lifetime, defined as $\tau_r \tau_t/(\tau_r + \tau_t)$, where τ_r and τ_t are the recombination time and trapping time, respectively, and D_a is the ambipolar diffusion coefficient. The ambipolar diffusion approximation can be shown to be valid from considerations based on the range of grating spacings and fluences used here [11]. For a distribution of carriers varying sinusoidally in space with period Λ, the solutions to Eq. (II.41) decay exponentially with a time constant $K/2$, where K is the *observed PP signal decay time* given by

$$K = \frac{2}{\tau_{fc}} + \frac{8\pi^2 D_a}{\Lambda^2}. \tag{II.42}$$

Therefore, for grating wavenumber $k_g = 2\pi/\Lambda$, a plot of K vs. $2k_g^2$, as shown in Fig. 8, gives a straight line with intercept $2/\tau_{fc}$ and slope D_a.

The solid line in Fig. 8 is drawn for reference and corresponds to $D_a = 3.0$ cm^2 s^{-1} and $\tau_{fc} = 12.0$ ns. Specifically, we find ambipolar diffusion coefficients 3.1 ± 1.5 cm^2 s^{-1} and 2.9 ± 1.0 cm^2 s^{-1}, and free carrier lifetimes 12.0 ± 9.0 ns and 12.5 ± 9.0 ns, for n- and p-type material, respectively.

For a laser-generated electron-hole plasma, the ambipolar diffusion coefficient is defined as

$$D_a = 2\frac{D_e D_h}{D_e + D_h} \tag{II.43}$$

where

$$D_{e,h} = \mu_{e,h}\frac{k_B T}{e}. \tag{II.44}$$

Eq. (II.44) is the Einstein relation between the electron-hole diffusion coefficient and mobilities, $\mu_{e,h}$, at temperature T. e is the modulus of the electronic charge and k_B is Boltzmann's constant. Assuming μ_e in the p-type material is equal
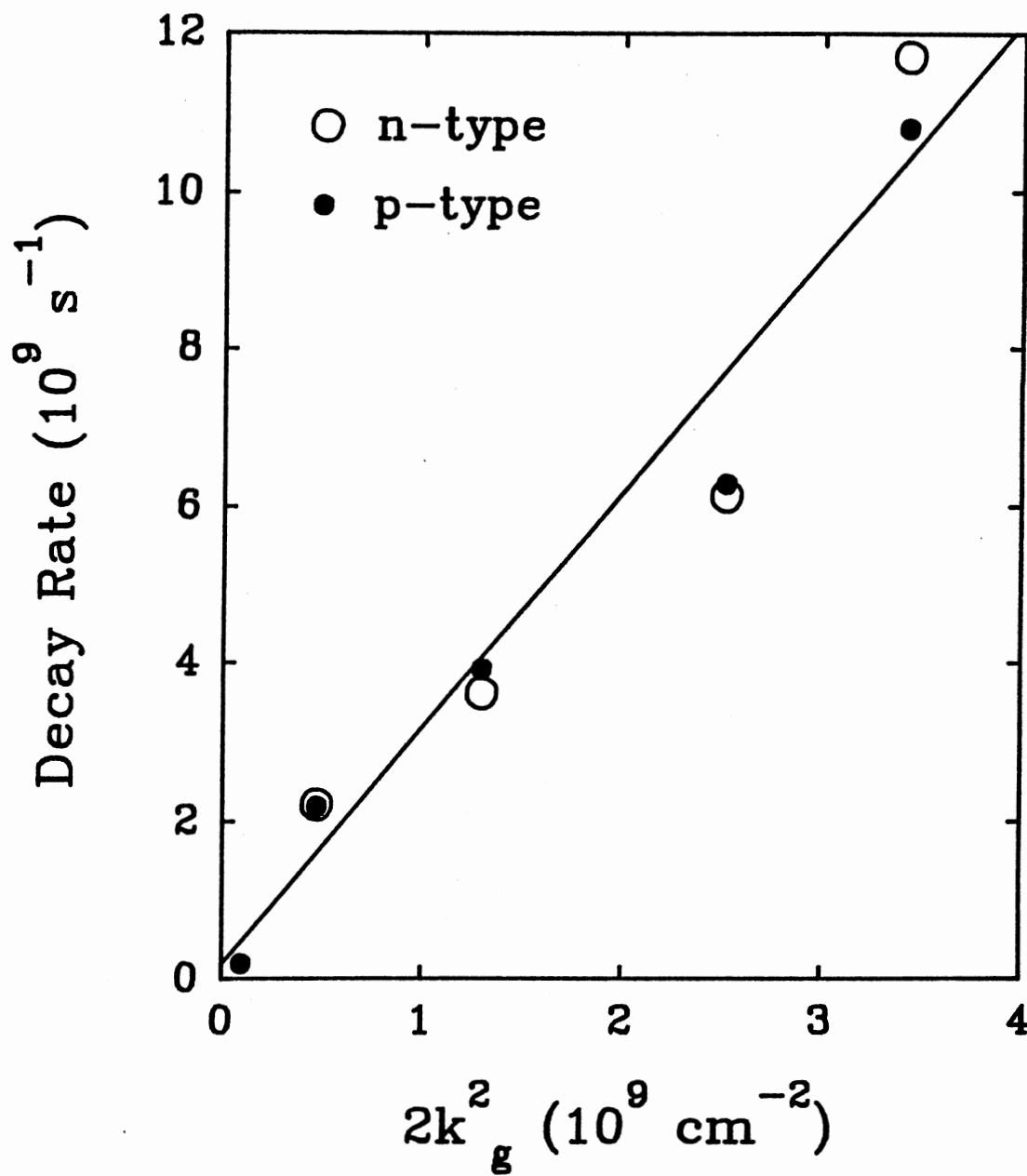
Figure 8. PP Signal Decay Rate K in CdTe as a Function of Twice the Square of the Grating Wavenumber.

to μ_e in the n-type material, and that μ_h in the n-type material is equal to μ_h in the p-type material, and using the measured room temperature values of the mobilities for these samples gives for both samples $D_a = 4.3$ cm^2 s^{-1}, in good agreement with the values determined by the picosecond laser-induced grating method.

Two-beam Self-Scattering

At sufficiently small write angles, multiple diffracted orders are observed on the side of the sample opposite that of the two incident write beams, as schematically depicted in Fig. 9. This effect, first observed in semiconductors by Woerdman and Bolger [7], is known as self-scattering, or Raman-Nath scattering [12], and defines the "thin grating" regime. Figure 10 shows the dependence of the first order scattered beam intensity on laser power density I_{exc} for p-type CdTe, with similar results obtaining for n-type material. As in the PP power dependence, the signal intensity is proportional to the third power of I_{exc} and saturation occurs near $I_{exc} = 3 \times 10^8$ W cm^{-2}.

The intensity of the ith order in self-scattering is given by [12]

$$I_i = AJ_i^2(\gamma \Delta n) \tag{II.45}$$

where

$$\gamma = \frac{2\pi l}{\lambda \cos \theta_{xtal}} \tag{II.46}$$

where A is a constant of proportionality, l is the grating thickness, Δn is the induced change in refractive index, θ is one-half the write beam crossing angle inside the material, and J_i is the ordinary Bessel function of integer order i. As a first approximation, l is taken to be the 0.1 cm sample thickness, since the length of the beam overlap region along the write angle bisector is much larger than the sample thickness at small write angles. The grating Q factor for this case is
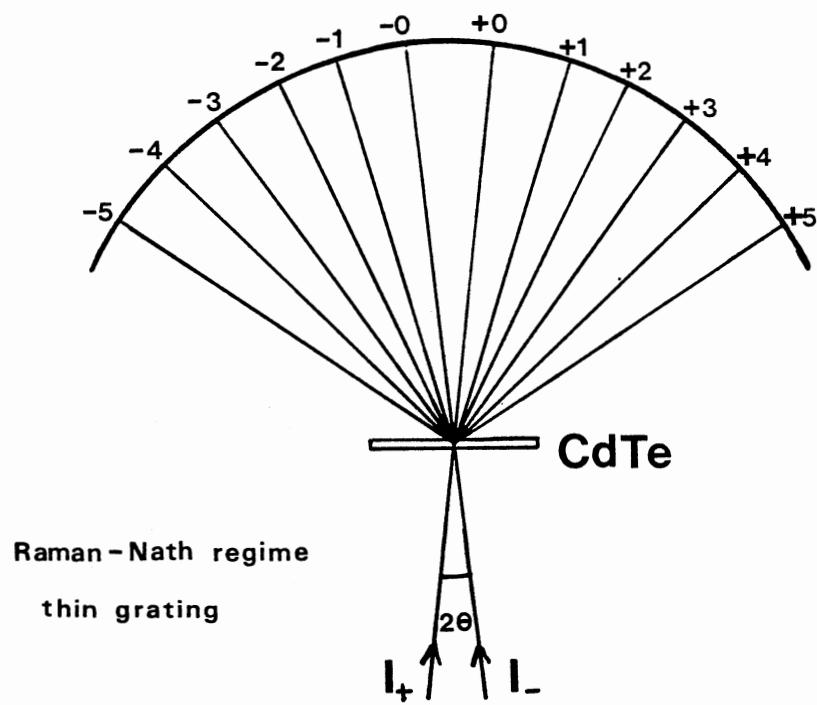
Figure 9. Schematic of Raman-Nath Self-scattering.
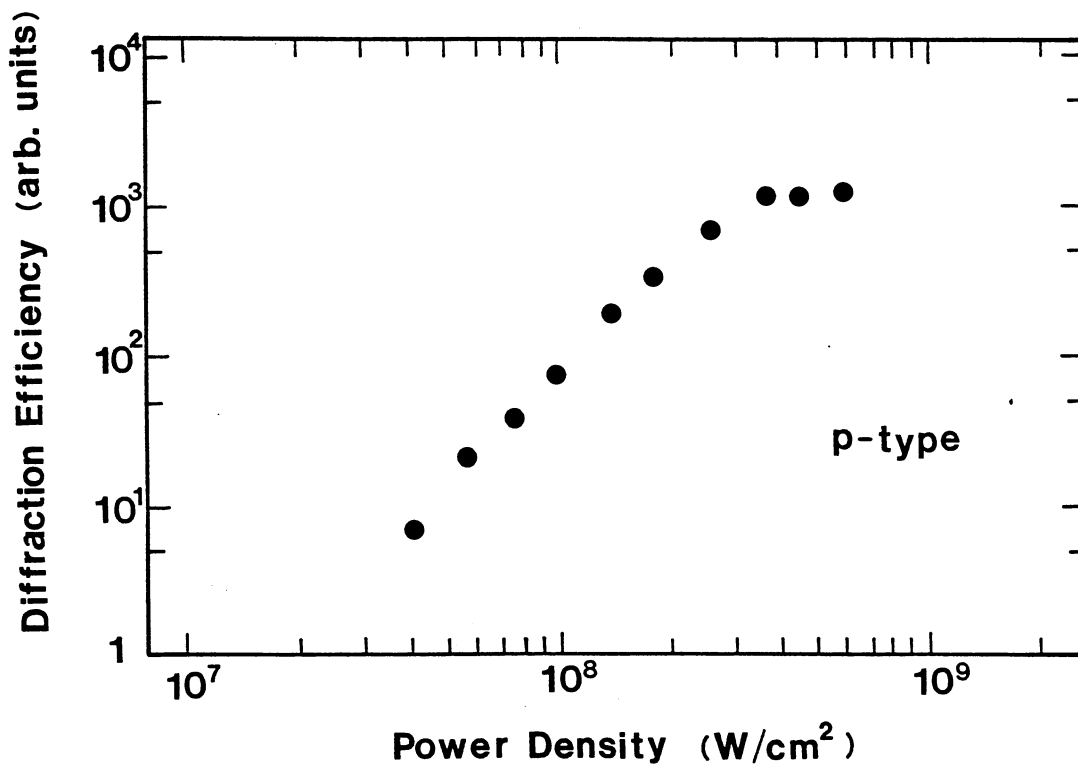
Figure 10. Dependence of the First Order SS Signal Intensity on the Write Beam Power Density for P-type CdTe.

$$Q = \lambda l / \Lambda^2 n_b \cos \theta_{xtal} \tag{II.47}$$

$$\approx 16. \tag{II.48}$$

The criteria for Raman-Nath scattering is $Q \ll 1$. However, the assumption of l being equal to the sample thickness is almost certainly overly optimistic, since beam depletion due to two-photon absorption will tend to restrict the depths of strong carrier (refractive index) modulation to the front layers of the sample. This reduced-thickness grating reduces the Q factor sufficiently to force the scattering process into the thin grating regime, and therefore provides preliminary justification for applying the Raman-Nath form of the scattering efficiency in Eq. (II.45).

Since both write beams, I_+ and I_- in Fig. 9, will scatter off the grating independently, there will be two significant contributions to each bright spot, one from, say, order i of I_+, and another from order $i + 1$ of I_-. We neglect the further scattering of thus scattered beams as a process of insignificantly high order. Thus, for equal write beam intensity, the expression for the scattering efficiency becomes

$$\eta_i = A[J_i^2(\gamma \Delta n) + J_{i+1}^2(\gamma \Delta n)] \tag{II.49}$$

Figure 11 shows examples of the relative intensities of the diffracted orders vs. order. A numerical fit of the data to Eq. (II.49), treating A and Δn as adjustable parameters, gives the free carrier-induced change in the refractive index. We find in the p- and n-type samples values of $\Delta n = 4.6 \times 10^{-4}$, and $\Delta n = 3.8 \times 10^{-4}$, respectively.

In a study complementing the pulse-probe work at 1.064 μm described above, we measured the absolute PP scattering efficiency in p-type CdTe as a function of excitation wavelength. The results are shown in Fig. 12, and were obtained using a tunable dye laser. The write angle for these measurements was 18°, measured outside the sample, corresponding to a grating wavelength of 3.4 μm.
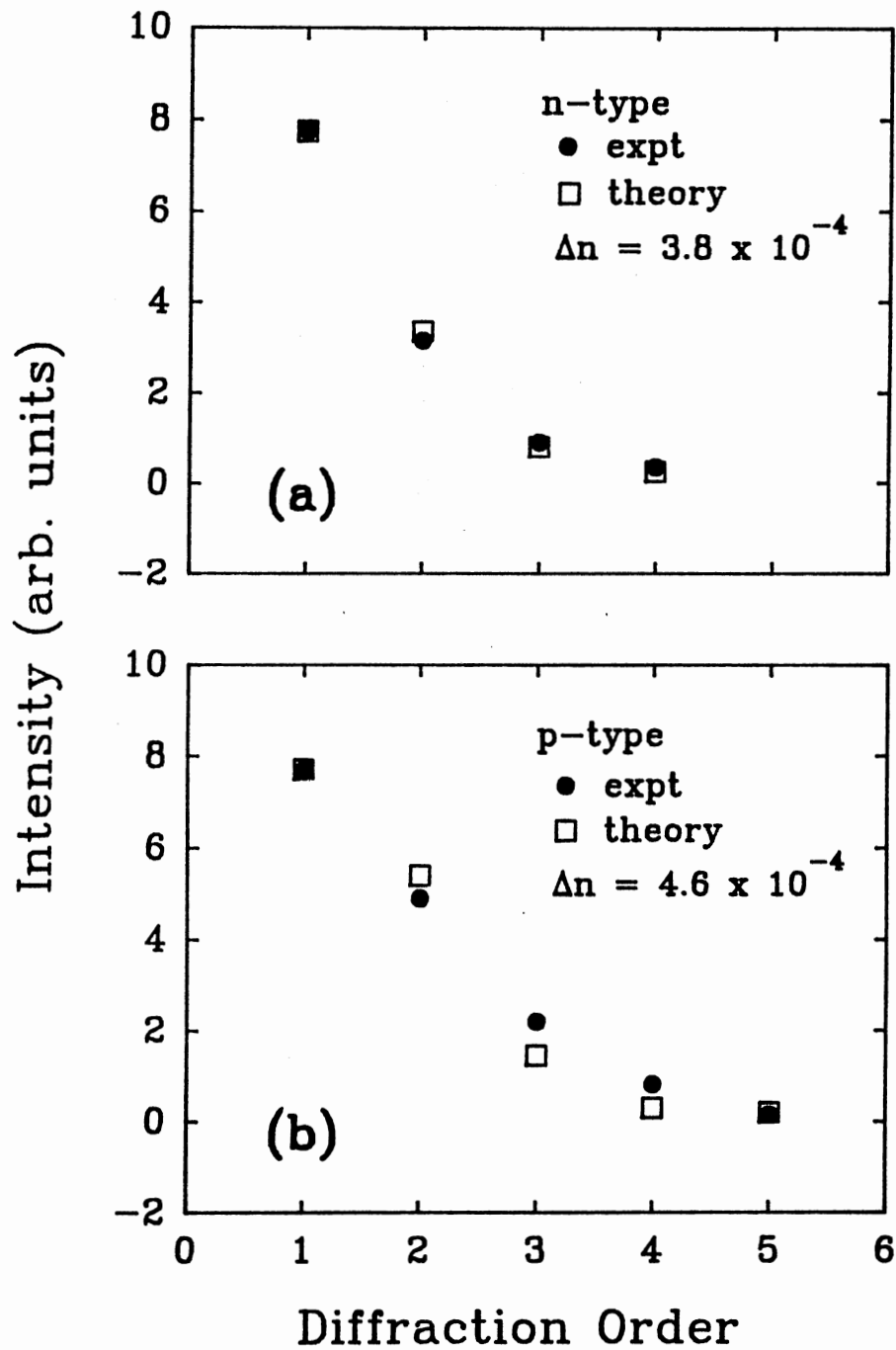
Figure 11. Raman-Nath Self-scattering in N- and P-type CdTe. (o) are Experimental Points and (□) is the Fit to the Raman-Nath Diffraction Efficiency. (a) N-type CdTe. (b) P-type CdTe.
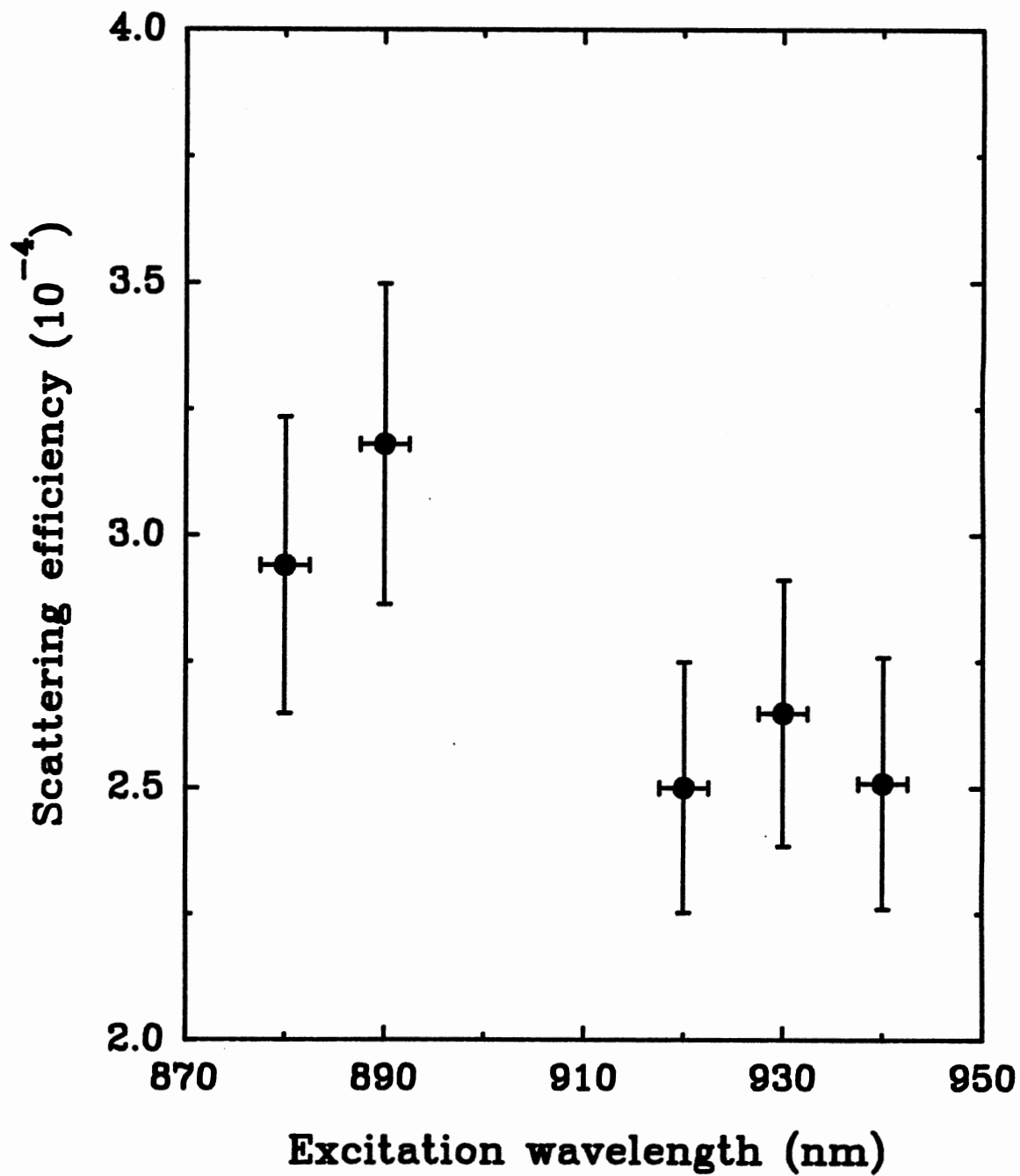
Figure 12. Absolute PP Scattering Efficiency as a Function of Excitation Wavelength in CdTe.

The excitation intensity I_{exc} was $\approx 1 \times 10^8$ W/cm^2. Although the write beams produce additional photocarriers (which increases the refractive index modulation) as the excitation wavelength is scanned nearer to resonance with the band edge energy, we observe no significant increase in the PP scattering efficiency due to resonant enhancement. The reason for this is that the probe beam, which is at the same wavelength as the write beams, also produces photocarriers more efficiently and therefore suffers increased attenuation as it passes through the material. Hence, the essentially constant scattering efficiency over the tens of nanometers shown in Fig. 12.

Discussion and Conclusions

The signals observed in laser-induced grating experiments such as those described here can be associated with bound charges, free carriers, and photorefractive effects. The bound charge contribution will be very small compared to the other contributions.

Before discussing particular results it is helpful to clarify what is meant by the term "photorefractive signal". In a material which has some nonvanishing tensor components of the electro-optic coefficient, an electric field present in such a direction as to couple into one of these nonvanishing components will produce a change in the refractive index, n, in the vicinity of the field through the linear electro-optic effect. If the index-modulating electric field is a space charge field arising from a charge distribution induced by laser beams incident on the material then it is called the photorefractive effect (PRE). The space charge field giving rise to the PRE can be associated with either a trapped charge distribution or with a spatial distribution of free charge carriers. An example of the latter case is that due to separating distributions of electrons and holes having different mobilities, as in the Dember effect.

Two features which were observed in the PP study are of particular interest: The general kinetics are similar for n- and p-type samples, and the long component of decay at large grating spacings in the n-type sample. The

observation that the results obtained in these experiments are the same for n- and p-type samples is evidence that we are dealing with band-to-band transitions in the production of electrons and holes.

The inflection in the decay near 1.75 ns at 15° indicates the presence of a PRE associated with trapped charge. To explain these long-lived contributions to the decay, we must consider the ultimate fate of the free carriers. Some will undergo linear or bimolecular recombination, terminating their contribution to the free-carrier, laser-induced change in the index of refraction. Others will relax into trap levels within the band gap, setting up a spatially modulated static space charge field. This field creates an additional index grating. This trapped charge grating is responsible for the long-lived index modulation. This modulation of n persists as long as the static space charge exists, which, for metastable impurity states, may be much longer than the free carrier lifetime.

At the larger write beam crossing angles, i.e., smaller grating spacings, the trapped charge photorefractive component of the PP signal is not observable because the free carriers have a smaller probability of finding a trap before the grating is destroyed. This trapped charge will have a spatially uniform distribution which will not give rise to a photorefractive grating. The trapped charge component of the PP signal will be considerably weaker when the grating spacing is smaller than the carrier diffusion length, L_d, than when it is larger than L_d. Although there is no sharp transition from one region to another, the grating spacing at which the trapped charge contribution to the signal may become important can be estimated from

$$\Lambda_c = \frac{\lambda}{2 \sin \theta_c} \simeq L_d = \sqrt{2 D_a \tau_{fc}}. \tag{II.50}$$

In the n-type sample this gives a value for the write angle $2\theta_c$ of about 22°, θ_c being measured outside the sample. Inspection of Fig. 6(b) shows that the long component of decay becomes negligible between 15° and 25°, which is consistent with this analysis.

Rough estimates can be made for some of the magnitudes of the different types of contributions to the observed signal. First consider the free carrier contribution. To confirm the assumption that the value of Δn obtained from the SS study is associated with free carrier effects, consider the number of carriers generated by a 18 ps FWHM Gaussian laser pulse through TPA,

$$N_{TPA} = \int_{-\infty}^{\infty} \frac{\beta I^2}{2\hbar\omega} \, dt. \tag{II.51}$$

Here β is the TPA coefficient I is the laser intensity, and $\hbar\omega$ is the laser photon energy. Using $I = 1.9 \times 10^8$ W cm^{-2}, and Van Stryland's [9] value of $\beta = 26$ cm GW^{-1} from gives $N_{TPA} \approx 3.0 \times 10^{16}$ cm^{-3}. This assumes no significant beam depletion due to free carrier absorption, so therefore N_{TPA} represents an upper bound on the carrier density.

The Drude model can be used to estimate the induced change in the refractive index due a distribution of free carriers. The change is given by

$$|\Delta n| = n_{eh} N_{Drude} \tag{II.52}$$

where Δn is the total change in refractive index, and n_{eh} is the change in refractive index per carrier. The latter is given by

$$n_{eh} = \frac{e^2}{2 n_b m_{eh}^\star \omega^2 \epsilon_0} \tag{II.53}$$

where n_b is the background index of refraction at 1.064 μm, ω is the laser frequency, $m_{eh}^\star = (m_e^\star m_h^\star)/(m_e^\star + m_h^\star)$ is the reduced optical effective mass of an electron-hole pair in CdTe [13] (which depends on the band structure and hence, carrier number density), and ϵ_0 is the free space permittivity. Using a value [14] of $n_b = 2.82$ and the value of N_{TPA} for N_{Drude} in Eqs. (II.52) and (II.53) predicts $\Delta n = 0.7 \times 10^{-4}$, well within an order of magnitude of the value obtained from the SS measurements. Thus this corroborates the assumption that the SS signal observed is due to the presence of a distribution of free carriers.

In both PP and SS experiments, the results exhibit a saturation in the signal intensity at excitation power densities between 2×10^7 and 3×10^8 W cm^{-2}. Several mechanisms may cause the observed saturation, including state- or band-filling [15,16], and free carrier absorption (FCA). The power density at which the latter process will be important is given by [17]

$$I_{FCA} = \sqrt{\frac{2\hbar\omega}{\tau_{fc}\beta\sigma d}} \qquad (II.54)$$

where σ is the FCA cross section. Assuming a value [13] of $\sigma = 1 \times 10^{-18}$ cm^2, Eq. (II.54) gives a value of $I_{FCA} = 2.4 \times 10^8$ W cm^{-2}, which is within the range of observed saturation power densities.

In summary, the nonlinear optical responses of CdTe on a picosecond time scale have been interpreted in terms of the generation and dynamics of electron-hole pairs. Contributions to the observed laser-induced changes in Δn were found from the initial free carrier distribution, the transient photorefractive signal associated with the spatially separated electron and hole distributions, and the photorefractive effect associated with trapped charge. No significant enhancement to the PP DFWM scattering efficiency was observed as the excitation wavelength was scanned toward the material band-edge.

CHAPTER III

PHOTOREFRACTIVE TWO-BEAM COUPLING

Introduction

Laser induced refractive index gratings provide an effective way to study various wave mixing phenomena in nonlinear optical materials. Because of their fast temporal response, high infrared sensitivity, and relatively large linear electrooptic coefficient, semiconductors such as CdTe have potential device applications in the area of fast optical switches and spatial light modulators [18,13,19].

Typically, in order to probe the nonlinear optical properties of a material, two copolarized write beams intersect inside the material to form a spatially sinusoidal interference pattern. In the regions of constructive interference charge is preferentially excited to the conduction and/or valence bands either through mid-gap defect ionization or band-to-band transitions. If the ionized charges do not quickly undergo recombination or trapping, they will diffuse away from the spatially-fixed, ionized defects and establish an electric field between themselves and the charged centers from which they were ionized. This space charge field E_{sc}, acting through the linear electrooptic effect, modulates the refractive index of the material; this light-induced refractive index modulation is the photorefractive effect.

The photorefractive effect in semiconductors using CW excitation has been observed in studies on CdTe:V [6], GaAs:EL2 [20], and InP:Fe [21]. Picosecond photorefractive effects have also been observed in these same materials [22]. Closely related CW work at 1.06 μm involving the electrooptic effect and photoconductivity has also been performed in the optical switching study by Steier *et al.* on CdTe:In [19]. Work on probe beam transmission in the presence of a strong

pump beam has also been done by Rückmann *et al.* in nonintentionally-doped CdTe and CdTe:Ge [23]. In the CdTe study undertaken by Valley *et al.* [22], mid-gap defect states introduced by the vanadium dopant provided the centers of charge photoionization necessary to produce the internal space charge field.

An electron-hole plasma can be produced at sufficiently high incident intensities in CdTe and other semiconductors by two-photon, band-to-band absorption, despite an absence of mid-gap defect states. Through the Dember effect [24], this plasma can give rise to an electric space charge field, and lead, therefore, to a picosecond photorefractive effect. The linear absorption coefficient at 1.064 μm of the sample of CdTe investigated in the work we present here is no greater than 0.1 cm^{-1}. Because the linear absorption coefficient in our material is so small, single-photon absorption contributes little to free-carrier populations. Through virtual-intermediate-state, two-photon absorption (TPA), however, significant free carrier populations can be produced, and, when spatially modulated, result in free carrier gratings.

In the absence of an appreciable mid-gap defect density, the charge distribution in this sample, therefore, consists of an electron-hole plasma. The initial electron-hole charge distribution, in phase with the irradiance distribution, will spatially modulate the refractive index as in the Drude model. However, for properly oriented crystals, the Dember field can couple into the linear electrooptic coefficient of the material to induce an additional refractive index grating through the photorefractive effect, which is phase shifted with respect to the free carrier grating and light intensity pattern. This phase shifted index grating can cause transfer of energy out of one laser beam and into the other at low to moderate fluences, with the direction of transfer dependent on the crystal orientation; at higher fluences the unshifted free carrier refractive index grating can cause orientation-independent transient energy transfer [5].

This paper describes what we believe to be the first observation of picosecond two-beam coupling (BC) in a sample of CdTe lacking appreciable linear absorption. The basic equations used to model the two-beam coupling interaction

presented here are a system of rate equations which govern the charge generation and migration and a wave equation which describes the gain (or loss) of the optical electric fields as they propagate through the material. Although the details of the solution are covered elsewhere [25], we restate here the key results for the sake of completeness.

A subsidiary demonstration of polarization rotation through scalar gratings (SPR) was also performed in single crystalline CdTe, showing that the material can be used as a polarization switch.

Theoretical Background

The picosecond beam coupling theory requires a set of rate equations for the charge generation and migration and an equation describing the change of the optical fields as they traverse the sample. The rate equations are given by

$$\frac{\partial p}{\partial t} = -(1/e)\nabla \cdot \vec{j}_p + \beta I^2/(2h\nu) \qquad \text{(III.1)}$$

$$\frac{\partial n}{\partial t} = (1/e)\nabla \cdot \vec{j}_n + \beta I^2/(2h\nu) \qquad \text{(III.2)}$$

$$\vec{j}_p = e\mu_p p\vec{E}_{sc} - \mu_p k_B T\nabla p \qquad \text{(III.3)}$$

$$\vec{j}_n = e\mu_n n\vec{E}_{sc} + \mu_n k_B T\nabla n \qquad \text{(III.4)}$$

$$\nabla \cdot \vec{E}_{sc} = (e/\epsilon)(p - n), \qquad \text{(III.5)}$$

where n and p are the electron and hole number densities, respectively, j_n and j_p are the electron and hole current densities, respectively, I is the irradiance, T is the absolute temperature, k_B is Boltzmann's constant, e is the electronic charge, ν is the optical field frequency, and ϵ is the dielectric constant. Table III contains the definitions of the remaining symbols, their numerical values and the references from which these values were taken.

In earlier work in this material [26] we found a free-carrier lifetime of approximately 12 ns. Therefore on picosecond time scales carrier recombination

TABLE I

ROOM TEMPERATURE MATERIAL PROPERTIES OF UNDOPED CDTE AT 1.064 μm *†

Parameter	Value	Reference
Refractive index, n_b	2.82	[14]
Dielectric constant, ϵ/ϵ_0	10.4	[13]
Electrooptic coefficient, r_{41} (pm/V)	5.5	[38]
Absorption coefficient, α (cm^{-1})	0.1	$\star$
Electron effective mass, m_e	0.1	[13]
Heavy-hole effective mass, m_e	0.4	[13]
Band gap, E_g (eV)	1.49	[13]
Electron mobility, μ_e (cm^2 V^{-1} s^{-1})	1050	$\star$
Hole mobility, μ_h (cm^2 V^{-1} s^{-1})	90	$\star$
Two-photon absorption coefficient, β (cm/GW)	26.0	[9]
Free-electron absorption cross section, s_{fc} (cm^2)	1×10^{-18}	[13]
Sample length, l (cm)	0.1	
Positive defect number density, N^+ (cm^{-3})	NA	
Neutral defect number density, N (cm^{-3})	NA	
Electron-photoionization cross section, s_e (cm^2)	NA	
Hole-photoionization cross section, s_h (cm^2)	NA	

* The quantity was obtained from measurements made in this paper.

† NA, value unknown.

and trapping can be neglected, hence the absence of such terms in the rate equations. The rate equations Eqs. (III.1)-(III.5) must be supplemented with a wave equation for the optical field. If the amplitude E of the optical frequency electric field is slowly varying compared to a wavelength (Slowly Varying Envelope approximation) and if the beams can be approximated by plane waves propagating at a small angle to the z direction, then the wave equation can be written as

$$\cos\theta\frac{\partial E}{\partial z} = i\delta_{PR}E_{sc}E + i\delta_D En - n_b\epsilon_0 c\beta \mid E \mid^2 E \qquad (III.6)$$
$$-s_{fc}nE/2 - \alpha_{np}E/2,$$

where θ is the angle between the direction of propagation and the z axis inside the crystal. The coordinate system is defined in Fig. 1. We have assumed that any refractive index changes can be separated into two parts, one due to the photorefractive effect, the other due to modulations due to free carrier (Drude) effects. These two contributions appear as δ_{PR} and δ_D, respectively, in Eq. (III.6) for the optical field. The conventional loss terms are represented by the *per carrier* s_{fc} free carrier absorption cross section and by what we call a *non-photorefractive* absorption coefficient α_{np}, defined as all linear absorption not creating an electron-hole pair or electron-empty trap complex.

The photorefractive coupling coefficient δ_{PR} is given by

$$\delta_{PR} = \pi r_{41}n_b^3/\lambda, \qquad (III.7)$$

where r_{41} is the electrooptic coefficient for this geometry, n_b is the background refractive index, and λ is the vacuum wavelength. The Drude-Lorentz or free carrier plasma coupling coefficient δ_D given by Jain and Klein [15] is

$$\delta_D = -\frac{\omega}{2cn_bN}\frac{\omega_N^2}{[\omega^2(1 - \omega^2/\omega_g^2)]}, \qquad (III.8)$$

where the plasma frequency for a number density N is given by $\omega_N^2 = e^2N/(\epsilon_0 m_e^*)$, ω is the optical frequency, ω_g is the band gap energy divided by $\hbar$ (Planck's constant divided by 2π), and m_e^* is the electron effective mass.

The term of central importance in the rate and optical field equations is that which contains the photorefractive coupling coefficient δ_{PR} in Eq. (III.6). The divergence operator in Poisson's equation in Eq. (III.5) induces a $\pi/2$ spatial phase shift of E_{sc} with respect to the irradiance pattern. Treating this phase shift as a complex number, the first term in the optical field equation becomes, after multiplication by the existing factor of $\sqrt{-1}$, strictly real, with the result that the optical field E suffers either a gain or loss, depending on the sign of r_{41} and therefore of δ_{PR}.

The experimental quantity of interest is the relative change in probe transmission $\Delta T/T_0 = (T - T_0)/T_0$, where T is the probe transmission in the presence of the pump, and T_0 is the probe transmission in the absence of the pump. The transmission in each case is obtained by numerically solving the coupled rate and optical field equations. For a sample of length l $\Delta T/T_0$ can be expressed as

$$\Delta T/T_0 = [\exp(-\alpha l \pm \Delta \alpha l + \Gamma l) - \exp(-\alpha l)]/\exp(-\alpha l), \qquad \text{(III.9)}$$

where the αl term represents probe absorption independent of the pump, $\Delta \alpha l$ represents probe absorption that depends on the pump, which may due to processes such as saturable absorption, two-photon absorption, transient energy transfer, or absorption gratings, and Γl represents probe photorefractive gain that depends on the pump. Since the photorefractive gain is dependent on crystal orientation, it can be separated from the isotropic contributions of probe gain or loss by measuring $\Delta T/T_0$ in two orientations - one differing from the other by a 180° rotation about the bisector of the write angle. The probe absorbance ΔA_{pr} is defined as the negative natural logarithm of the probe transmission, $-\ln T_{pr}$, therefore the relationship between $\Delta T/T_0$ and the change in probe absorbance ΔA is

$$\Delta A \quad = \quad A_{pr}(\text{with pump}) - A_{pr}(\text{without pump}) \qquad \text{(III.10)}$$

$$= \ln(T_0/T)$$

$$= -\ln[\Delta T/T_0 + 1],$$

which, upon using the expression for $\Delta T/T_0$ in Eq. (III.9), becomes

$$\Delta A = \ln[\exp(-\alpha l)/\exp(-\alpha l + \Gamma l \pm \Delta \alpha l)] \qquad \text{(III.11)}$$

$$= -(\Gamma l \pm \Delta \alpha l).$$

From the expressions for ΔA in Eqs. (III.10) and (III.11), and from the fact that Γ changes sign under a 180° rotation about the write beam angle bisector we obtain for the photorefractive gain and loss, respectively,

$$\Gamma = -(1/2l)\ln\left[\frac{(\Delta T/T_0)^{(\pi)} + 1}{(\Delta)^{(0)} + 1}\right] \qquad \text{(III.12)}$$

$$\Delta \alpha = \pm(1/2l)\ln\left\{[(\Delta T/T_0)^{(\pi)} + 1][(\Delta)^{(0)} + 1]\right\}, \qquad \text{(III.13)}$$

where the superscript (0) denotes measurements made in the orientation for photorefractive probe gain and (π) denotes measurements made in an orientation for probe beam loss.

For the case where the write beams are cross-polarized, no grating is formed in the material, and therefore no photorefractive probe beam gain occurs. The probe beam will, however, undergo losses due to linear and two-photon absorption. For this material, over the range of irradiances considered, TPA dominates linear absorption [26]. Neglecting linear absorption, the equations which govern the signal beam intensity, I_s, in the presence of the pump I_p are, for a large pump to probe ratio

$$\frac{dI_s}{dz} = -\beta I_s I_p \qquad \text{(III.14)}$$

$$\frac{dI_p}{dz} = -\beta I_p^2, \qquad \text{(III.15)}$$

where τ is the Gaussian pulse width, ρ_0 is the $1/e^2$ Gaussian beam radius, $I_s = I_s^{(0)}\exp[-(t^2/\tau^2 + \rho^2/\rho_0^2)]$, $I_p = I_p^{(0)}\exp[-(t^2/\tau^2 + \rho^2/\rho_0^2)]$, and $I^{(0)} = \mathcal{E}/(\pi^{3/2}\rho_0^2\tau)$,

for incident energy $\mathcal{E}$. Solving the equations for dI_s/dz and dI_p/dz in Eqs. (III.14) and (III.15), respectively, for I_s gives

$$I_s(\rho, t) = \frac{I_s^{(0)} \exp[-(t^2/\tau^2 + \rho^2/\rho_0^2)]}{I_p^{(0)} \beta l \exp[-(t^2/\tau^2 + \rho^2/\rho_0^2)] + 1} \qquad \text{(III.16)}$$

Numerical integration over the temporal and spatial variables provides a value of $\Delta T/T_0$ as a function of $\mathcal{E}$ for the case of cross-polarized write beams.

Experimental Procedure

In all of the pulsed laser work described below the source of excitation was an actively and passively mode locked $Y_3Al_5O_{12}$:Nd^{3+} (YAG:Nd) laser operating at its fundamental wavelength of 1.064 μm. The laser full-width-half maximum (FWHM) Gaussian pulse width τ, which was determined by autocorrelation, was 18 ps. The laser repetition rate was 10 Hz. In the study to determine the CW beam coupling response of our material, a 200 mW, linearly polarized, diode-pumped CW YAG:Nd laser was used.

The polished, high resistivity, p-type single crystalline CdTe used in these experiments was grown by Eagle-Picher Research Laboratories, where the Hall electron and hole mobilities were also measured. Crystal growth details are the same as those described earlier [26]. Table 1 lists the 1.064 μm, room temperature material parameters of the sample used. The sample cut and orientation with respect to the laser write beams for the BC experiment are shown in Fig. 13. The pump:probe ratio of the σ polarized write beams was 10:1. The angle between the write beams inside the crystal was 11.2°, corresponding to a grating period 1.9 μm. The combination of 1 mm sample thickness and 11.2° crossing angle indicates the experiment was performed in the Bragg, or thick grating, regime. The zero time delay between the two write beams was determined by replacing, in the sample plane, the CdTe sample with a LiNbO$_3$ crystal and adjusting an optical variable delay line to achieve a maximum in the second harmonic signal intensity generated along the bisector of the write beam angle. The transmitted
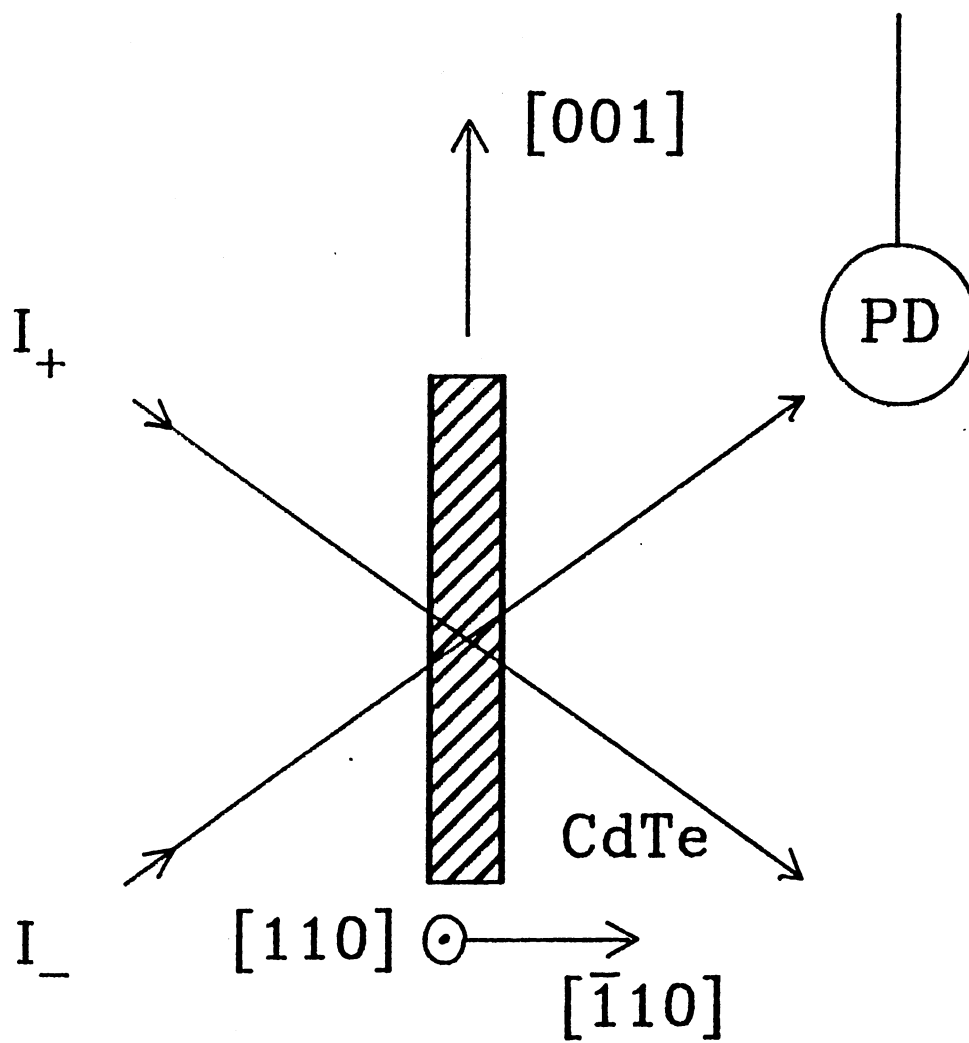
Figure 13. Picosecond Two-beam Coupling Geometry.

laser beams were then monitored as a function of total fluence with an infrared-sensitive photodiode.

In the SPR study, two pump beams are crossed in the sample at an angle of 13.7°, with one of the write beams σ polarized and the other having equal components of σ and π polarizations. In this configuration, the σ components of the two write beams writes a free carrier refractive index grating in the sample, and the π component present in the pump beam scatters off the grating into the direction of transmission of the purely σ beam. The ratio of the σ components of the write beams was 13:1. The π polarized signal was then monitored as a function of increasing irradiance with an infrared-sensitive photodiode. The sample used in this study had the same electrical properties as that used in the beam coupling experiment. However, the polished front and back faces were parallel to the (100) and ($\bar{1}$00) crystallographic planes, respectively. The remaining edges were parallel to the (010) and (001) planes, respectively.

Experimental Results

Picosecond Beam Coupling

Figure 14 shows the result of picosecond beam coupling on high resistivity p-type CdTe using copolarized write beams. The open circles denote the measured values of $\Delta T/T_0$ for the orientation where energy transfer is from pump to probe while the solid circles denote $\Delta T/T_0$ for the orientation where the transfer is from probe to pump. The dashed lines indicate the solution of the rate and optical field equations, Eqs. (III.1)-(III.5) and Eq. (III.6), respectively, based on the literature values of the material parameters, for the change in probe transmission in the two different crystal orientations. The solid lines indicate a better fit to the data, using $r_{41} = 10$ pm/V, $\beta = 50$ cm/GW, and value of δ_D one third the value of that given by the expression for δ_D in Eq. (III.8). Figure 15 shows the gain and loss curves obtained by applying Eqs. (III.12) and (III.13) for gain and loss, respectively, to the experimental data and to the theoretical fit.

Figure 14. $\Delta T/T_0$ as a Function of Total Fluence for the Case of Copolarized Write Beams. Open Circles Denote Data for the Orientation where Energy Transfer is from Pump to Probe and Solid Circles for the Case of Transfer from Probe to Pump. The Dashed Lines Indicate the Theoretical Results Based on the Literature Values of the Parameters for CdTe in Table I. The Solid Lines are the Theoretical Results Based on the Increased Values of the TPA Coefficient and Electrooptic Coefficient as Discussed in the Text.
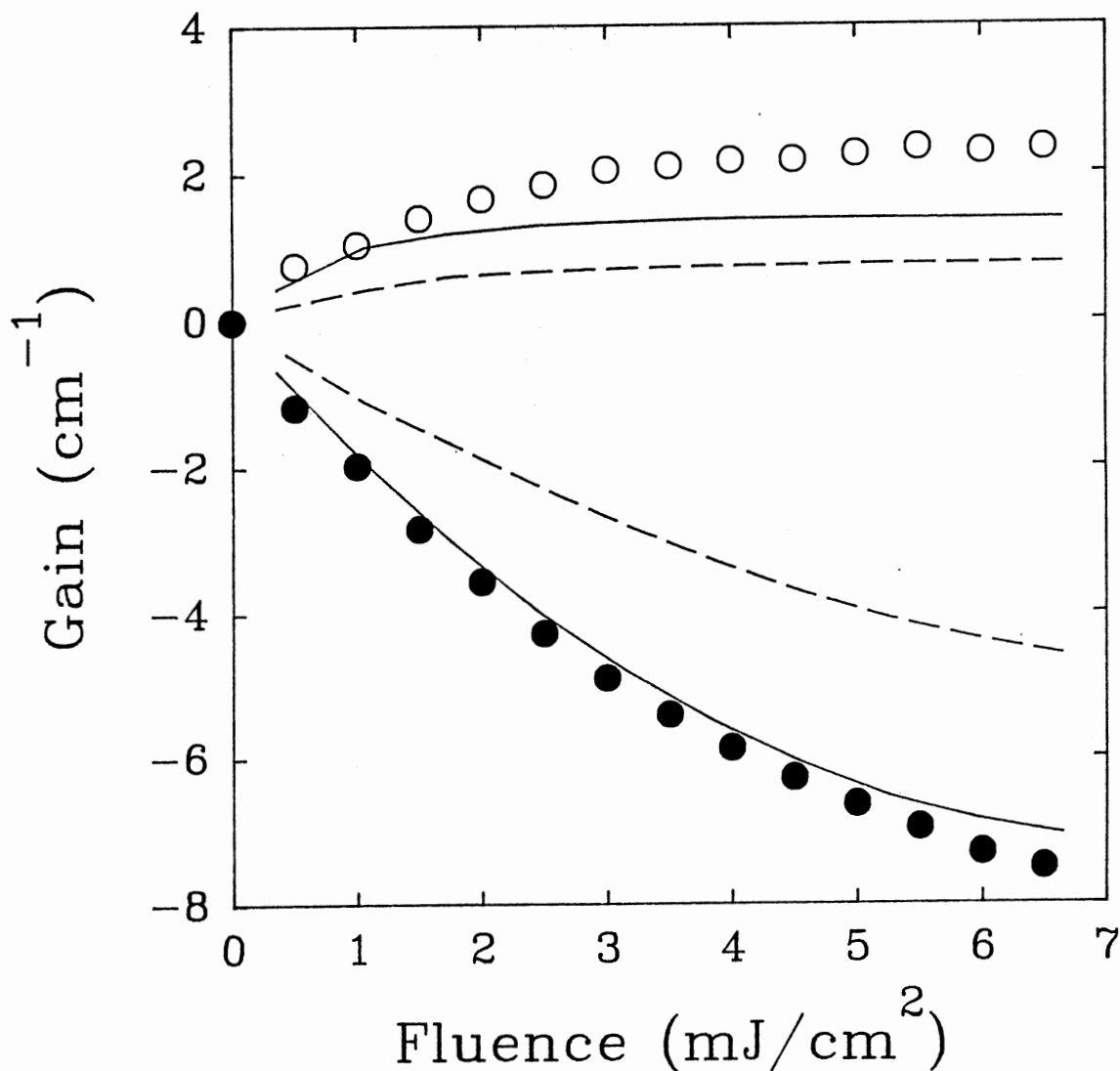
Figure 15. Photorefractive Gain and TPA Loss as a Function of Total Fluence for Copolarized Write Beams. Open Circles Denote Photorefractive Probe Beam Gain and Solid Circles Denote Pump-dependent Probe Loss, Due Primarily to TPA. The Points were Obtained from Smoothing the Data in Fig. 14; Interpolation was used to Obtain Points Lying between Actual Data Points. The Dashed Lines Indicate the Theoretical Results Based on the Literature Values of the Parameters for CdTe in Table I. The Solid Lines are the Theoretical Results Based on the Increased Values of the TPA Coefficient and Electrooptic Coefficient as Discussed in the Text.

Figure 16 shows the results of a measurement of $\Delta T/T_0$ using cross-polarized write beams. The dashed line represents the theoretical result based on Eq. (III.16) using the literature value of β. The solid line is the corresponding result using $\beta = 50$ cm/GW.

For the same experimental geometry, but using a CW YAG:Nd laser instead of a pulsed laser, we find that this same sample displays *no* CW beam coupling signal for incident irradiances in the 10 W/cm^2 range using copolarized write beams and a grating spacing of 1.4 μm.

Polarization Rotation by Scalar Gratings

Many types of optical spatial light modulators are based on changing the state of the polarization of a light beam. One particular method of optical switching or limiting made possible through laser induced gratings is scalar polarization rotation [27]. The technique consists of crossing two write beams I_1 and I_2, where I_1 is σ polarized and I_2 contains equal components of π and σ polarizations, in the sample in the usual manner. The σ components of I_1 and I_2 write a index grating in the nonlinear material and the π component of I_2, incident at the Bragg angle, scatters off the grating in the direction of the transmitted I_1 beam. Figure 17 shows the dependence of the π signal in the direction of I_1 as a function of the total σ polarization irradiance for undoped n- and p-type CdTe. In this configuration, the device can be used as an optical switch if the detector is placed along the I_1 direction, or as an optical limiter if placed along the direction of I_2. Assuming operation in the 500 MW/cm^2 range, an 18 picosecond pulse width, and a square pixel ten microns on a side, we find that energies on the order of a nanojoule are sufficient to operate such a device. In addition, significant enhancements to the rotation effect have been demonstrated by using photorefractive polarization rotation [28].
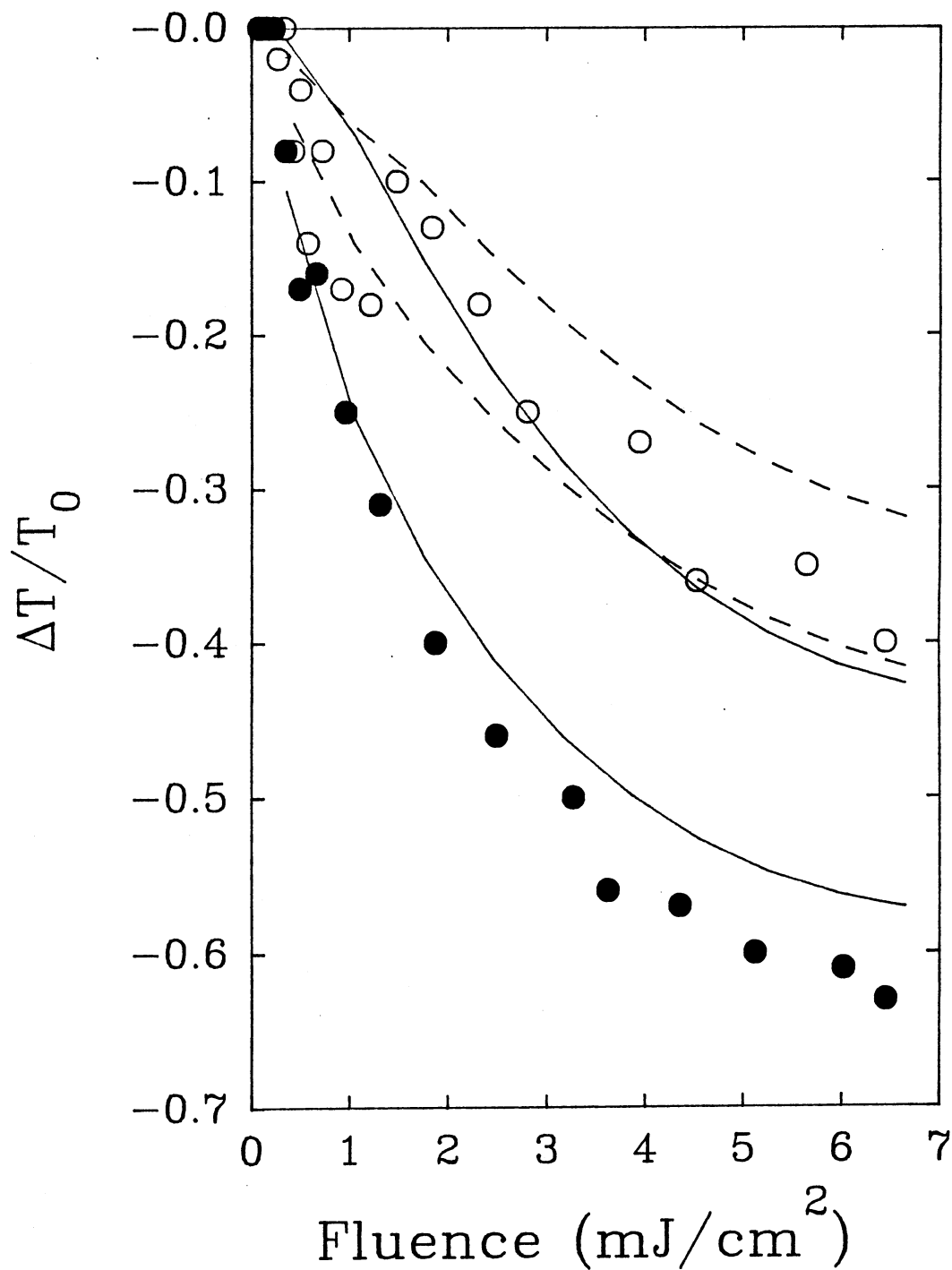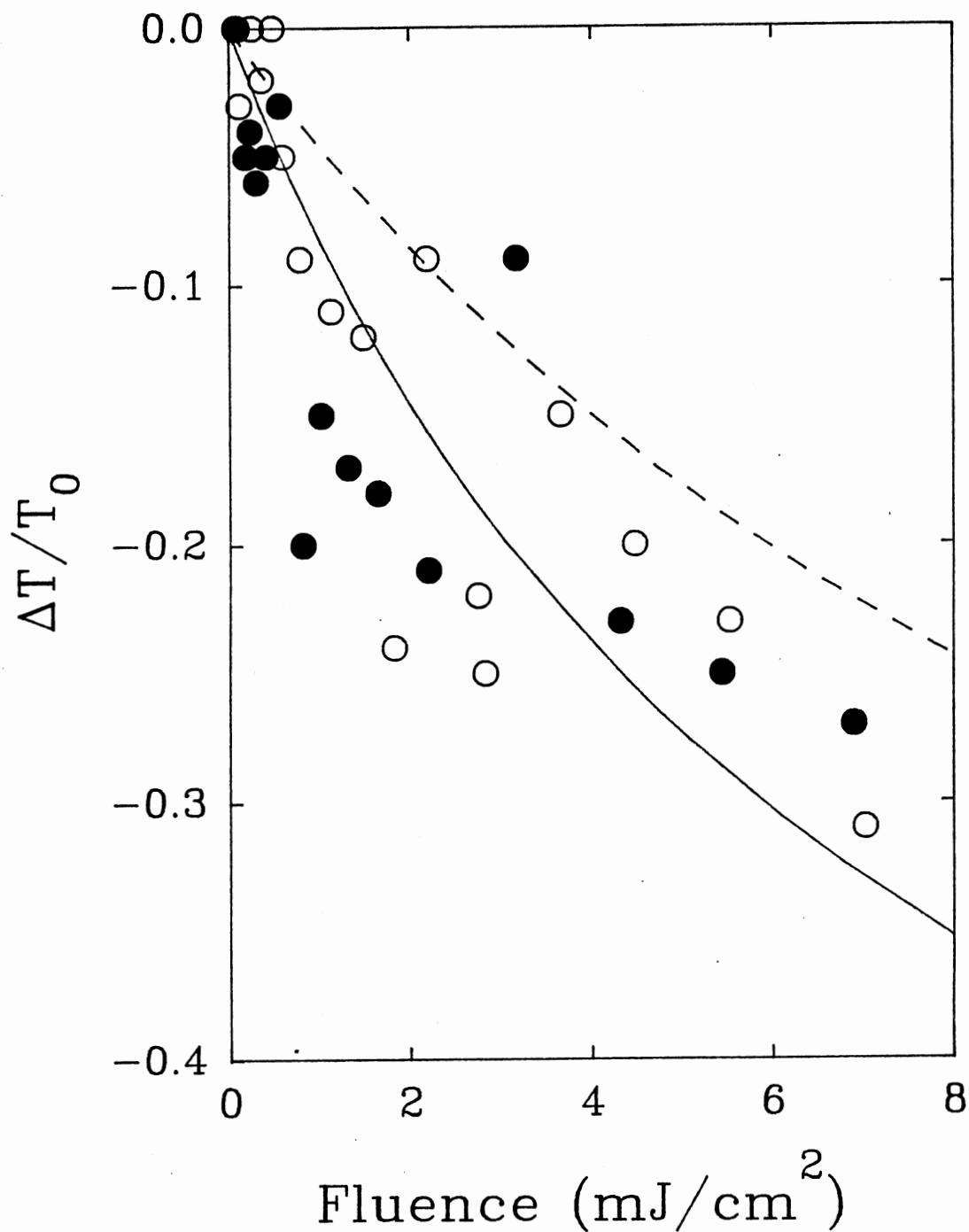
Figure 16. $\Delta T/T_0$ as a Function of Total Fluence for the Case of Cross-polarized Write Beams. The Open Circles Denote Data Acquired in an Orientation that Otherwise Would Have Led to Probe Beam Gain, and the Solid Circles Denote Data Acquired in an Orientation that Otherwise Would Have Led to Pump-dependent Probe Loss. The Solid Line is the Theoretical Result Based on Eq. (III.16).
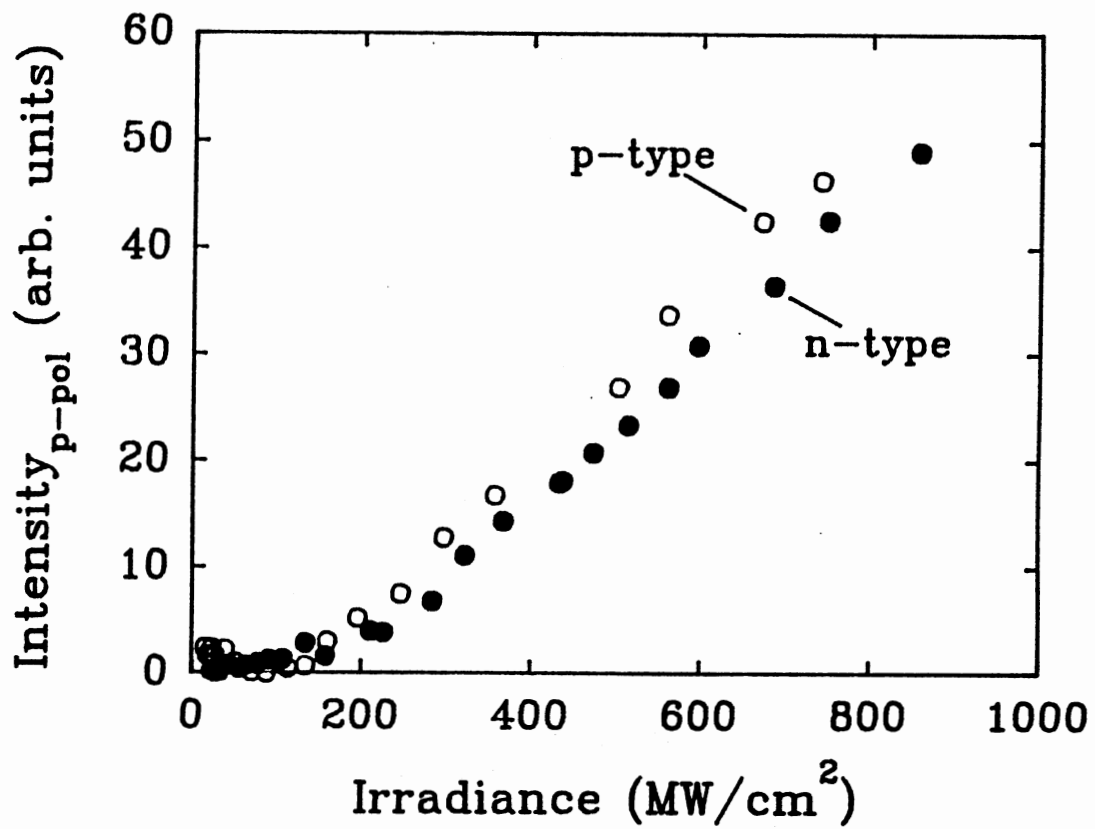
Figure 17. Experimental Results of Scalar Grating Polarization Rotation as a Function of Incident Irradiance in Undoped N- and P-type CdTe.

Discussion and Conclusion

The picosecond BC results in Fig. 14 show several features which are of particular interest. First, since the sample showed no CW beam coupling, we can assume that linear absorption plays at best a minor role in photocarrier production; therefore, the pulsed-laser results constitute the first observation of picosecond photorefractive two-beam coupling in a material which displays neither appreciable intrinsic nor mid-gap defect absorption. As such, the photorefractive gain occurring in the probe beam must originate as a two-photon absorption process, out of which arises a Dember field produced by separating distributions of electrons and holes. Such an effect has been observed in GaAs [20,22,29] but it was accompanied by non-negligible contributions from linear absorption. GaAs has significant linear absorption at 1.064 μm due to the native mid-gap EL2 level located 820 meV below the conduction band, so that both charge migration from ionized EL2 levels and TPA processes can provide the space charge field required for photorefractive beam coupling. In our CdTe, where there is no significant absorption from mid-gap levels, the spatial separation of the charge distributions is due to the significant difference in the mobilities of the electrons and holes.

With the exception of the electron and hole absorption cross sections, s_e and s_h the values of the material parameters in Table 1 are taken from literature sources. Since the linear absorption coefficient is quite small in this material, we have used $s_e = s_h = 0$ in the numerical modelling. For material parameters based on those literature values and for fluences greater than 1 mJ cm^{-2}, we observe values of $\Delta T/T_0$ which are consistently less, or more negative, than those predicted by the theory. This may due to one or more types of increased absorption seen by the probe beam, either enhanced free carrier absorption or TPA. Also, the separation between the two experimental curves is larger than that predicted by the theory for those same literature value parameters, meaning that the photorefractive probe beam gain is larger than that predicted by the theory. A better fit to the data, as shown in Fig. 14, is obtained by adjusting β

and r_{41} to twice their literature values. The TPA coefficient has been reported to be 26 cm/GW [9]. However, several mechanisms, which can vary from sample to sample, may affect this value, such as the anisotropy of β [30] and other competing nonlinear effects, such as bulk second harmonic generation [31–33]. The value of 50 cm/GW is therefore tenable. The required value of $r_{41} = 10$ pm/V is more problematic, but may nonetheless be considered an effective electrooptic coefficient, operative in the excited, highly dynamic, state of the semiconductor during and just after excitation, in contrast with the literature value obtained under equilibrium conditions. Moreover, Martynov *et al.* [34] have shown that the electrooptic coefficient exhibits an impurity content dependence, which may be related to the increased value we require to fit the data. The reduced value of the Drude-Lorentz coupling coefficient to one third of its theoretical value is not unreasonable, since the exact form of the corresponding term in the optical field in Eq. (III.6) is not well understood or agreed upon.

We also note that the power densities considered here, assuming a photoinduced carrier density described by $dN/dt = \beta I^2/(2\hbar\omega)$, induce a carrier density $N \approx 10^{16}$ cm^{-3}, corresponding to a plasma frequency of roughly 10^{13} Hz, well below the frequency of the optical field. We also neglect refractive index changes due to phenomena such as band renormalization, band filling, and state filling because the carrier densities required to produce these effects is typically at least an order of magnitude larger than those produced here [35,36,16].

The results of Fig. 16 correspond to the case where the pump and probe beams are cross polarized. No grating is written in the material and therefore, for this geometry, no photorefractive gain takes place and the two curves are expected to overlap. The smooth solid curve is a plot of the cross-polarized $\Delta T/T_0$ given by Eq. (III.16) using a value of $\beta = 50$ cm/GW. Despite a certain amount of noise in the data, it is clear that there is no gross difference between the two orientations. The theoretical plot using $\beta = 50$ cm/GW better describes the data than the value of β from other samples in the existing literature, and is

therefore consistent with the value of β needed to obtain a good fit to the data in Fig. 15.

Summary and Conclusions

In summary, we have observed what we believe to be the first instance of picosecond photorefractive two-beam coupling in a material which exhibits very little linear absorption, but has a high two-photon absorption coefficient. No CW beam coupling signal was observed in this material at the irradiances investigated. The observed average photorefractive gain $\Gamma = 2.3$ cm^{-1} is believed to arise out of a Dember space charge field produced by the separation of electrons and holes, and shows that this undoped material has potential applications in the area of beam manipulation and other fields of optical processing. Polarization rotation by scalar gratings in undoped CdTe was also demonstrated and may prove to be an additional technique in the area of laser beam manipulation, owing to its nJ/μm^2 turn-on power density.

CHAPTER IV

SECOND HARMONIC GENERATION

Introduction

Because of their potential applications in optical device technology [13,18], the optical properties of semiconductors such as CdTe have been the subject of widespread and intense investigation. Among the various studies undertaken on these materials are those in which the nonlinear interaction of interest depends on laser-induced charge generation. Recent examples of such work include pulse-probe degenerate four-wave mixing (PP DFWM) and Raman-Nath self-scattering in CdTe [26,6,40], and picosecond two-beam coupling in CdTe, CdTe:Ge, CdTe:V, GaAs:EL2, and InP:Fe [41,29,22,23]. Because of their dependence on charge generation in the semiconductor bulk, it is important to accurately account for the physical mechanisms of photocarrier production in the course of modelling these nonlinear interactions.

Aside from the usual carrier generation mechanisms in semiconductors of single- and two-photon band-to-band absorption, and single- and two-photon absorption from defect levels to the conduction or valence band, an alternative method of photocarrier production in materials lacking inversion symmetry is absorption of internally generated frequency-doubled light, if the energy gap E_g is less than $2\hbar\omega$. One of the areas in which this second harmonic generation (SHG) process will be important is in the description of the various contributing mechanisms to the measured value of the two-photon absorption (TPA) coefficient. Despite considerable effort in quantifying the TPA coefficient in CdTe, and other semiconductors, its value remains known only with limited accuracy, due to a lack of knowledge of contributing mechanisms, as well as their relative strength

[9,42,33]. The absorption of any internally generated frequency-doubled radiation may, therefore, represent a nontrivial contribution to the measured TPA coefficient, or other absorption-dependent phenomena. Preliminary results [31] on 1 mm thick single-crystal, undoped CdTe have already shown the ratio of the number of photons created via SHG to the number created through all other TPA processes to be approximately 0.04. We extend that work here by investigating the dependence of the SHG efficiency on sample thickness, the angular dependence of the observed signals to quantify any enhancement to the conversion efficiency due to phase matching, and to determine the origin of the SHG signal, be it bulk or surface.

Theoretical Background

In this section the basic expressions describing the second order nonlinear optical effect of *second harmonic generation* or *frequency doubling* are derived. We also treat the dependence of the resultant frequency-doubled intensity on the Cartesian components of the input fields. Finally, the results are specialized to the case of materials with $\bar{4}3m$ symmetry, such as cadmium telluride.

We begin by writing the wave equation for the electric field inside what is assumed to be a lossless ($\sigma = 0$) material.

$$\nabla^2 E = \mu_0 \epsilon \frac{\partial^2 E}{\partial t^2} + \mu_0 \frac{\partial^2 P_{NL}}{\partial t^2} \tag{IV.1}$$

for nonlinear polarization P_{NL}, and permittivity ϵ. All waves are assumed to travel in the $\hat{z}$ direction. Anticipating a three-wave ($\chi^{(2)}$) process, we write for the total electric field inside the material

$$E_{tot} = E_i^{(\omega_1)}(z,t) + E_j^{(\omega_2)}(z,t) + E_l^{(\omega_3)}(z,t) \tag{IV.2}$$

whose components are defined by

$$E_i^{(\omega_1)}(z,t) = \frac{1}{2}[E_{1i}(z)\exp[i(k_1 z - \omega_1 t)] + c.c.] \tag{IV.3}$$

$$E_j^{(\omega_2)}(z,t) = \frac{1}{2}\left[E_{2j}(z)\exp[i(k_2 z - \omega_2 t)] + c.c.\right] \tag{IV.4}$$

$$E_l^{(\omega_3)}(z,t) = \frac{1}{2}\left[E_{3l}(z)\exp[i(k_3 z - \omega_3 t)] + c.c.\right] \tag{IV.5}$$

where $E_{\alpha\beta}$ is the field amplitude of the βth Cartesian component oscillating at angular frequency ω_α, and c.c. denotes the complex conjugate. Assuming propagation along the z-direction and $\partial/\partial x = \partial/\partial y = 0$, we obtain for the spatial derivative of the ith field component oscillating at ω_α

$$\nabla^2 E \approx \frac{1}{2}\left(2ik_\alpha E'_{\alpha 1} - k_\alpha^2 E_{\alpha i}\right)\exp[i(k_\alpha z - \omega_\alpha t)], \tag{IV.6}$$

where the prime denotes differentiation with respect to z. In deriving this expression we have used the Slowly Varying Envelope approximation (SVE), which is to neglect the second derivatives with respect to z. From Appendix A the ith component of the nonlinear polarization oscillating at $\omega_3 = \omega_1 + \omega_2$ can be written

$$[P_{NL}(-\omega_3; \omega_1, \omega_2)]_i = d_{ijk}E_{1j}E_{2k}\exp\left\{i[(k_1 + k_2)z - (\omega_1 + \omega_2)t]\right\} \tag{IV.7}$$

where the d_{ijk} are the elements of the second order nonlinear susceptibility tensor referred to the crystallographic axes of the nonlinear material. Subtituting the fields and nonlinear polarization into the wave equation of Eq. (IV.1), keeping on both sides only those terms oscillating at ω_3, and assuming that the input fields remain largely undiminished as they propagate through the material leads to the single equation describing the evolution of the frequency-doubled field

$$E'_{3l} = i\omega\sqrt{\mu_0/\epsilon_3}\,d_{lij}E_{1i}E_{2j}\exp(i\Delta k z) \tag{IV.8}$$

where

$$\omega = \omega_1 \tag{IV.9}$$

$$= \omega_3/2, \tag{IV.10}$$

and

$$\Delta k = k_3^{(l)} - k_1^{(i)} - k_2^{(j)} \qquad \text{(IV.11)}$$

Note that Δk vanishes, or efficient *phase matching* occurs, only when the refractive index at the fundamental wavelength is twice that at the doubled wavelength for a given component. Such is the case for proper crystal orientation in certain birefringent materials.

Integrating Eq. (IV.8) from $z = 0$ to crystal thickness l gives

$$E_{3l}(l) = 2\omega\sqrt{\mu_0/\epsilon_3}d_{lij}E_{1i}E_{2j}\frac{\exp(i\Delta kl - 1)}{\Delta kl}. \qquad \text{(IV.12)}$$

where the leading factor of 2 results from the sum over i, j.

The quantity in which we are interested is the intensity $[I(l)]_l$ of the lth polarization component in the frequency-doubled beam at $z = l$, given by

$$
\begin{aligned}
[I(l)]_l &= \frac{1}{2}\sqrt{\epsilon_3/\mu_0}E_{3l}E_{3l}^{\star} & \text{(IV.13)} \\
&= \frac{1}{2}\sqrt{\mu_0/\epsilon_3}\omega^2 d_{lij}^2 E_{1i}^2 E_{2j}^2 \frac{\sin^2(\Delta kl/2)}{(\Delta kl/2)^2} & \text{(IV.14)} \\
&= \frac{1}{2}\sqrt{\mu_0/\epsilon_3}\omega^2 d_{lij}^2 E_{1i}^2 E_{1j}^2 \frac{\sin^2(\Delta kl/2)}{(\Delta kl/2)^2}. & \text{(IV.15)}
\end{aligned}
$$

where in the last of these equations we have assumed that the two input fields originate in the same input beam.

To describe the dependence of the intensity of frequency-doubled light as the components of the input fields $E_{1\beta}$ vary, we can proceed in one of two ways. We may fix the nonlinear material in space and allow the input field polarization vectors to rotate, or we may fix the field polarization vectors, referring them to a convenient laboratory frame, and rotate the crystal in the opposite direction. Although the two approaches lead to equivalent results, we shall follow the latter, where the crystal is presumed to rotate. The effective elements $(d_{ijk})_{eff}$ then change as the crystal rotates, and are given by [43]

$$d_{eff} = \sum_{ijk} \hat{b}_i d_{ijk} \hat{a}_j \hat{a}_k \qquad \text{(IV.16)}$$

where $\hat{a}$ and $\hat{b}$ are the unit polarization vectors of the input field and frequency-doubled field, respectively, referred to the *crystallographic axes ijk*. Inspection of Eq. (IV.12) for the frequency-doubled field E_3 shows that $\hat{b}$ may be either *parallel or perpendicular* to $\hat{a}$.

For cadmium telluride (point group $\bar{4}3m$), all but the following elements d_{ijk} are nonzero [44]

$$d_{123} = d_{132} \qquad \text{(IV.17)}$$

$$d_{213} = d_{231} \qquad \text{(IV.18)}$$

$$d_{312} = d_{321}. \qquad \text{(IV.19)}$$

Moreover, each of these elements is equal to each other. This single value is hereafter referred to as simply d. Performing the prescribed sum in Eq. (IV.16) leads to

$$d_{eff} = 2d(a_2 a_3 b_1 + a_1 a_3 b_2 + a_1 a_2 b_3) \qquad \text{(IV.20)}$$

We consider two cases: one for which the input field propagation vector $\vec{k}$ is anti-parallel to the [110] crystallographic direction, and the other where $\vec{k}$ is anti-parallel to the [111] crystallographic direction. (Hereafter, integers in square brackets denote crystallographic directions). In either case, two frames of reference sharing a common origin are required, a *laboratory* frame and *crystal* frame.

In the first case, for propagation anti-parallel to [110], the laboratory frame, or primed frame, is obtained by rotating the crystal frame about the $\hat{z}$-axis through an angle $\Theta = \pi/4$. The vectors $\hat{a}'$ and $\hat{b}'$ referred to the laboratory frame are

$$\hat{a}' = \begin{pmatrix} 0 \\ \sin\phi \\ \cos\phi \end{pmatrix} \qquad (IV.21)$$

$$\hat{b}' = \begin{pmatrix} 0 \\ -\cos\phi \\ \sin\phi \end{pmatrix} \qquad (IV.22)$$

where ϕ is the angle between $\hat{a}'$ and [001]. $\hat{a}$ and $\hat{b}$ are then obtained from their primed counterparts by applying the rotation operator $\mathcal{R}_\Theta$

$$\hat{a} = \mathcal{R}_\Theta \hat{a}' \qquad (IV.23)$$

$$\hat{b} = \mathcal{R}_\Theta \hat{b}' \qquad (IV.24)$$

where

$$\mathcal{R}_\Theta = \begin{pmatrix} \cos\Theta & -\sin\Theta & 0 \\ \sin\Theta & \cos\Theta & 0 \\ 0 & 0 & 1 \end{pmatrix}, \qquad (IV.25)$$

for *positive* angle Θ. This yields

$$\hat{a} = \begin{pmatrix} -\sin\Theta\sin\phi \\ \cos\Theta\sin\phi \\ \cos\phi \end{pmatrix} \qquad (IV.26)$$

$$\hat{b} = \begin{pmatrix} \sin\Theta\cos\phi \\ -\cos\Theta\cos\phi \\ \sin\phi \end{pmatrix}. \qquad (IV.27)$$

Using these crystal-frame components in the expression for d_{eff} in Eq. (IV.20) gives the angular dependence of the parallel ($\hat{b} \parallel \hat{a}$) and perpendicular ($\hat{b} \perp \hat{a}$)

polarization components of the frequency-doubled light for the case of incidence normal to a (110) crystallographic face

$$I(2\omega)_{\parallel} \quad \propto \quad (d_{eff})_{\parallel}^2 \tag{IV.28}$$

$$\propto \quad \sin^4\phi \cos^2\phi \tag{IV.29}$$

$$I(2\omega)_{\perp} \quad \propto \quad (d_{eff})_{\perp}^2 \tag{IV.30}$$

$$\propto \quad \sin^2\phi(1 - 3\cos^2\phi)^2 \tag{IV.31}$$

Again, this treatment assumes that the input field polarization vectors are *fixed* with respect to the laboratory frame.

In the second case, for an input field propagation vector $\vec{k}$ anti-parallel to [111], the laboratory frame is obtained from the crystal frame by two consecutive rotations. The first is a positive rotation about the crystal $\hat{z}$-axis by $\pi/4$, giving rise to the primed coordinate system. The second rotation occurs about the $\hat{y}'$-axis (which coincides with [$\bar{1}$10]) through an angle $\Psi = \arccos\sqrt{1/3} \approx 54.7°$, taking $\hat{z}'$ into the [111] direction, giving rise to the doubly-primed coordinate system. The components of $\hat{a}''$ and $\hat{b}''$, where the double primes denote the laboratory frame, are

$$\hat{a}'' = \begin{pmatrix} \sin\psi \\ \cos\psi \\ 0 \end{pmatrix} \tag{IV.32}$$

$$\hat{b}'' = \begin{pmatrix} -\cos\psi \\ \sin\psi \\ 0 \end{pmatrix} \tag{IV.33}$$

where ψ is the angle between $\hat{a}''$ and $\hat{y}''$, or, equivalently, between $\hat{a}''$ and [$\bar{1}$10]. The crystal coordinates are obtained from those in the laboratory frame by applying the rotation operators $\mathcal{R}_\Theta$ and $\mathcal{R}_\Psi$

$$\hat{a} = \mathcal{R}_\Theta \mathcal{R}_\Psi \hat{a}'' \tag{IV.34}$$

$$\hat{b} = \mathcal{R}_\Theta \mathcal{R}_\Psi \hat{b}'' \tag{IV.35}$$

where $\mathcal{R}_\Theta$ is defined in Eq. (IV.25) and

$$\mathcal{R}_\Psi = \begin{pmatrix} \cos\Psi & 0 & \sin\Psi \\ 0 & 1 & 0 \\ -\sin\Psi & 0 & \cos\Psi \end{pmatrix}, \tag{IV.36}$$

again noting that Ψ is a *positive* angle. The components of the vectors $\hat{a}$ and $\hat{b}$ are then

$$\hat{a} = \begin{pmatrix} \cos\Theta\cos\Psi\sin\psi - \sin\Theta\cos\psi \\ \sin\Theta\cos\Psi\sin\psi + \cos\Theta\cos\psi \\ -\sin\Psi\sin\psi \end{pmatrix} \tag{IV.37}$$

$$\hat{b} = \begin{pmatrix} -\cos\Theta\cos\Psi\cos\psi - \sin\Theta\sin\psi \\ -\sin\Theta\cos\Psi\cos\psi + \cos\Theta\sin\psi \\ \sin\Psi\cos\psi \end{pmatrix} \tag{IV.38}$$

This gives for the case of incidence normal to a (111) crystallographic face

$$I(2\omega)_\parallel \propto (d_{eff})^2_\parallel \tag{IV.39}$$

$$I(2\omega)_\parallel \propto \sin^2 3\psi \tag{IV.40}$$

$$I(2\omega)_\perp \propto (d_{eff})^2_\parallel \tag{IV.41}$$

$$I(2\omega)_\perp \propto \cos^2 3\psi. \tag{IV.42}$$

Experimental Procedure

In all of the work described below the source of excitation was an actively and passively mode locked $Y_3Al_5O_{12}$:Nd^{3+} (YAG:Nd) laser operating at its fundamental wavelength of 1.064 μm. The laser full-width-half maximum (FWHM) Gaussian pulse width τ, which was determined by autocorrelation, was 18 ps. The laser repetition rate was 10 Hz.

The polished, high resistivity, p-type single crystalline CdTe used in these experiments was grown by Eagle-Picher Research Laboratories. Crystal growth details are the same as those described earlier [26]. The experimental geometry, shown in Fig. 18, is the same as that used in our preliminary work on SHG in 1 mm thick samples of CdTe [31]. Three different materials were investigated here to determine the film thickness dependence of the SHG efficiency. Two samples were Bridgman-grown material, one with dimensions 1 cm $\times$ 1 cm $\times$ 127 μm, the other 1 cm $\times$ 1 cm $\times$ 254 μm, each grown on a sapphire substrate. The orientation of these samples is the same: a polished face parallel to the (110) plane, and remaining edges parallel to the ($\bar{1}$10) and (001) planes, respectively. Material oriented in this way is hereafter referred to as "(110)" material. The third sample was a 6 μm thick film of MOCVD CdTe deposited on an optical quality ZnSe substrate. Although the exact orientation of this sample was unknown, knowledge of the growth characteristics suggests that the polished face was parallel to the (111) plane. The sample had no other well defined directions. Material oriented in this way is hereafter referred to as "(111)" material. The Eagle-Picher Lot Numbers for the 127, 254, and 6 μm thick material are FC89277-01-18, FC89277-01-16, FC89320, respectively.

Experimental Results

The contributions to TPA are known to be dependent on various material parameters of the samples used in the experiment, such as the anisotropy of TPA [30] and impurity levels in the forbidden gap. SHG in semiconductors
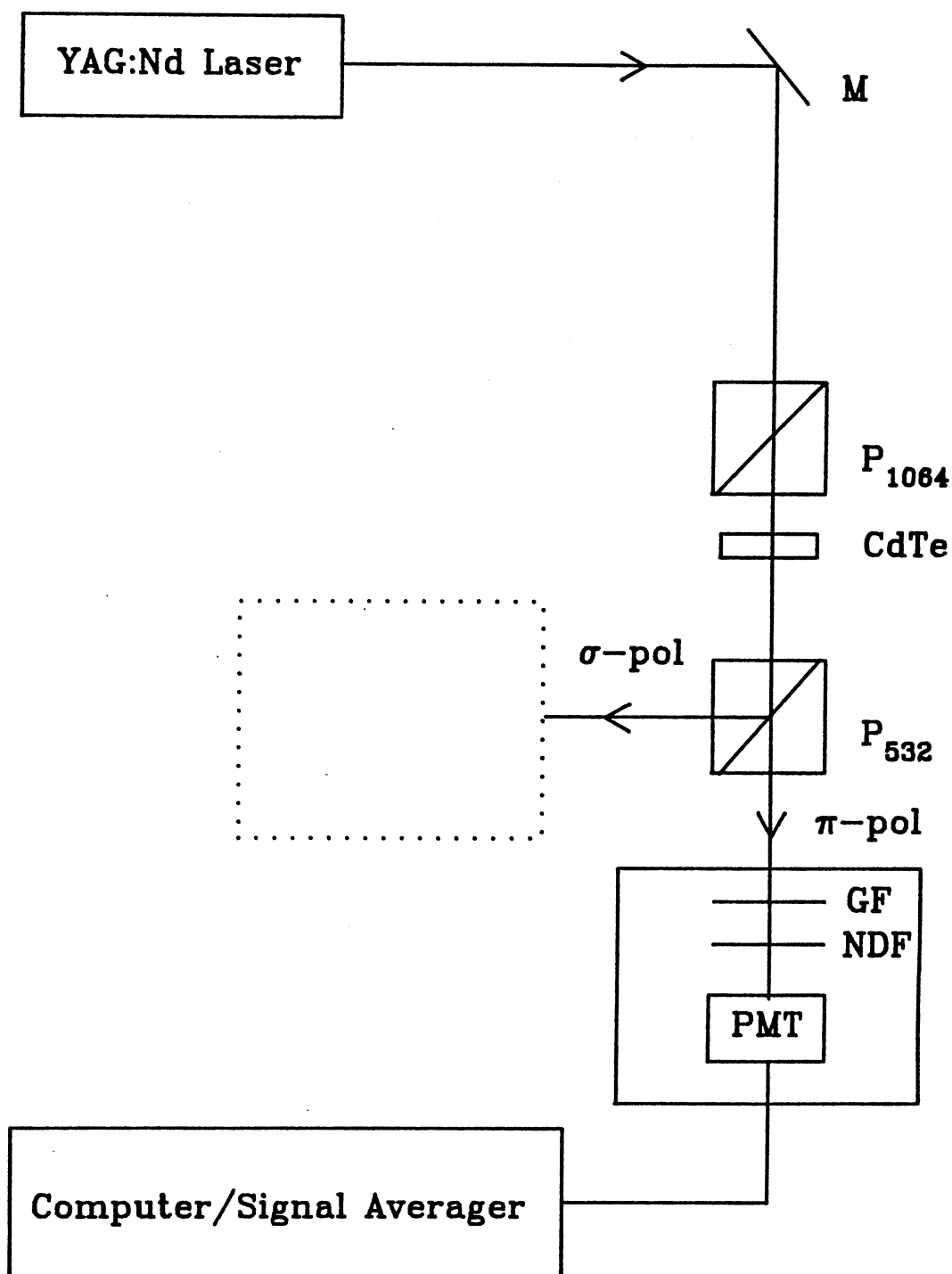
Figure 18. Experimental Geometry Used in the SHG Investigation. M, Mirror; $P_{1.064}$, Polarizing Beam Splitter Coated for 1.064 μm; CdTe, CdTe Sample; P_{532}, Polarizing Beam Splitter Coated for 532 nm; GF, Green Filter (Corning Filter #1-56); NDF, Neutral Density Filter; PMT, Photomultiplier Tube.

has been observed in reflection geometries at air-surface interfaces in several III-V compounds [45,46], in transmission geometries at 10.6 μm [47,48], and in internally generated SHG in semiconductor lasers [49–51]. There have also been observations of transmitted SHG [52,53], similar to that reported here, where the frequency-doubled radiation lies above the intrinsic absorption edge of the material. However, to our knowledge SHG followed by single photon absorption has not been considered as a mechanism leading to a laser-induced free carrier population in the context of measurements of the TPA coefficient or in the analysis of photorefractive effects in this material. In either of linear or two-photon band-to-band absorption, or SHG followed by single photon absorption, a charge distribution is produced which can affect the nonlinear interaction of interest. The mechanism of charge generation is, however, quite different, and should be considered in the modelling of these interactions.

Preliminary results [31] were presented on a 1 mm thick sample of (110) material. The dependence of the second harmonic intensity was determined both as a function of the angle ϕ between the optical electric field unit vector $\hat{e}$ and the [001] crystallographic direction at constant pump intensity and the absolute efficiency of SHG on pump intensity for constant ϕ. The variation of the σ and π polarization components of the second harmonic intensity with ϕ was found to agree well with the theoretical model of bulk SHG, where the σ component is defined as the polarization component of second harmonic light generated perpendicular to $\hat{e}$, and the π component is that generated parallel to $\hat{e}$. In that study it was also found that in the 100 MW cm^{-2} intensity range, the ratio of the total number of photocarriers created via absorption of frequency-doubled light to that created via all other TPA processes to be about 0.04. Although this ratio is small, its presence should be addressed in charge generation models. It is also of some interest to note that, using proper eye protection, the transmitted SHG signal was easily visible to the eye in moderate to low room lighting.

It was thought that for diminishing sample thickness, an increased efficiency might be obtained owing to the absence of a mismatch between the SHG

coherence length and the sample thickness. We measured the absolute signal intensity in three additional samples, two Bridgman-grown samples on sapphire substrates, one of 127 μm and the other of 254 μm thickness, and the third an MOCVD film of thickness 6 μm, grown on a ZnSe substrate. We recorded the same ($\pm 5\%$) absolute π component signal intensity emerging from the sample in each of the two Bridgman samples, and a signal intensity half that in the 6 μm, thin film material. For purposes of comparison, the absolute SHG signal intensity of the 1 mm thick sample used in our preliminary study [31] was remeasured and found to be the same to within experimental error as that recorded in the 127 and 254 μm Bridgman materials, under the same pump conditions. The measurements were made on the π signal component at the angle for which the SHG signal was maximum.

The angular dependences of the π and σ component SHG signal intensities for incidence on a (110) plane are given by

$$I_\pi(2\omega) \propto P_\pi^2(2\omega) = 9E_p^2(\omega)\chi^2 \sin^4\phi \cos^2\phi \qquad \text{(IV.43)}$$

$$I_\sigma(2\omega) \propto P_\sigma^2(2\omega) = E_p^2(\omega)\chi^2 \sin^2\phi(1 - 3\cos^2\phi)^2, \qquad \text{(IV.44)}$$

respectively, where $E_p(\omega)$ is the amplitude of the optical electric field oscillating at angular frequency ω, $P(2\omega)$ is the induced nonlinear polarization oscillating at 2ω, and $\chi = \chi_{123} = \chi_{213} = \chi_{312}$ is the bulk second harmonic generation contribution to $\chi^{(2)}$ in materials with $\bar{4}3m$ symmetry. The experimentally observed angular dependence of the π and σ polarization components in the 127 μm and 254 μm (110) samples is shown in Fig. 19. The theoretical curves corresponding to Eqs. (IV.43) and (IV.44) are shown as solid lines. We obtain agreement with the theory over the full range of angles, with the exception of the π component signal near $\phi = 90°$, where the signal falls short of the predicted intensity by a factor of about 2/3. This same diminished π component signal intensity at $\phi = 90°$ is observed in all three (110) materials.
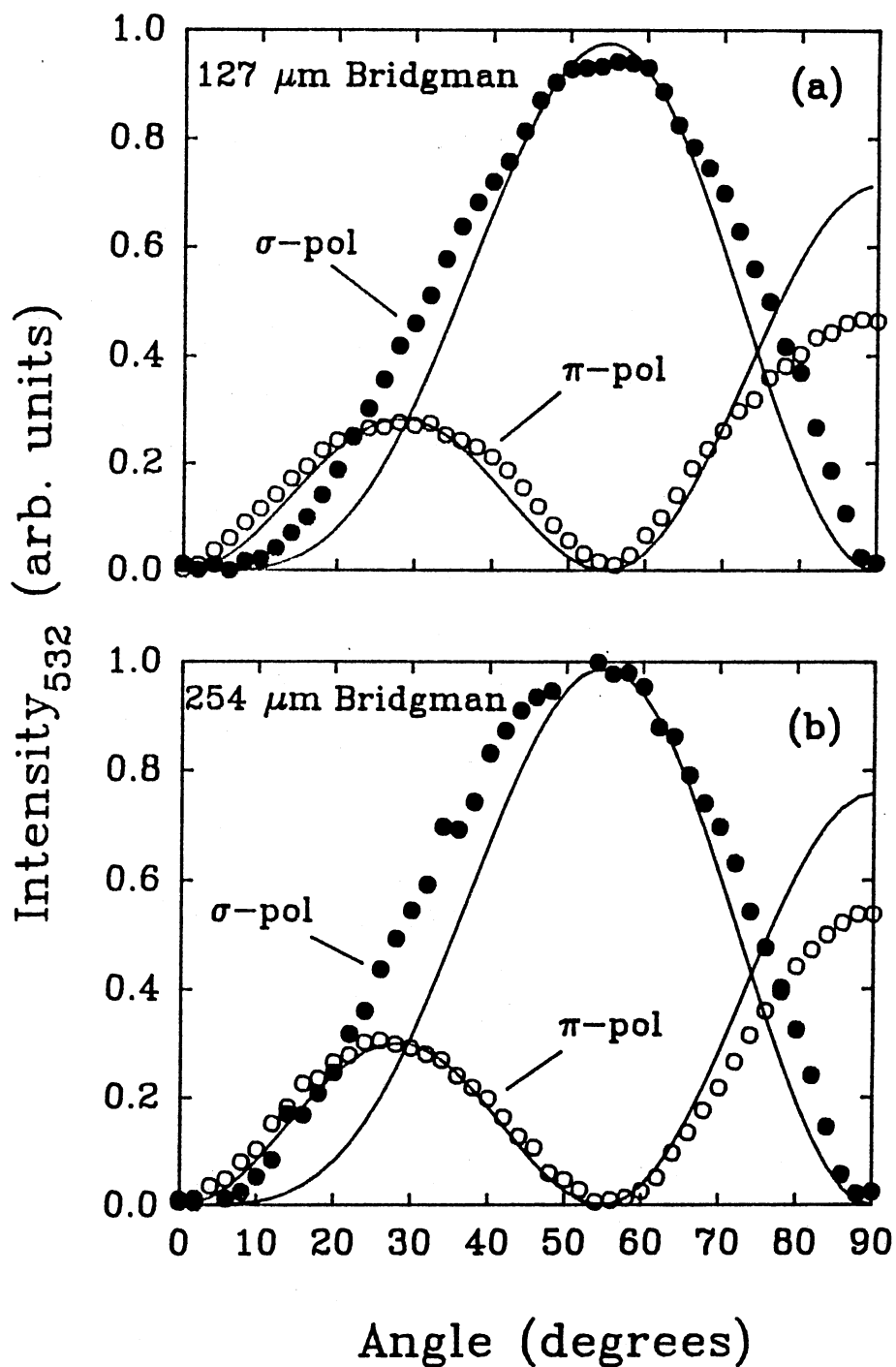
Figure 19. SHG Signal Intensity as a Function of Crystal Orientation in (110) Bridgman Material. (a) 127 μm-thick material, (b) 254 μm-thick material. Open Circles Denote the π Polarization Component, and Solid Circles Denote the σ Component. The Angle, ϕ, is Defined in the Text. The Solid Lines are the Corresponding Bulk Theoretical Curves.

The angular dependences of the π and σ component SHG signal intensities for incidence normal to a (111) plane are given by

$$I_\pi(2\omega) \propto P_\pi^2(2\omega) = (2/3)E_p^2(\omega)\chi^2 \sin^2 3\psi \qquad \text{(IV.45)}$$

$$I_\sigma(2\omega) \propto P_\sigma^2(2\omega) = (2/3)E_p^2(\omega)\chi^2 \cos^2 3\psi, \qquad \text{(IV.46)}$$

respectively, where ψ is the angle lying in the (111) crystallographic plane between $\hat{e}$ and the $[\bar{1}10]$ crystallographic direction. Figure 20(a) shows for the thin film MOCVD material the dependence of the σ component second harmonic intensity on ψ; Fig. 20(b) shows the π component signal intensity dependence on ψ. The theoretical curves corresponding to Eqs. (IV.45) and (IV.46) are shown as solid lines.

Assuming a uniform value of the frequency conversion efficiency along the fundamental laser beam path in the sample (equivalent to neglecting Maker oscillations), the total number of frequency-doubled photons N_t generated in the crystal may be estimated from

$$N_t = \alpha l N_{pmt} \qquad \text{(IV.47)}$$

where α is the absorption coefficient at 532 nm, N_{pmt} is the number of 532 nm photons reaching the photodetector, and l is the sample thickness. Figure 21 shows the total second harmonic conversion efficiency η vs. input laser intensity, where η is defined as the ratio of N_t to the number of 1064 nm photons introduced into the sample. The intensity at which η saturates, $I \approx 200$ MW/cm^2, is consistent with the saturation intensities observed in our other picosecond wave-mixing work [26], and is again attributed to free-carrier absorption. The measurement of η was performed on (110) material for second harmonic light polarized parallel to the excitation beam, at an angle between the [001] direction and the polarization vector of the excitation beam that maximized the frequency-doubled signal.

Figure 22 shows the frequency-doubled signal at 461 nm obtained by
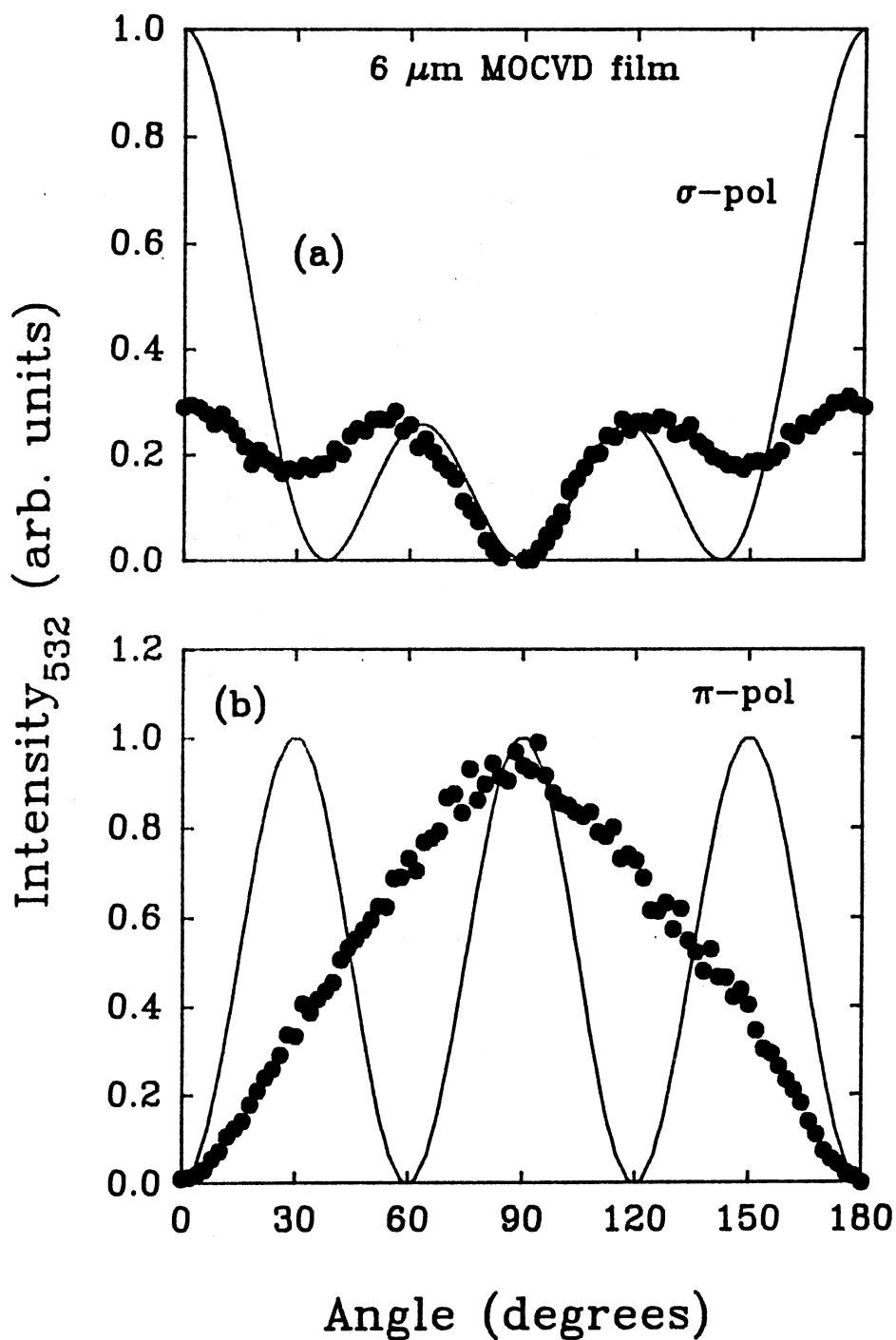
Figure 20. SHG Signal Intensity as a Function of Crystal Orientation in 6 μm-thick MOCVD Material. (a) σ Polarization Component, (b) π Polarization Component. The Angle, ψ, is Defined in the Text. The Solid Lines are the Corresponding Bulk Theoretical Curves.
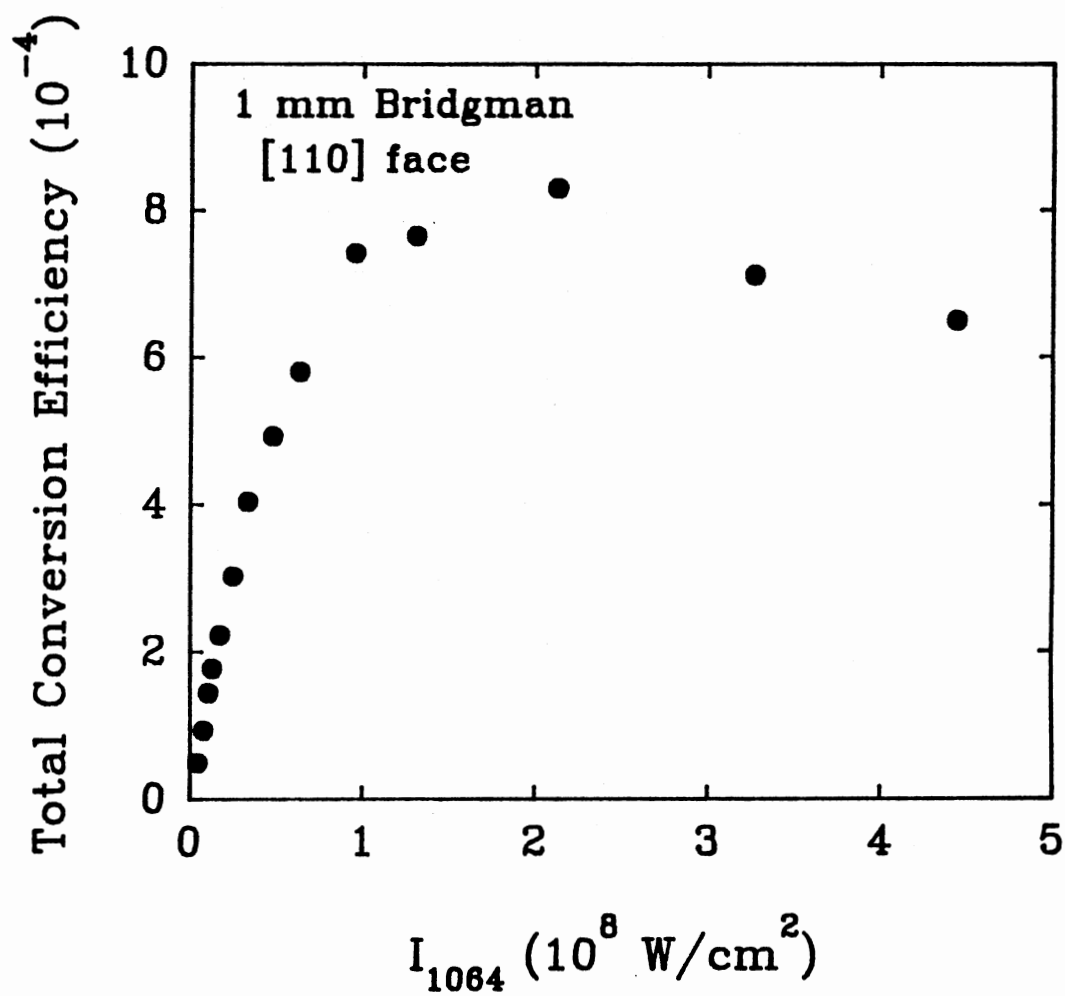
Figure 21. Dependence of the Total π-polarized SHG Conversion Efficiency of (110) CdTe on the Intensity of the Fundamental Beam.
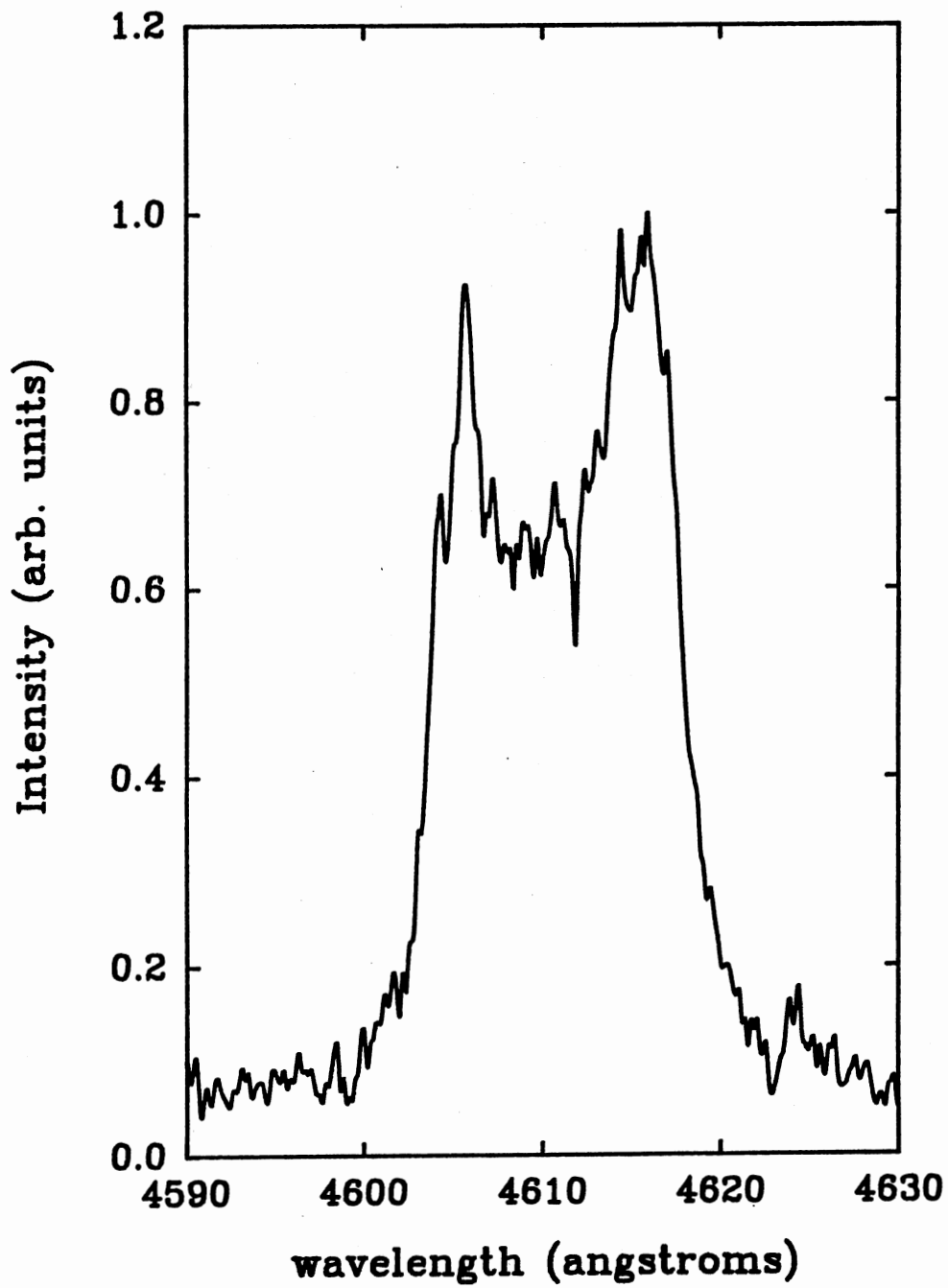
Figure 22. Frequency-doubled Signal As a Function of Wavelength Under 921 nm Excitation in (110) CdTe. The Finite Width of the Frequency-doubled Emission is Due to the Structure of the Pump Laser Emission.

pumping the 1 mm thick, (110) sample with the output of a short cavity dye laser centered near 921 nm, demonstrating that the frequency-doubling in CdTe is not limited to 1.064 μm excitation.

Discussion and Conclusions

The agreement of the data obtained on the (110) material with the theoretical curves based on the bulk material is quite good, suggesting that most of the observed signal in these particular samples has its origin in bulk SHG. Referring to Figs. 19(a) and 19(b) for the (110) material, it is seen, however, that there is a discrepancy between experiment and theory in the π polarization component at $\phi = 90°$, where the observed signal intensity falls short of the theoretical value by a factor of about 2/3. For this angle, $\hat{e}$ points along the [$\bar{1}10$] crystallographic direction. This shortfall in signal strength was attributed in our preliminary work to increased free photocarrier absorption. However, the diminution in signal strength at $\phi = 90°$ does not depend strongly on incident laser intensity. An alternative mechanism may be rooted in a dependence of the linear absorption coefficient on the orientation of $\hat{e}$ with respect to the crystallographic axes, viz. a dichroic effect. It is also possible that a change in the phase matching conditions, caused by photocarrier-induced refractive index changes, is responsible for the smaller signal strength [33]. A similar decrease in signal intensity under these conditions was observed in our earlier study [31], leading us to conclude that we are observing a material property rather than an artifact of experimental parameters.

The presumed-(111) type MOCVD material shows results that are quite different than the bulk (111) SHG theory predicts. For this sample, neither the crystallographic orientation or the quality of the film are well characterized. If the film is to a degree polycrystalline, or if growth did not occur along (111) planes, the observed signal is not expected to obey the bulk, single-crystal equations used above. A reasonable explanation of the deviation of the observed signals from the bulk (111) theory would credit each of these effects in some measure.

In the theory of SHG [44], the second harmonic power per unit area is modulated spatially by the factor which gives rise to Maker fringes [54,55]

$$\frac{\sin^2(\Delta kl/2)}{(\Delta kl/2)^2} \qquad \text{(IV.48)}$$

where $\Delta k = k^{(2\omega)} - 2k^{(\omega)}$ is the phase mismatch, and l is the sample thickness. This results assumes a low sample electrical conductivity. The coherence length l_c is defined as the distance between adjacent peaks of Eq. (IV.48) and is given by

$$\begin{aligned} l_c &= \frac{2\pi}{\Delta k} \qquad \text{(IV.49)} \\ &= \frac{\lambda}{2(n^{(2\omega)} - n^{(\omega)})} \end{aligned}$$

for free-space fundamental wavelength λ. The coherence length puts an upper limit on the maximum useful thickness of an efficient second harmonic generator. Using values of the refractive index of CdTe [14,56] of $n_{1.064} = 2.82$ and $n_{532} = 3.2$ at 1.064 μm and 532 nm, respectively, gives a coherence length of 1.4 μm. The absorption length l_{abs}, defined as the reciprocal of the absorption coefficient at 532 nm, is approximately 0.17μm, using [57] a value of $\alpha = 6 \times 10^4$ cm^{-1}. This suggests that very little enhancement, even for film thicknesses approaching the coherence length, is obtained by varying film thickness, since any newly-generated frequency-doubled light in the bulk is almost immediately absorbed.

With the exception of the MOCVD sample, the experimental results discussed above are consistent, in the limit of negligible pump depletion, with signals of constant absolute intensity in samples thicker than l_{abs}. We therefore find no enhancement owing to decreasing film thickness for the range of thicknesses considered here. This contrasts sharply with the increase in efficiency realized in transparent materials where the indices of refraction at both the fundamental and doubled frequency are largely real so that phase matching techniques can be applied [44,55]. The origin of the factor of two difference in the signal strength

in the MOCVD film remains unknown and may be related to a combination of unknown film quality and sample symmetry.

In summary, we have studied transmission geometry optical second harmonic generation in several thin films of CdTe and have found that the absolute registered second harmonic intensity is constant for three samples of well-defined symmetry, and a factor of two less for a thin MOCVD film, whose properties are not well characterized. In both types of samples the magnitude of the frequency-doubled signals is large enough to contribute to free carrier populations. In the materials of well-defined symmetry we find an angular dependence of the SHG signal intensity consistent with signals originating in the material bulk. The deviation of the presumed-(111) MOCVD SHG signals from the bulk (111) theory is attributed to a combination of unknown crystal symmetry and possible polycrystalline effects.

CHAPTER V

SUMMARY AND CONCLUSIONS

The experimental results of several picosecond, near-infrared nonlinear optical studies performed on the II-VI unintentionally-doped semiconductor cadmium telluride (CdTe) have been reported. The results of a series of experiments performed to determine the PP DFWM response of CdTe under picosecond laser excitation reveals the nonlinear response of the material can be described by the free-carrier optical nonlinearity. From these measurements values of the the ambipolar diffusion coefficient and free-carrier lifetime are deduced. The results of thin-grating, two-beam scattering are presented, from which is deduced the laser-induced refractive index change. An investigation of band-edge enhancement of the PP DFWM response is also presented, and shows that in this particular sample for the conditions of excitation investigated no significant enhancement to the absolute scattering efficiency vs. excitation wavelength is had, with an average scattering efficiency of approximately 10^{-4}. A description is presented of the first observation of picosecond photorefractive two-beam coupling in a material (undoped CdTe) lacking appreciable linear absorption, along with the first observation of polarization rotation by scalar gratings.

We have reported the results of a series of measurements made of second harmonic generation in a transmission geometry in various thicknesses of CdTe. We find that the second harmonic light originates in the material bulk rather than at the exit surface, and that no significant enhancement to the conversion efficiency is obtained by varying the sample thickness, down to a thickness of roughly six times the second harmonic generation coherence length. Results are presented for both 1064 nm and 921 nm excitation.

BIBLIOGRAPHY

1. R. Magnusson and T. Gaylord, J. Opt. Soc. Am. **67**, 1165 (1977),

2. M. Moharam and T. Gaylord, J. Opt. Soc. Am. **73**, 1105 (1983),

3. T. K. Gaylord and M. Moharam, Proc. IEEE **73**, 894 (1985),

4. W. Klein and B. D. Cook, IEEE Trans. Sonics Ultrason. **SU-14**, 123 (1967),

5. A. Smirl, G. Valley, K. Bohnert, and T. Boggess, Jr., IEEE J. Quant. Electron. **QE-24**, 289 (1988).

6. R. Bylsma, P. Bridenbaugh, D. Olson, and A. Glass, Appl. Phys. Lett. **51**, 889 (1987).

7. J. Woerdman and B. Bolger, Phys. Lett. A **30**, 164 (1969).

8. V. Kremenitskii, S. Odulov, and M. Soskin, Phys. Status Solidi A **51**, K63 (1979).

9. E.W. Van Stryland, H. Vanherzeele, M.A. Woodall, M.J. Soileau, A.L. Smirl, S. Guha, and T.F. Boggess, Jr. , Opt. Eng. **24**, 613 (1985).

10. A. Maruani, IEEE J. Quant. Electron. **QE-16**, 558 (1980).

11. G. C. Valley, Hughes Research Laboratories, Malibu, CA, (unpublished) (1988).

12. C. Raman and N. Nath, Proc. Ind. Acad. Sci. **2**, 413 (1935).

13. K. Zanio, *Cadmium Telluride*, volume 13 of *Semiconductors and Semimetals: A Treatise*, Academic, New York, 1978.

14. K. Hellwege and A. Hellwege, editors, *Landolt-Börnstein Numerical Data and Functional Relationships in Science and Technology*, volume 11, Springer-Verlag, New York, 1979.

15. R. Jain and M. Klein, *Optical Phase Conjugation*, Academic, Orlando, FL, 1983.

16. T. Moss, Phys. Status Solidi B **101**, 555 (1980).

17. A. Bugayev and A. Vankov, (unpublished).

18. P. Günter and J.-P. Huignard, editors, *Photorefractive Materials and Their Applications I*, Springer-Verlag, New York, 1988.

19. W. H. Steier, J. Kumar, and M. Ziari, Appl. Phys. Lett. **53**, 840 (1988).

20. M. Klein, Opt. Lett. **9**, 350 (1984).

21. G. C. Valley, S. McCahon, and M. Klein, Jour. Appl. Phys. **64**, 6684 (1988).

22. G. C. Valley, J. Dubard, A. L. Smirl, and A. Glass, Opt. Lett. **14**, 961 (1989).

23. I. Rückman, J. Kornack, J. Kolenda, and M. Petrauskas, Phys. Status Solidi B **158**, 769 (1990).

24. J. I. Pankove, *Optical Processes in Semiconductors*, Prentice-Hall, Englewood Cliffs, New Jersey, 1971.

25. G. C. Valley and A. L. Smirl, IEEE J. Quant. Electron. **QE-24**, 304 (1988).

26. M. S. Petrovic, A. Suchocki, R. C. Powell, G. Cantwell, and J. Aldridge, Jour. Appl. Phys. **66**, 1359 (1989).

27. K. Hill, Appl. Opt. **10**, 1695 (1971).

28. A. L. Smirl, J. Dubard, A. Cui, T. F. Boggess, and G. C. Valley, Opt. Lett. **4**, 242 (1989).

29. G. C. Valley, A. L. Smirl, and M. Klein, Opt. Lett. **11**, 647 (1986).

30. S. J. Bepko, Phys. Rev. B **12**, 669 (1975).

31. M. S. Petrovic, A. Suchocki, R. C. Powell, G. Cantwell, and J. Aldridge, Appl. Phys. Lett. **56**, 1632 (1990).

32. M. S. Petrovic, A. Suchocki, R. C. Powell, G. C. Valley, and G. Cantwell, to be published (1991).

33. C. A. Schwartz, J.-L. Oudar, and E. M. Batifol, IEEE J. Quant. Electron. **QE-11**, 616 (1975).

34. V. Martynov, E. Zeragiya, A. Solovev, and Y. Shaldin, Opt. Spectrosc. (USSR) **65**, 46 (1988).

35. H. Saito and E. Göbel, Phys. Rev. B **31**, 2360 (1986).

36. F. Majumder, H.-E. Swoboda, K. Kempf, and C. Klingshirn, Phys. Rev. B **32**, 2407 (1985).

37. H.J. Eichler, guest editor, IEEE J. Quant. Electron. **QE-22**, 1194 (1986).

38. V. Bagaev, T. Belousova, Y. Berozashvili, and D. Lordkipanidze, Sov. Phys. - Semicond. **3**, 1418 (1970).

39. J. Kiefer and A. Yariv, Appl. Phys. Lett. **15**, 26 (1969).

40. I. Rückman, M. Petrauskas, V. Netikšis, G. Tamulaitis, and J. Halfpap, Phys. Status Solidi B **142**, 629 (1987).

41. M. S. Petrovic, A. Suchocki, R. C. Powell, and G. Cantwell (unpublished, 1990).

42. M. Weber, editor, *Handbook of Laser Science and Technology*, CRC Press, Inc., Boca Raton, FL, 1986.

43. R. Hopf and G. Stegeman, *Applied Classical Electrodynamics*, Wiley, New York, 1986,

44. A. Yariv, *Quantum Electronics*, Wiley, New York, third edition, 1989.

45. J. Ducuing and N. Bloembergen, Phys. Rev. Lett. **10**, 474 (1963).

46. G. Akhundov, A. Agaeva, V. Salmanov, Y. Sharonov, and I. Yaroshetskii, Sov. Phys. - Semicond. **7**, 826 (1973).

47. C. Patel, Phys. Rev. Lett. **16**, 613 (1966).

48. M. Piltch, C. Cantrell, and R. Sze, Jour. Appl. Phys. **47**, 3514 (1976).

49. T. Furuse and I. Sakuma, Opt. Comm. **35**, 413 (1980).

50. M. Garfinkel and W. Engeler, Appl. Phys. Lett. **3**, 178 (1963).

51. J. Armstrong, M. I. Nathan, and A. W. Smith, Appl. Phys. Lett. **127**, 68 (1963).

52. R. Miller, D. Kleinman, and A. Savage, Phys. Rev. Lett. **11**, 146 (1963).

53. R. Soref and H. Moos, Jour. Appl. Phys. **35**, 2152 (1964).

54. P. Maker, R. Terhune, M. Nisenoff, and C. Savage, Phys. Rev. Lett. **8**, 21 (1962).

55. Y. Shen, *The Principle of Nonlinear Optics*, Wiley, New York, 1984.

56. M. Cardona, Jour. Appl. Phys. **36**, 2181 (1965).

57. F. H. Pollak, *II-VI Semiconducting Compounds, 1967 International Conference*, Benjamin, New York, 1967.

58. J. Armstrong, N. Bloembergen, J. Ducuing, and P. Pershan, Phys. Rev. **127**, 1918 (1962).

59. G. Baldwin, *An Introduction to Nonlinear Optics*, Plenum Press, New York, 1969.

60. P. N. Butcher, *Nonlinear Optical Phenomena*, Bulletin No. 200, Ohio State University Engineering Publications, 1965.

61. W. Chang, *Principles of Nonlinear Optics*, Addison-Wesley, Reading, MA, 1969.

62. C. Cohen-Tannoudji, B. Diu, and F. Laloe, *Quantum Mechanics*, Vol. I and II, Wiley, New York, 1977.

63. U. Fano, Rev. Mod. Phys. **29**, 74 (1957).

64. R. Jain and M. Klein, *Optical Phase Conjugation*, Academic, Orlando, FL, 1983.

65. G. Fowles, editor, *Analytical Mechanics*, Holt, Rinehart, and Winston, New York, third edition, 1977.

66. H. Goldstein, editor, *Classical Mechanics*, Addison-Wesley, Reading, MA, 1950.

67. R. Karplus and J. Schwinger, Phys. Rev. **73**, 1020 (1948).

68. P. Kelley, B. Lax, and P. Tannenwald, *Physics of Quantum Electronics*, McGraw-Hill, 1966.

69. L. Landau and E. Lifshitz, *Mechanics*, volume 1 of *Course of Theoretical Physics*, Pergamon Press, Oxford, third edition, 1976.

70. S. Levine, *Quantum Physics of Electronics*, MacMillan, New York, 1965.

71. D. Marcuse, *Principles of Quantum Electronics*, Academic, New York, 1980.

72. C. Morrison and M. Tobin, Classical derivation of nonlinear susceptibilities for the 32 crystal classes in the harmonic oscillator approximation, Technical Report HDL-TR-2078, Harry Diamond Research Laboratories, Adelphi, MD, 20783-1197, 1986.

73. R. Newman, *Infra-red Studies of Crystal Defects*, Taylor and Francis, LTD, London, 1973.

74. W. Panofsky and M. Phillips, *Classical Electricity and Magnetism*, Addison-Wesley, Reading, MA, 1962.

75. R. Pantell and H. Putthoff, *Fundamentals of Quantum Electronics*, Wiley, New York, 1969.

76. F. Robinson, *Macroscopic Electromagnetism*, Pergamon Press, Oxford, 1973.

77. R. Seeley, *Calculus of Several Variables*, Scott, Foresman and Co. Glenview, IL, 1970.

78. J. Ward, Rev. Mod. Phys. **37** (1965).

APPENDICES

APPENDIX A

CLASSICAL ANHARMONIC OSCILLATOR

CLASSICAL ANHARMONIC OSCILLATOR

It is the purpose of this appendix to discuss the derivation and form of the nonlinear optical constants in the classical anharmonic oscillator approximation. We begin by writing the equation of motion for the anharmonic oscillator

$$m\frac{d^2\vec{r}}{dt^2} = -e\vec{E} - \vec{\nabla}U(r), \tag{A.1}$$

where m is the oscillator effective mass, $\vec{r}$ is the position of the electron, $\vec{E}$ is the driving optical electric field, and

$$U(r) = U = U^{(2)} + U^{(3)} + U^{(4)} \tag{A.2}$$

is the anharmonic potential to order four in the displacement r. Generally,

$$
\begin{aligned}
U^{(2)} &= \sum_{i=1}^{3} \alpha_i Q_i^{(2)} \\
U^{(3)} &= \sum_{i=0}^{9} \beta_i Q_i^{(3)} \\
U^{(4)} &= \sum_{i=1}^{15} \gamma_i Q_i^{(4)},
\end{aligned} \tag{A.3}
$$

where the α_i, β_i, and γ_i are the expansion coefficients of the polynomials $Q^{(n)}$ of order n = 2, 3, and 4. In treating a particular point group we require that the potential be invariant under the group symmetry operation, or

$$\mathcal{O}U = U \tag{A.4}$$

80

for symmetry operation $\mathcal{O}$. When applying the symmetry operation in Eq. (A.4) to U we will find that generally not all the expansion coefficients are nonzero, so that the potential simplifies.

We take as a specific example the construction of the invariant potential for the point group S_4. Crystal class S_4 is a cyclic group containing the single generator S_4 which gives

$$
\begin{aligned}
S_4(x,y,z) &= (y,-x,-z), \\
S_4^2(x,y,z) &= (-x,-y,z), \\
S_4^3(x,y,z) &= (-y,x,-z).
\end{aligned}
\tag{A.5}
$$

The general form for the second order potential $U^{(2)}$ is

$$
U^{(2)} = \alpha_1 x^2 + \alpha_2 y^2 + \alpha_3 z^2,
\tag{A.6}
$$

and becomes under the application of the symmetry operation in Eq. (A.4) becomes

$$
S_4 U^{(2)} = \alpha_2 x^2 + \alpha_1 y^2 + \alpha_3 z^2.
\tag{A.7}
$$

Making a one-to-one correspondence between similar terms in x, y, and z in the expressions for $U^{(2)}$ and $S_4\, U^{(2)}$ in Eqs. (A.6) and (A.7), respectively, we find the following

$$
\begin{aligned}
\alpha_1 &= \alpha_2 \\
\alpha_2 &= \alpha_1 \\
\alpha_3 &= \alpha_3.
\end{aligned}
\tag{A.8}
$$

The second order contribution to the potential U is therefore

$$
\begin{aligned}
U^{(2)} &= \alpha_1(x^2 + y^2) + \alpha_3 z^2 \\
&= \frac{1}{2} m_x \omega_x^2 (x^2 + y^2) + \frac{1}{2} m_z w_z^2 z^2,
\end{aligned}
\tag{A.9}
$$

where, for the linear solution, we have taken $\alpha_i = m_i \omega_i^2/2$. The m_i are the oscillator effective masses in the $i = x, y$ and z direction.

Moving now to the third order potential $U^{(3)}$ and referring to Table I, we can see that generally $U^{(3)}$ is

$$U^{(3)} = \frac{1}{3}\beta_1 x^3 + \frac{1}{3}\beta_2 y^3 + \frac{1}{3}\beta_3 z^3 + \beta_4 x^2 y + \beta_5 x^2 z \tag{A.10}$$
$$+ \beta_6 x y^2 + \beta_7 y^2 z + \beta_8 x z^2 + \beta_9 y z^2 + 2\beta_0 xyz.$$

With the application of the symmetry operation of Eq. (A.4) U_3 becomes

$$S_4 U_3 = -\frac{1}{3}\beta_2 x^3 + \frac{1}{3}\beta_1 y^3 - \frac{1}{3}\beta_3 z^3 + \beta_6 x^2 y - \beta_7 x^2 z \tag{A.11}$$
$$-\beta_4 x y^2 - \beta_5 y^2 z - \beta_9 x z^2 + \beta_8 y z^2 + 2\beta_0 xyz.$$

Making the same one-to-one correspondence between similar terms in x, y, and z in (A.10) and (A.11) leads to the following relationships among the third order coefficients

$$\begin{aligned}
\beta_1 &= -\beta_2, \quad \beta_2 = \beta_1 \\
\beta_3 &= -\beta_3, \quad \beta_4 = \beta_6 \\
\beta_5 &= -\beta_7, \quad \beta_6 = -\beta_4 \\
\beta_7 &= -\beta_5, \quad \beta_8 = -\beta_9 \\
\beta_9 &= \beta_8, \quad \beta_0 = \beta_0.
\end{aligned} \tag{A.12}$$

Examination of these equations leads to the conclusion that only those involving β_5, β_7, and β_0 are self-consistent; therefore, these are the only nonzero coefficients in U_3 for point group S_4, with $\beta_5 = -\beta_7$. All other $\beta_i = 0$. This gives

$$U_3 = \beta_5(x^2 - y^2)z + 2\beta_0 xyz. \tag{A.13}$$

We turn our attention now to the fourth order potential $U^{(4)}$, given generally by

TABLE II

POLYNOMIALS OF ORDER n, $Q_i^{(n)}$, AND EXPANSION COEFFICIENT IN POTENTIAL ENERGY $U^{(n)}$

Expansion Coefficient	$Q_i^{(n)}$
α_1	$\frac{1}{2}x^2$
α_2	$\frac{1}{2}y^2$
α_3	$\frac{1}{2}z^2$
β_1	$\frac{1}{3}x^3$
β_2	$\frac{1}{3}y^3$
β_3	$\frac{1}{3}z^3$
β_4	x^2y
β_5	x^2z
β_6	xy^2
β_7	y^2z
β_8	xz^2
β_9	yz^2
β_0	$2xyz$
γ_1	$\frac{1}{4}x^4$
γ_2	$\frac{1}{4}y^4$
γ_3	$\frac{1}{4}z^4$
γ_4	x^3y
γ_5	x^3z
γ_6	xy^3
γ_7	y^3z
γ_8	xz^3
γ_9	yz^3
γ_{10}	$\frac{3}{2}x^2y^2$
γ_{11}	$\frac{3}{2}x^2z^2$
γ_{12}	$\frac{3}{2}y^2z^2$
γ_{13}	$3x^2yz$
γ_{14}	$3xy^2z$
γ_{15}	$3xyz^2$

$$U^{(4)} = \frac{1}{4}\gamma_1 x^4 + \frac{1}{4}\gamma_2 y^4 + \frac{1}{4}\gamma_3 z^4 + \gamma_4 x^3 y + \gamma_5 x^3 z + \gamma_6 x y^3 \qquad (A.14)$$

$$+\gamma_7 y^3 z + \gamma_8 x z^3 + \gamma_9 y z^3 + \frac{3}{2}\gamma_{10} x^2 y^2 + \frac{3}{2}\gamma_{11} x^2 z^2 + \frac{3}{2}\gamma_{12} y^2 z^2$$

$$+3\gamma_{13} x^2 y z + 3\gamma_{14} x y^2 z + 3\gamma_{15} x y z^2.$$

Applying Eq. (A.4) to this gives

$$S_4 U^{(4)} = \frac{1}{4}\gamma_2 x^4 + \frac{1}{4}\gamma_1 y^4 + \frac{1}{4}\gamma_3 z^4 - \gamma_6 x^3 y + \gamma_7 x^3 z - \gamma_4 x y^3 \qquad (A.15)$$

$$-\gamma_5 y^3 z + \gamma_9 x z^3 - \gamma_8 y z^3 + \frac{3}{2}\gamma_{10} x^2 y^2 + \frac{3}{2}\gamma_{12} x^2 z^2 + \frac{3}{2}\gamma_{11} y^2 z^2$$

$$-3\gamma_{14} x^2 y z + 3\gamma_{13} x y^2 z - 3\gamma_{15} x y z^2.$$

A comparison of (A.14) and (A.15) yields

$$\gamma_1 = \gamma_2, \quad \gamma_2 = \gamma_1 \qquad (A.16)$$

$$\gamma_3 = \gamma_3, \quad \gamma_4 = -\gamma_6$$

$$\gamma_5 = \gamma_7, \quad \gamma_6 = -\gamma_4$$

$$\gamma_7 = -\gamma_5, \quad \gamma_8 = \gamma_9$$

$$\gamma_9 = -\gamma_8, \quad \gamma_{10} = \gamma_{10}$$

$$\gamma_{11} = \gamma_{12}, \quad \gamma_{12} = \gamma_{11}$$

$$\gamma_{13} = -\gamma_{14}, \quad \gamma_{14} = \gamma_{13}$$

$$\gamma_{15} = -\gamma_{15}.$$

Examination of these equations reveals that only those involving γ_1, γ_2, γ_3, γ_4, γ_6, γ_{10}, γ_{11}, and γ_{12} are self-consistent, therefore these are the only nonzero coefficients in $U^{(4)}$ for class S_4, with $\gamma_1 = \gamma_2$, $\gamma_4 = -\gamma_6$, and $\gamma_{11} = \gamma_{12}$. We therefore have for $U^{(4)}$

$$U^{(4)} = \frac{1}{4}\gamma_1(x^4 + y^4) + \frac{1}{4}\gamma_3 z^4 + \frac{1}{4}\gamma_4 x y(x^2 - y^2) \qquad (A.17)$$

$$+\frac{3}{2}\gamma_{10} x^2 y^2 + \frac{3}{2}\gamma_{12}(x^2 + y^2)z^2.$$

This completes the construction of the invariant potential U for crystal class S_4 through order 4. We will not solve the equation of motion for this class, but reserve that for the more general case of crystal class C_1, the potential for which we now address.

Because crystal class C_1 has no symmetry all of the terms in Table 1 will be present in U. Substitution of the full expression for U from Eq. (A.2) into the equation of motion Eq. (A.1) gives for the three components

$$
\begin{aligned}
m_x\ddot{x} = & -eE_x - m_x\omega_x^2 x - \beta_1 x^2 - 2\beta_4 xy - 2\beta_5 xz - \beta_6 y^2 \qquad (A.18)\\
& -\beta_8 z^2 - \beta_0 yz - \gamma_1 x^3 - 3\gamma_4 x^2 y - 3\gamma_5 x^2 z - \gamma_6 y^3\\
& -\gamma_8 z^3 - 3\gamma_{10}xy^2 - 3\gamma_{11}xz^2 - 6\gamma_{13}xyz - 3\gamma_{14}y^2 z - 3\gamma_{15}yz^2,
\end{aligned}
$$

$$
\begin{aligned}
m_y\ddot{y} = & -eE_y - m_y\omega_y^2 y - \beta_2 x^2 - \beta_4 x^2 - 2\beta_6 xy - \beta_7 yz \qquad (A.19)\\
& -\beta_9 z^2 - 2\beta_0 xz - \gamma_2 y^3 - \gamma_4 x^3 - 3\gamma_6 xy^2 - 3\gamma_7 y^2 z\\
& -\gamma_9 z^3 - 3\gamma_{10}x^2 y - 3\gamma_{12}yz^2 - 3\gamma_{13}x^2 z - 6\gamma_{14}xyz - 3\gamma_{15}xz^2,
\end{aligned}
$$

and

$$
\begin{aligned}
m_z\ddot{z} = & -eE_z - m_z\omega_z^2 z - \beta_3 z^2 - \beta_5 x^2 - \beta_7 y^2 - 2\beta_8 xz \qquad (A.20)\\
& -2\beta_9 yz - 2\beta_0 xy - \gamma_3 z^3 - \gamma_5 x^3 - \gamma_7 y^3 - 3\gamma_8 xz^2\\
& -3\gamma_9 yz^2 - 3\gamma_{11}x^2 z - 3\gamma_{12}y^2 z - 3\gamma_{13}x^2 y - 3\gamma_{14}xy^2 - 6\gamma_{15}xyz.
\end{aligned}
$$

Reflecting the perturbational approach we shall adopt, we let

$$
\begin{aligned}
E_q & \rightarrow E_q \delta \qquad\qquad\qquad (A.21)\\
q & \rightarrow q_1\delta + q_2\delta^2 + q_3\delta^3,
\end{aligned}
$$

where E is the optical electric field, q is the displacement, which can be either x, y, or z, with each consisting of a first, second, and third order contribution.

The parameter δ serves only as a tag so that we might track the various orders of the solution through the calculations. Once the first, second, and third order equations of motion have been written down, δ will be set equal to unity. Terms in δ of order higher than 3 will not be considered, as such terms were not included in the original form of the solution in Eq. (A.21).

Substituting the form of the solution from Eq. (A.21) into the equation of motion and collecting on like powers of δ gives us through third order the solutions in x, y, and z

$$m_x \ddot{x}_1 = -eE_x - m_x \omega_x^2 x_1 \tag{A.22}$$

$$m_x \ddot{x}_2 = -m_x \omega_x^2 x_2 - \beta_1 x_1^2 - 2\beta_4 x_1 y_1 - 2\beta_5 x_1 z_1 - \beta_6 y_1^2 \tag{A.23}$$
$$-\beta_8 z_1^2 - 2\beta_0 y_1 z_1$$

$$m_x \ddot{x}_3 = -m_x \omega_x^2 x_3 - 2\beta_1 x_1 x_2 - 2\beta_4 (x_1 y_2 + x_2 y_1) \tag{A.24}$$
$$-2\beta_5 (x_1 z_2 + x_2 z_1) - 2\beta_6 y_1 y_2 - 2\beta_8 z_1 z_2 - 2\beta_0 (y_1 z_2 + y_2 z_1)$$
$$-\gamma_1 x_1^3 - 3\gamma_4 x_1^2 y_1 - 3\gamma_5 x_1^2 z_1 - \gamma_6 y_1^3 - \gamma_8 z_1^3 - 3\gamma_{10} x_1 y_1^2$$
$$-3\gamma_{11} x_1 z_1^2 - 6\gamma_{13} x_1 y_1 z_1 - 3\gamma_{14} y_1^2 z_1 - 3\gamma_{15} y_1 z_1^2,$$

$$m_y \ddot{y}_1 = -eE_y - m_y \omega_y^2 y_1 \tag{A.25}$$

$$m_y \ddot{y}_2 = -m_y \omega_y^2 y_2 - \beta_2 y_1^2 - \beta_4 x_1^2 - 2\beta_6 x_1 y_1 - 2\beta_7 y_1 z_1 \tag{A.26}$$
$$-\beta_9 z_1^2 - 2\beta_0 x_1 z_1$$

$$m_y \ddot{y}_3 \;=\; -m_y \omega_y^2 y_3 - 2\beta_2 y_1 y_2 - 2\beta_4 x_1 x_2 - 2\beta_6 (x_2 y_1 + x_1 y_2) \qquad \text{(A.27)}$$

$$-2\beta_7 (y_1 z_2 + y_2 z_1) - 2\beta_9 z_1 z_2 - 2\beta_0 (x_1 z_2 + x_2 z_1) - \gamma_2 y_1^3$$

$$-\gamma_4 x_1^3 - 3\gamma_6 x_1 y_1^2 - 3\gamma_7 y_1^2 z_1 - \gamma_9 z_1^3 - 3\gamma_{10} x_1^2 y_1$$

$$-3\gamma_{12} y_1 z_1^2 - 3\gamma_{13} x_1^2 z_1 - 6\gamma_{14} x_1 y_1 z_1 - 3\gamma_{15} x_1 z_1^2,$$

and

$$m_z \ddot{z}_1 \;=\; -eE_z - m_z \omega_z^2 z_1 \qquad \text{(A.28)}$$

$$m_z \ddot{z}_2 \;=\; -m_z \omega_z^2 z_2 - \beta_3 z_1^2 - \beta_5 x_1^2 - \beta_7 y_1^2 - 2\beta_8 x_1 z_1 \qquad \text{(A.29)}$$

$$-2\beta_9 y_1 z_1 - 2\beta_0 x_1 y_1$$

$$m_z \ddot{z}_3 \;=\; -m_z \omega_z^2 z_3 - 2\beta_3 z_1 z_2 - 2\beta_5 x_1 x_2 - 2\beta_7 y_1 y_2 \qquad \text{(A.30)}$$

$$-2\beta_8 (x_2 z_1 + x_1 z_2) - 2\beta_9 (y_2 z_1 + y_1 z_2) - 2\beta_0 (x_1 y_2 + x_2 y_1) \,\text{(A.31)}$$

$$-\gamma_3 z_1^3 - \gamma_5 x_1^3 - \gamma_7 y_1^3 - 3\gamma_8 x_1 z_1^2$$

$$-3\gamma_9 y_1 z_1^2 - 3\gamma_{11} x_1^2 z_1 - 3\gamma_{12} y_1^2 z_1 - 3\gamma_{13} x_1^2 y_1 - 3\gamma_{14} x_1 y_1^2$$

$$-6\gamma_{15} x_1 y_1 z_1.$$

Let us assume for the form of the optical electric field

$$\vec{E} = \sum_{\alpha,j} E_j^{(\alpha)} e^{iw_j t} \hat{a}_\alpha \qquad \text{(A.32)}$$

where $E_j^{(\alpha)}$ is the αth component of the electric field oscillating at angular frequency ω_j and $\hat{a}_\alpha$ is a unit vector in the α direction. For an input optical field with n Fourier components, the index j takes on values $-n, -n+1, \ldots, -1, 1, \ldots, n-1, n$, with the understanding that $\omega_j = -\omega_{-j}$, and $E_j^{(\alpha)} = (E_{-j}^{(\alpha)})^*$ where $(*)$

denotes the complex conjugate. The wave vector $\vec{k}$ dependence of E will be suppressed in this discussion since it does not enter directly into the calculations at this time. It may be inserted into the final results so that one might discuss the notion of *phase matching.*

Let us take as an example for solution the x component of the first order equation of motion. Substituting the x component of the optical electric field in Eq. (A.32) into the equation of motion Eq. (A.22) gives

$$m_x \ddot{x}_1 = -e \sum_j E_j^{(x)} e^{i\omega_j t} - m_x \omega_x^2 x_1. \tag{A.33}$$

Assuming a trial solution of the form

$$x_1 = \sum_j x_1^{(j)} e^{i\omega_j t}, \tag{A.34}$$

and performing the differentiation yields

$$-m_x \sum_j \omega_j^2 x_1^{(j)} e^{i\omega_j t} = -e \sum_j E_j^{(x)} e^{i\omega_j t} - m_x \sum_j \omega_x^2 x_1^{(j)} e^{i\omega_j t}. \tag{A.35}$$

Equating coefficients of synchronous terms gives the $x_1^{(j)}$

$$x_1^{(j)} = -\frac{E_j^{(x)}}{D_x(\omega_j)}, \tag{A.36}$$

where $D_i(\omega_j) = (m_i/e)(\omega_i^2 - \omega_j^2)$. Similar operations lead to the first order y and z coefficients

$$y_1^{(j)} = -\frac{E_j^{(y)}}{D_y(\omega_j)} \tag{A.37}$$

$$z_1^{(j)} = -\frac{E_j^{(z)}}{D_z(\omega_j)}, \tag{A.38}$$

from which follow the first order solutions

$$x_1 = -\sum_j \frac{E_j^{(x)}}{D_x(\omega_j)} e^{i\omega_j t} \tag{A.39}$$

$$y_1 = -\sum_j \frac{E_j^{(y)}}{D_y(\omega_j)} e^{i\omega_j t} \tag{A.40}$$

$$z_1 = -\sum_j \frac{E_j^{(z)}}{D_z(\omega_j)} e^{i\omega_j t}. \tag{A.41}$$

The polarization P in the α direction is related to the nth order displacement q_n through

$$P_\alpha^{(n)} = -Neq_n \tag{A.42}$$

where N is the number of displaced electrons and e is the modulus of the electronic charge (a positive number). However, we may also expand the polarization in powers of the electric field E

$$P_\alpha = \sum_j \chi_{\alpha j}^{(1)} E^{(j)} + \sum_{j,k} \chi_{\alpha jk}^{(2)} E^{(j)} E^{(k)} + \sum_{j,k,l} \chi_{\alpha jkl}^{(3)} E^{(j)} E^{(k)} E^{(l)} + \ldots \tag{A.43}$$

A comparison of these two forms of the polarization gives the linear susceptibility $\chi^{(1)}$

$$\chi_{\alpha\alpha}^{(1)}(\omega_j) = \frac{Ne}{D_\alpha(\omega_j)}. \tag{A.44}$$

Note that x_1 contains *no frequency components not contained in the driving field* E_x, reflecting the fact that x_1 is the first order solution; it therefore describes only linear optical effects. We shall continue to refer to Eqs. (A.42) and (A.43) throughout this work, as we seek the nonlinear susceptibility tensor elements.

We now proceed to the second order solution in x. Substituting the first order solutions in $x, y,$ and z into the second order equation of motion Eq. (A.23) for x gives

$$m_x\ddot{x}_2 = -m_x\omega_x^2 x_2 - (e/m)^2 \sum_{j,k} \left(\frac{\beta_1 E_j^x E_k^x}{(\omega_x^2 - \omega_j^2)(\omega_x^2 - \omega_k^2)} \right. \quad (A.45)$$

$$\frac{2\beta_4 E_j^x E_k^y}{(\omega_x^2 - \omega_j^2)(\omega_y^2 - \omega_k^2)} + \frac{2\beta_5 E_j^x E_k^z}{(\omega_x^2 - \omega_j^2)(\omega_z^2 - \omega_k^2)} + \frac{\beta_6 E_j^y E_k^y}{(\omega_y^2 - \omega_j^2)(\omega_y^2 - \omega_k^2)}$$

$$\left. \frac{\beta_8 E_j^z E_k^z}{(\omega_z^2 - \omega_j^2)(\omega_z^2 - \omega_k^2)} + \frac{2\beta_0 E_j^y E_k^z}{(\omega_y^2 - \omega_j^2)(\omega_z^2 - \omega_k^2)} \right) e^{i(\omega_j + \omega_k)t}.$$

As in the first order case, we try a solution x_2 that has the same time dependence as the driving term. Let x_2 be of the form

$$x_2 = \sum_{j,k} x_2^{(j,k)} e^{i(\omega_j + \omega_k)t}. \quad (A.46)$$

Substitution of this into the equation of motion and equating coefficients of synchronous terms gives

$$x_2^{(j,k)} = -\frac{(e/m)^2}{[\omega_x^2 - (\omega_j + \omega_k)^2]} \left(\frac{\beta_1 E_j^x E_k^x}{(\omega_x^2 - \omega_j^2)(\omega_x^2 - \omega_k^2)} \right. \quad (A.47)$$

$$+\frac{2\beta_4 E_j^x E_k^y}{(\omega_x^2 - \omega_j^2)(\omega_y^2 - \omega_k^2)} + \frac{2\beta_5 E_j^x E_k^z}{(\omega_x^2 - \omega_j^2)(\omega_z^2 - \omega_k^2)} + \frac{\beta_6 E_j^y E_k^y}{(\omega_y^2 - \omega_j^2)(\omega_y^2 - \omega_k^2)}$$

$$\left. \frac{\beta_8 E_j^z E_k^z}{(\omega_z^2 - \omega_j^2)(\omega_z^2 - \omega_k^2)} + \frac{2\beta_0 E_j^y E_k^z}{(\omega_y^2 - \omega_j^2)(\omega_z^2 - \omega_k^2)} \right) e^{i(\omega_j + \omega_k)t},$$

from which follows the second order solution in x

$$x_2 = -(e/m)^2 \sum_{j,k} \frac{1}{[\omega_x^2 - (\omega_j + \omega_k)^2]} \left(\frac{\beta_1 E_j^x E_k^x}{(\omega_x^2 - \omega_j^2)(\omega_x^2 - \omega_k^2)} \right. \quad (A.48)$$

$$+\frac{2\beta_4 E_j^x E_k^y}{(\omega_x^2 - \omega_j^2)(\omega_y^2 - \omega_k^2)} + \frac{2\beta_5 E_j^x E_k^z}{(\omega_x^2 - \omega_j^2)(\omega_z^2 - \omega_k^2)} + \frac{\beta_6 E_j^y E_k^y}{(\omega_y^2 - \omega_j^2)(\omega_y^2 - \omega_k^2)}$$

$$\left. \frac{\beta_8 E_j^z E_k^z}{(\omega_z^2 - \omega_j^2)(\omega_z^2 - \omega_k^2)} + \frac{2\beta_0 E_j^y E_k^z}{(\omega_y^2 - \omega_j^2)(\omega_z^2 - \omega_k^2)} \right) e^{i(\omega_j + \omega_k)t}.$$

Similar operations provide the second order solutions in y and z

$$y_2 = -(e/m)^2 \sum_{j,k} \frac{1}{[\omega_y^2 - (\omega_j^2 + \omega_k^2)]} \left(\frac{\beta_2 E_j^y E_k^y}{(\omega_y^2 - \omega_j^2)(\omega_y^2 - \omega_k^2)} \right. \quad (A.49)$$

$$\frac{\beta_4 E_j^x E_k^x}{(\omega_x^2 - \omega_j^2)(\omega_x^2 - \omega_k^2)} + \frac{2\beta_6 E_j^x E_k^y}{(\omega_x^2 - \omega_j^2)(\omega_y^2 - \omega_k^2)} + \frac{2\beta_7 E_j^y E_k^z}{(\omega_y^2 - \omega_j^2)(\omega_z^2 - \omega_k^2)}$$

$$\left. \frac{\beta_9 E_j^z E_k^z}{(\omega_z^2 - \omega_j^2)(\omega_z^2 - \omega_k^2)} + \frac{2\beta_0 E_j^x E_k^z}{(\omega_x^2 - \omega_j^2)(\omega_z^2 - \omega_k^2)} \right) e^{i(\omega_j + \omega_k)t}.$$

and

$$z_2 = -(e/m)^2 \sum_{j,k} \frac{1}{[\omega_z^2 - (\omega_j^2 + \omega_k^2)]} \left(\frac{\beta_3 E_j^z E_k^z}{(\omega_z^2 - \omega_j^2)(\omega_z^2 - \omega_k^2)} \right. \tag{A.50}$$

$$\frac{\beta_5 E_j^x E_k^x}{(\omega_x^2 - \omega_j^2)(\omega_x^2 - \omega_k^2)} + \frac{\beta_7 E_j^y E_k^y}{(\omega_y^2 - \omega_j^2)(\omega_y^2 - \omega_k^2)} + \frac{2\beta_8 E_j^x E_k^z}{(\omega_x^2 - \omega_j^2)(\omega_z^2 - \omega_k^2)}$$

$$\left. \frac{2\beta_9 E_j^y E_k^z}{(\omega_y^2 - \omega_j^2)(\omega_z^2 - \omega_k^2)} + \frac{2\beta_0 E_j^x E_k^y}{(\omega_x^2 - \omega_j^2)(\omega_y^2 - \omega_k^2)} \right) e^{i(\omega_j + \omega_k)t},$$

respectively, where we have for simplicity assumed that the effective masses are equal. These expressions for x_2, y_2, and z_2 are sufficient to describe nonlinear effects arising from the second order polarization.

Let us now take as an example second harmonic generation to show how we might extract the nonlinear second order susceptibility tensor elements for a particular wave mixing process. Considering the x component of the polarization, and letting the optical pump field consist of the single Fourier component $\omega = \omega_p$, we focus on those terms in Eq. (A.48) oscillating at $2\omega_p$. This gives

$$x_2(2\omega_p) = -\frac{(e/m)^3}{(\omega_x^2 - 4\omega_p^2)} \left(\frac{\beta_1 E^{(x)} E^{(x)}}{(\omega_x^2 - \omega_p^2)(\omega_x^2 - \omega_p^2)} \right. \tag{A.51}$$

$$+ \frac{2\beta_4 E^{(x)} E^{(y)}}{(\omega_x^2 - \omega_p^2)(\omega_y^2 - \omega_p^2)} + \frac{2\beta_5 E^{(x)} E^{(z)}}{(\omega_x^2 - \omega_p^2)(\omega_z^2 - \omega_p^2)}$$

$$+ \frac{\beta_6 E^{(y)} E^{(y)}}{(\omega_y^2 - \omega_p^2)(\omega_y^2 - \omega_p^2)} + \frac{\beta_8 E^{(z)} E^{(z)}}{(\omega_z^2 - \omega_p^2)(\omega_z^2 - \omega_p^2)}$$

$$\left. + \frac{2\beta_0 E^{(y)} E^{(z)}}{(\omega_y^2 - \omega_p^2)(\omega_z^2 - \omega_p^2)} \right) e^{i2\omega_p t} + c.c.$$

Knowing that the second order polarization P for displacement x_2 is given by

$$P_x^{(2)}(2\omega_p) = -Nex_2(2\omega_p) \tag{A.52}$$

$$= \sum_{j,k} \chi^{(2)}_{xjk} E^{(j)} E^{(k)}$$

we can identify the values of the elements of the second order nonlinear optical susceptibility tensor $\chi^{(2)}_{xjk}$. For example, for $j = k = x$, we have

$$\chi^{(2)}_{xxx} = \frac{N(e/m)^3}{(\omega_x^2 - 4\omega_p^2)} \frac{\beta_1}{(\omega_x^2 - \omega_p^2)^2} + c.c. \qquad (A.53)$$

Now that we have obtained the first and second order solutions in x, y, and z, we can proceed to third order. Because of the considerable amount of algebraic overhead in transcribing these equations we will only discuss the third order solution in the variable x, and even then we will keep only those terms involving the γ_i. Let us assume a form of the third order solution given by

$$x_3 \doteq \sum_{j,k,l} x_3^{(j,k,l)} e^{i(\omega_j + \omega_k + \omega_l)t}. \qquad (A.54)$$

Substitution of this, and the lower order solutions, into Eq. (A.24), and equating coefficients of synchronous terms in the γ_i yields

$$x_3 = -(e/m)^4 \sum_{j,k,l} \frac{e^{i(\omega_j + \omega_k + \omega_l)t}}{[\omega_x^2 - (\omega_j + \omega_k + \omega_l)^2]} \times \qquad (A.55)$$

$$\left(\frac{\gamma_1 E_j^{(x)} E_k^{(x)} E_l^{(x)}}{(\omega_x^2 - \omega_j^2)(\omega_x^2 - \omega_k^2)(\omega_x^2 - \omega_l^2)} + \frac{3\gamma_4 E_j^{(x)} E_k^{(x)} E_l^{(y)}}{(\omega_x^2 - \omega_j^2)(\omega_x^2 - \omega_k^2)(\omega_y^2 - \omega_l^2)} \right.$$

$$+ \frac{3\gamma_5 E_j^{(x)} E_k^{(x)} E_l^{(z)}}{(\omega_x^2 - \omega_j^2)(\omega_x^2 - \omega_k^2)(\omega_z^2 - \omega_l^2)} + \frac{\gamma_6 E_j^{(y)} E_k^{(y)} E_l^{(y)}}{(\omega_y^2 - \omega_j^2)(\omega_y^2 - \omega_k^2)(\omega_y^2 - \omega_l^2)}$$

$$+ \frac{\gamma_8 E_j^{(z)} E_k^{(z)} E_l^{(z)}}{(\omega_z^2 - \omega_j^2)(\omega_z^2 - \omega_k^2)(\omega_z^2 - \omega_l^2)} + \frac{3\gamma_{10} E_j^{(x)} E_k^{(y)} E_l^{(y)}}{(\omega_x^2 - \omega_j^2)(\omega_y^2 - \omega_k^2)(\omega_y^2 - \omega_l^2)}$$

$$+ \frac{3\gamma_{11} E_j^{(x)} E_k^{(z)} E_l^{(z)}}{(\omega_x^2 - \omega_j^2)(\omega_z^2 - \omega_k^2)(\omega_z^2 - \omega_l^2)} + \frac{6\gamma_{13} E_j^{(x)} E_k^{(y)} E_l^{(z)}}{(\omega_x^2 - \omega_j^2)(\omega_y^2 - \omega_k^2)(\omega_z^2 - \omega_l^2)}$$

$$\left. + \frac{3\gamma_{14} E_j^{(y)} E_k^{(y)} E_l^{(z)}}{(\omega_y^2 - \omega_j^2)(\omega_y^2 - \omega_k^2)(\omega_z^2 - \omega_l^2)} + \frac{3\gamma_{15} E_j^{(y)} E_k^{(z)} E_l^{(z)}}{(\omega_y^2 - \omega_j^2)(\omega_z^2 - \omega_k^2)(\omega_z^2 - \omega_l^2)} \right),$$

where we have again assumed for simplicity that the effective masses are equal.

As an example of how to extract the values of the third order nonlinear susceptibility tensor let us consider third harmonic generation. In this case the

input optical pump field has only one Fourier component $\omega = \omega_p$. The nonlinear response from the medium then gives rise to a polarization oscillating at $3\omega_p$. Writing only those terms in γ_i oscillating at $3\omega_p$ in Eq. (A.55) we have

$$
\begin{aligned}
x_3(3\omega_p) = & -\frac{(e/m)^4}{(\omega_x^2 - 9\omega_p^2)}\left(\frac{2\gamma_1 E^{(x)}E^{(x)}E^{(x)}}{(\omega_x^2 - \omega_p^2)(\omega_x^2 - \omega_p^2)(\omega_x^2 - \omega_p^2)}\right. \\
& + \frac{3\gamma_4 E^{(x)}E^{(x)}E^{(x)}}{(\omega_x^2 - \omega_p^2)(\omega_x^2 - \omega_p^2)(\omega_x^2 - \omega_p^2)} + \frac{3\gamma_5 E^{(x)}E^{(x)}E^{(z)}}{(\omega_x^2 - \omega_p^2)(\omega_x^2 - \omega_p^2)(\omega_z^2 - \omega_p^2)} \\
& + \frac{\gamma_6 E^{(y)}E^{(y)}E^{(y)}}{(\omega_y^2 - \omega_p^2)(\omega_y^2 - \omega_p^2)(\omega_y^2 - \omega_p^2)} + \frac{\gamma_8 E^{(z)}E^{(z)}E^{(z)}}{(\omega_z^2 - \omega_p^2)(\omega_z^2 - \omega_p^2)(\omega_z^2 - \omega_p^2)} \\
& + \frac{3\gamma_{10} E^{(x)}E^{(y)}E^{(y)}}{(\omega_x^2 - \omega_p^2)(\omega_y^2 - \omega_p^2)(\omega_y^2 - \omega_p^2)} + \frac{3\gamma_{11} E^{(x)}E^{(z)}E^{(z)}}{(\omega_x^2 - \omega_p^2)(\omega_z^2 - \omega_p^2)(\omega_z^2 - \omega_p^2)} \\
& + \frac{6\gamma_{13} E^{(x)}E^{(y)}E^{(z)}}{(\omega_x^2 - \omega_p^2)(\omega_y^2 - \omega_p^2)(\omega_z^2 - \omega_p^2)} + \frac{3\gamma_{14} E^{(y)}E^{(y)}E^{(z)}}{(\omega_y^2 - \omega_p^2)(\omega_y^2 - \omega_p^2)(\omega_z^2 - \omega_p^2)} \\
& \left. + \frac{3\gamma_{15} E^{(y)}E^{(z)}E^{(z)}}{(\omega_y^2 - \omega_p^2)(\omega_z^2 - \omega_p^2)(\omega_z^2 - \omega_p^2)}\right) e^{i3\omega_p t} + c.c.
\end{aligned}
\tag{A.56}
$$

Knowing that the third order polarization P for displacement x_3 is given by

$$
\begin{aligned}
P_x^{(3)}(3\omega_p) &= -Nex_3(3\omega_p) \tag{A.57} \\
&= \sum_{j,k,l} \chi_{xjkl}^{(3)}(3\omega_p)E^{(j)}E^{(k)}E^{(l)}e^{i3\omega_p t}
\end{aligned}
$$

where $j, k,$ and l are each summed over the Cartesian components $x, y,$ and z, a comparison of Eq. (A.56) and (A.57) gives

$$
\chi_{xxxx}^{(3)} = \frac{N(e/m)^4}{(\omega_x^2 - 9\omega_p^2)}\frac{2\gamma_1}{(\omega_x^2 - \omega_p^2)(\omega_x^2 - \omega_p^2)(\omega_x^2 - \omega_p^2)} + c.c. \tag{A.58}
$$

APPENDIX B

SEMICLASSICAL DENSITY MATRIX

SEMICLASSICAL DENSITY MATRIX

It is the purpose of this appendix to discuss the form and derivation of the nonlinear optical constants in the semiclassical density matrix approximation. The density matrix method in quantum mechanics allows us to gain information about a physical system without precise knowledge of the system's wave functions $|\psi(t)\rangle$. In place of this exact knowledge of the wavefunctions we substitute our knowledge of the probability of the system taking on a certain wavefunction.

Consider a system whose wavefunction is at time t

$$| \psi(t)\rangle = \sum_n c_n(t) \mid u_n\rangle \tag{B.1}$$

where the kets u_n form an orthonormal basis for the state space and the coefficients $c_n(t)$ satisfy the relationship

$$\sum_n \mid c_n(t) \mid^2 = 1, \tag{B.2}$$

an expression of the fact that the $\psi(t)$'s are normalized. If we now consider an observable $\hat{A}$ with matrix elements

$$A_{np} = \langle u_n \mid \hat{A} \mid u_p\rangle, \tag{B.3}$$

then the mean value of $\hat{A}$ at the instant t is

$$
\begin{aligned}
\langle A\rangle(t) &= \langle \psi(t) \mid \hat{A} \mid \psi(t)\rangle \\
&= \langle \sum_n c_n^*(t)u_n \mid \hat{A} \mid \sum_p c_p(t)u_p\rangle \\
&= \sum_{n,p} c_n^*(t)c_p(t)A_{np}.
\end{aligned} \tag{B.4}
$$

95

Eq. (B.4) shows that the coefficients $c_n(t)$ enter into the mean values through quadratic expressions of the form $c_n^*(t)c_p(t)$. These are simply the matrix elements of the operator

$$\hat{\rho}(t) = \mid \psi(t)\rangle\langle\psi(t) \mid \tag{B.5}$$

taken between the basis vectors $\mid u_p\rangle$ and $\mid u_n\rangle$. That is,

$$
\begin{aligned}
\rho_{pn} &= \langle u_p \mid \hat{\rho}(t) \mid u_n\rangle \\
&= \langle u_p \mid \psi(t)\rangle\,\langle\psi(t) \mid u_n\rangle \\
&= \langle u_p \mid \sum_i c_i(t)u_i\rangle\langle\sum_j c_j^*(t)u_j \mid u_n\rangle \\
&= \sum_{i,j} c_i(t)c_j^*(t)\langle u_p \mid u_i\rangle\langle u_j \mid u_n\rangle \\
&= \sum_{i,j} c_i(t)c_j^*(t)\delta_{pi}\delta_{nj} \\
&= c_n^*(t)c_p(t).
\end{aligned} \tag{B.6}
$$

The operator $\hat{\rho}(t)$ is called the *density operator* and its matrix elements ρ_{pn} constitute the *density matrix*. We will now show that the specification of $\hat{\rho}(t)$ suffices to characterize the physical properties of the system; that is, it will allow us to obtain all the physical information that can be calculated using the kets $\psi(t)$.

According to the statement of normalization of the $\psi(t)$ in Eq. (B.2) and the relationship between the ρ_{pn} and expansion coefficients $c_k(t)$ in Eq. (B.6), a sum over the diagonal elements of $\hat{\rho}(t)$ results in unity, or,

$$
\begin{aligned}
\sum_n \mid c_n(t) \mid^2 &= \sum_n \rho_{nn}(t) \\
&= \mathrm{Tr}[\hat{\rho}(t)] \\
&= 1.
\end{aligned} \tag{B.7}
$$

The mean value of $\hat{A}$ given in Eq. (B.4) may be rewritten by combining Eq. (B.3) for the matrix elements of $\hat{A}$ with the result for the matrix elements of $\hat{\rho}(t)$ in Eq. (B.6). This produces

$$
\begin{aligned}
\langle A(t) \rangle &= \sum_{n,p} [c_n^*(t) c_p(t)][A_{np}] \qquad &\text{(B.8)} \\
&= \sum_{n,p} [\rho_{pn}][A_{np}] \\
&= \sum_{n,p} [\langle u_p \mid \hat{\rho}(t) \mid u_n \rangle][\langle u_n \mid \hat{A} \mid u_p \rangle] \\
&= \sum_{p} \langle u_p \mid \hat{\rho}(t) \hat{A} \mid u_p \rangle \\
&= \text{Tr}[\hat{\rho}(t) \hat{A}],
\end{aligned}
$$

where the fourth line follows from the third due to closure. *

The time evolution of the density operator may be obtained with the aid of Schrödinger's equation,

$$
i\hbar \frac{d}{dt} \mid \psi(t) \rangle = \hat{H} \mid \psi(t) \rangle , \qquad \text{(B.9)}
$$

so that

$$
\begin{aligned}
\frac{d\hat{\rho}(t)}{dt} &= \frac{d}{dt} \mid \psi(t) \rangle \langle \psi(t) \mid \qquad &\text{(B.10)} \\
&= \left(\frac{d}{dt} \mid \psi(t) \rangle \right) \langle \psi(t) \mid + \mid \psi(t) \rangle \left(\frac{d}{dt} \langle \psi(t) \mid \right) \\
&= \frac{1}{i\hbar} \hat{H} \mid \psi(t) \rangle \langle \psi(t) \mid + \frac{1}{(-i\hbar)} \mid \psi(t) \rangle \langle \psi(t) \mid \hat{H} \\
&= \frac{-i}{\hbar} \left[\hat{H}, \hat{\rho}(t) \right] ,
\end{aligned}
$$

where $\hat{H}$ is the Hamiltonian of the system.

Let us consider more closely the commutator given in Eq. (B.10) by noting that the Hamiltonian consists of two terms

$$
\hat{H} = \hat{H}_0 + \hat{V} \qquad \text{(B.11)}
$$

*A brief discussion of closure can be found in Appendix F .

where $\hat{H}_0$ is the unperturbed diagonal Hamiltonian of the system and $\hat{V}$ is an applied perturbation. Substituting this total Hamiltonian into the equation of motion for $\hat{\rho}(t)$ in Eq. (B.10) gives

$$
\begin{aligned}
\frac{d\hat{\rho}(t)}{dt} &= -\frac{i}{\hbar}\left[\hat{H}_0+\hat{V},\hat{\rho}(t)\right] \\
&= -\frac{i}{\hbar}\left[\left(\hat{H}_0+\hat{V}\right)\hat{\rho}(t)-\hat{\rho}(t)\left(\hat{H}_0+\hat{V}\right)\right] \\
&= -\frac{i}{\hbar}\left[\hat{H}_0\hat{\rho}(t)-\hat{\rho}(t)\hat{H}_0+\hat{V}\hat{\rho}(t)-\hat{\rho}(t)\hat{V}\right] \\
&= -\frac{i}{\hbar}\left\{\left[\hat{H}_0,\hat{\rho}(t)\right]+\left[\hat{V},\hat{\rho}(t)\right]\right\}.
\end{aligned}
\tag{B.12}
$$

This result may be written for a particular matrix element of $d\hat{\rho}(t)/dt$

$$
\frac{d\rho_{ij}}{dt} = -\frac{i}{\hbar}\left[\hat{H}_0,\hat{\rho}(t)\right]_{ij}-\frac{i}{\hbar}\left[\hat{V},\hat{\rho}(t)\right]_{ij}.
\tag{B.13}
$$

Let us consider the first term in this equation. We have

$$
\left[\hat{H}_0,\hat{\rho}(t)\right]_{ij} = \left[\begin{pmatrix} H_{11}^0 & H_{12}^0 & H_{13}^0 \\ H_{21}^0 & H_{22}^0 & H_{23}^0 \\ H_{31}^0 & H_{32}^0 & H_{33}^0 \end{pmatrix}\begin{pmatrix} \rho_{11} & \rho_{12} & \rho_{13} \\ \rho_{21} & \rho_{22} & \rho_{23} \\ \rho_{31} & \rho_{32} & \rho_{33} \end{pmatrix} - \begin{pmatrix} \rho_{11} & \rho_{12} & \rho_{13} \\ \rho_{21} & \rho_{22} & \rho_{23} \\ \rho_{31} & \rho_{32} & \rho_{33} \end{pmatrix}\begin{pmatrix} H_{11}^0 & H_{12}^0 & H_{13}^0 \\ H_{21}^0 & H_{22}^0 & H_{23}^0 \\ H_{31}^0 & H_{32}^0 & H_{33}^0 \end{pmatrix}\right]_{ij},
\tag{B.14}
$$

assuming a three-level system and where $H_{ij}=H_{ii}\delta_{ij}=\mathcal{E}_i\delta_{ij}$ for energy $\mathcal{E}_i$ of the ith level of the system. Following the usual prescription for taking a matrix product, Eq. (B.14) can be cast as

$$
\begin{aligned}
\left[\hat{H}_0,\hat{\rho}(t)\right]_{ij} &= \sum_n H_{in}^0\rho_{nj}-\sum_n \rho_{in}H_{nj}^0 \\
&= \sum_n\left(H_{in}^0\rho_{nj}\delta_{in}-\rho_{in}H_{nj}^0\delta_{nj}\right) \\
&= (\mathcal{E}_i-\mathcal{E}_j)\rho_{ij} \\
&= \hbar\omega_{ij}\rho_{ij},
\end{aligned}
\tag{B.15}
$$

where $\omega_{ij} \equiv (\mathcal{E}_i - \mathcal{E}_j)/\hbar$. With this, Eq. (B.13) for the equation of motion becomes

$$\frac{d\rho_{ij}}{dt} = -i\omega_{ij}\rho_{ij} - \frac{i}{\hbar}[\hat{V}, \hat{\rho}(t)]_{ij}. \tag{B.16}$$

Let us now make explicit the perturbational nature of our approach. We shall let the following take effect:

$$V \quad \rightarrow \quad \delta V \tag{B.17}$$

$$\rho_{ij} \quad \rightarrow \quad \rho_{ij}^{(0)} + \delta\rho_{ij}^{(1)} + \delta^2\rho_{ij}^{(2)} + \delta^3\rho_{ij}^{(3)}, \tag{B.18}$$

where the parameter δ serves, as in the classical discussion, as a tag to track the various orders of the final solution. Substitution of these last two equations into the equation of motion Eq. (B.16) leaves us with

$$\frac{d}{dt}\left(\rho_{ij}^{(0)} + \delta\rho_{ij}^{(1)} + \delta^2\rho_{ij}^{(2)}\right) = -i\omega_{ij}\left(\rho_{ij}^{(0)} + \delta\rho_{ij}^{(1)} + \delta^2\rho_{ij}^{(2)}\right) \tag{B.19}$$
$$-\frac{i}{\hbar}\left[\delta V, \rho_{ij}^{(0)} + \delta\rho_{ij}^{(1)} + \delta^2\rho_{ij}^{(2)}\right].$$

By expanding the commutator and equating like powers of δ we find

$$\frac{d\rho_{ij}^{(n)}}{dt} = -i\omega_{ij}\rho_{ij}^{(n)} - \frac{i}{\hbar}\left[V, \rho^{(n-1)}\right]_{ij}, \tag{B.20}$$

showing that solutions in order n depend on solutions of order $n-1$. The zeroth order solution is $\rho_{ij}^{(0)} = \bar{\rho}_{ij}\delta_{ij}$, where the physical meaning of the Kronecker δ_{ij} lies in our foreknowledge that only diagonal elements of $\hat{\rho}(t)$ (which are proportional to the population in state i) are nonzero at thermal equilibrium (denoted by the superscript (0)). In the absence of a perturbation there is no phase coherence between states i and j, a coherence which would otherwise manifest itself as nonzero off-diagonal matrix elements.

Before we attempt to solve this particular equation, let us take for a moment a slightly more general type of situation, solve it, and then make the identifications useful to us at the end. Consider a differential equation of the form

$$\frac{dy(t)}{dt} = i\omega y(t) + g(t). \tag{B.21}$$

Assume a solution of the form $y(t) = C(t)e^{i\omega t}$ and substitute it into the differential equation for y in Eq. (B.21) to give

$$e^{i\omega t}\frac{dC}{dt} + i\omega e^{i\omega t}C = i\omega C e^{i\omega t} + g(t), \tag{B.22}$$

which, upon solving for dC/dt and integrating, gives

$$C(t) = \int_{-\infty}^{t} e^{-i\omega t'}g(t')dt', \tag{B.23}$$

from which follows the solution $y(t)$

$$y(t) = e^{i\omega t}\int_{-\infty}^{t} e^{-i\omega t'}g(t')dt'. \tag{B.24}$$

Making the identifications

$$y(t) \;\rightarrow\; \rho_{ij}^{(n)} \tag{B.25}$$

$$\omega \;\rightarrow\; -\omega_{ij} \tag{B.26}$$

$$g(t) \;\rightarrow\; -\frac{i}{\hbar}\left[V, \rho^{(n-1)}\right]_{ij} \tag{B.27}$$

leaves us with an extremely powerful integral equation for the ρ_{ij}:

$$\rho_{ij}^{(n)} = -\frac{i}{\hbar}e^{-i\omega_{ij}t}\int_{-\infty}^{t} e^{i\omega_{ij}t'}\left[V, \rho^{(n-1)}\right]_{ij}(t')dt'. \tag{B.28}$$

For Eq. (B.28) to agree with what is actually observed in physical systems, we must supplement it in such a way as to ensure that the various ρ_{ij} go to zero at $t = -\infty$. This is done by adding a phenomenological damping term to the equation of motion in Eq. (B.20) to give

$$\frac{d\rho_{ij}^{(n)}}{dt} = -i\omega_{ij}\rho_{ij}^{(n)} - \frac{i}{\hbar}\left[V, \rho^{(n-1)}\right]_{ij} - \Gamma_{ij}\rho_{ij}^{(n)}, \tag{B.29}$$

where Γ_{ij} is equal to the decay rate of level i when $i = j$ (so-called T_1 processes) and equal to the dephasing rate between states i and j when $i \neq j$ (T_2 processes). With this new damping term, the integral equation for ρ_{ij} given by Eq. (B.28) becomes

$$\rho_{ij}^{(n)} = -\frac{i}{\hbar}e^{-i(\omega_{ij}-i\Gamma_{ij})t} \int_{-\infty}^{t} e^{i(\omega_{ij}-i\Gamma_{ij})t'} \left[V, \rho^{(n-1)}\right]_{ij}(t')dt'. \tag{B.30}$$

What remains of this discussion of nonlinear optical constants will rest almost entirely on this most broad-shouldered equation for the ρ_{ij}.

Let us now specify the applied perturbation by impressing on the system an external optical electric field of the form

$$\vec{E}(t) = \sum_{\alpha,j} \hat{a}_\alpha E_j^{(\alpha)} e^{i\omega_j t}, \tag{B.31}$$

for unit polarization vector $\hat{a}_\alpha$ in the αth direction, field amplitude $E_j^{(\alpha)}$ oscillating at ω_j, and Fourier component ω_j. As was done in the classical case for a field consisting of n Fourier components, j ranges from $-n, -n+1, \ldots, -1, 1, \ldots, n-1, n$, with the understanding that $\omega_j = -\omega_{-j}$ and that $E_j^\alpha = (E_{-j}^\alpha)^*$. As in the classical discussion, the the dependence of $\vec{E}$ on the wave vector $\vec{k}$ will be suppressed since $\vec{k}$ does not directly affect the calculations, but can, of course, be inserted back into the results when *phase matching* must be considered.

As was alluded to earlier, we will for the sake of example assume a three-level system characterized by discrete energy levels $\mathcal{E}_1 < \mathcal{E}_2 < \mathcal{E}_3$, each corresponding to an angular frequency $\omega_1 < \omega_2 < \omega_3$, respectively, with the ω_i obtained from the relation $\mathcal{E}_i = \hbar\omega_i$. We also assume that level 1 is the only level with a population at thermal equilibrium.

Assuming an electric dipole transition *, we have for the perturbation V

$$V = -e\vec{r}\cdot\vec{E} \tag{B.32}$$

---

*A derivation of the form of the electric dipole interaction can be found in Appendix D.

$$= \vec{\mu} \cdot \vec{E}$$
$$= \sum_{\alpha,j} \mu_\alpha E_j^{(\alpha)} e^{i\omega_j t},$$

where e is the electronic charge (taken to be positive), $\vec{r}$ is the position of the electron about the nucleus, and $\vec{\mu} = -e\vec{r}$ is the electric dipole moment. The perturbation matrix element is then

$$
\begin{aligned}
V_{ij} &= \langle \psi_j \mid V \mid \psi_i \rangle \\
&= \langle \psi_j \mid \vec{\mu} \cdot \vec{E} \mid \psi_i \rangle \\
&= \langle \psi_j \mid \sum_{\alpha,j} \mu_\alpha E_j^{(\alpha)} e^{i\omega_j t} \mid \psi_i \rangle \\
&= \sum_{\alpha,j} E_j^{(\alpha)} e^{i\omega_j t} \langle \psi_j \mid \mu_\alpha \mid \psi_i \rangle \\
&= \sum_{\alpha,j} E_j^{(\alpha)} e^{i\omega_j t} (\mu_\alpha)_{ij},
\end{aligned}
\tag{B.33}
$$

where the dipole matrix element is defined as

$$(\mu_\alpha)_{ij} = \langle \psi_j \mid \mu_\alpha \mid \psi_i \rangle. \tag{B.34}$$

The matrix of V then takes the form

$$
V = \begin{pmatrix}
0 & V_{12} & V_{13} \\
V_{21} & 0 & V_{23} \\
V_{31} & V_{32} & 0
\end{pmatrix}. \tag{B.35}
$$

Because the states of the system have a definite parity and because V is an odd operator, matrix elements taken between states of the same parity vanish, and therefore the diagonal elements of V are zero. In addition, we may choose the phase of the wave functions such that $\mu_{ij} = \mu_{ji}$.

We are interested in the polarization P given by

$$P_\alpha = N\mathrm{Tr}(\rho\mu_\alpha), \tag{B.36}$$

where we have used Eq. (B.8) in calculating the expectation value of $\vec{\mu}$. Let us deal for the time being with the dipole moment of a single electron, $\mathrm{Tr}(\rho\mu_\alpha)$, only later generalizing to the total polarization given in Eq. (B.36). We have

$$
\begin{aligned}
\langle\mu_\alpha\rangle &= \mathrm{Tr}(\rho\mu_\alpha) && \text{(B.37)}\\
&= \sum_{i,k}\rho_{ik}(\mu_\alpha)_{ki}\\
&= \rho_{12}(\mu_{11})_\alpha + \rho_{13}(\mu_{31})_\alpha + \rho_{21}(\mu_{12})_\alpha + \rho_{23}(\mu_{32})_\alpha + \rho_{31}(\mu_{13})_\alpha + \rho_{32}(\mu_{23})_\alpha\\
&= (\mu_{12})_\alpha(\rho_{12}+\rho_{12}^*) + (\mu_{13})_\alpha(\rho_{13}+\rho_{13}^*) + (\mu_{23})_\alpha(\rho_{23}+\rho_{23}^*)
\end{aligned}
$$

where we have used $\mu_{ii}=0$, $\mu_{ij}=\mu_{ji}$, and $\rho_{ij}=\rho_{ji}^*$. We are therefore left with the conceptually simple task of calculating to third order each of the elements ρ_{12}, ρ_{13}, and ρ_{32}.

Since the requisite algebra to climb to the heights of third order in the density matrix expansion is quite involved and not particularly instructive past a certain point, our approach will be to do a few calculations to sample the mechanics of the process, and then to simply quote the remaining results, noting only the more interesting points.

Let us begin by considering ρ_{12}. From the integral equation for the ρ_{ij} in Eq. (B.30) we have

$$
\rho_{12}^{(1)} = -\frac{i}{\hbar}e^{-i(\omega_{12}-i\Gamma_{12})t}\int_{-\infty}^{t} e^{i(\omega_{12}-i\Gamma_{12})t'}\left[V,\rho^{(0)}\right]_{12}(t')\,dt'. \qquad \text{(B.38)}
$$

Focussing attention on the commutator

$$
\left[V,\rho^{(0)}\right]_{12} =
\left[
\begin{pmatrix}
0 & V_{12} & V_{13}\\
V_{21} & 0 & V_{23}\\
V_{31} & V_{32} & 0
\end{pmatrix}
\begin{pmatrix}
\bar\rho_{11}^{(0)} & 0 & 0\\
0 & 0 & 0\\
0 & 0 & 0
\end{pmatrix}
\right.
\qquad \text{(B.39)}
$$
$$
\left.
- \begin{pmatrix}
\bar\rho_{11}^{(0)} & 0 & 0\\
0 & 0 & 0\\
0 & 0 & 0
\end{pmatrix}
\begin{pmatrix}
0 & V_{12} & V_{13}\\
V_{21} & 0 & V_{23}\\
V_{31} & V_{32} & 0
\end{pmatrix}
\right]_{12}
$$

$$= -\bar{\rho}_{11}^{(0)} V_{12},$$

where in the form of $\rho^{(0)}$ we see a reflection of the assumption that only level 1 has a thermal equilibrium population. Substitution of this into the integral equation Eq. (B.38) for $\rho_{12}^{(1)}$ and using the form of V_{12} in by Eq. (B.33) gives

$$
\begin{aligned}
\rho_{12}^{(1)} &= \frac{i\bar{\rho}_{11}^{(0)}}{\hbar} e^{-i(\omega_{12}-i\Gamma_{12})t} \sum_{\alpha,j} (\mu_\alpha)_{12} E_j^{(\alpha)} \int_{-\infty}^{t} e^{i(\omega_{12}+\omega_j-i\Gamma_{12})t'} dt' \qquad (\text{B.40}) \\
&= \frac{\bar{\rho}_{11}^{(0)}}{\hbar} \sum_{\alpha,j} \frac{(\mu_\alpha)_{12} E_j^{(\alpha)} e^{i\omega_j t}}{(\omega_{12}+\omega_j-i\Gamma_{12})}.
\end{aligned}
$$

Similar operations for $\rho_{13}^{(1)}$ lead to

$$\rho_{13}^{(1)} = \frac{\bar{\rho}_{11}^{(0)}}{\hbar} \sum_{\alpha,j} \frac{(\mu_\alpha)_{13} E_j^{(\alpha)} e^{i\omega_j t}}{(\omega_{13}+\omega_j-i\Gamma_{13})}, \qquad (\text{B.41})$$

and

$$\rho_{23}^{(1)} = 0, \qquad (\text{B.42})$$

since $[V,\rho^{(0)}]_{23} = 0$. This completes the calculation of the required first order terms and leaves us with the first order density matrix

$$\rho^{(1)} = \begin{pmatrix} 0 & \rho_{12}^{(1)} & \rho_{13}^{(1)} \\ \rho_{21}^{(1)} & 0 & 0 \\ \rho_{31}^{(1)} & 0 & 0 \end{pmatrix}. \qquad (\text{B.43})$$

As a final example of how to calculate the $\rho_{ij}^{(n)}$ let us consider a second order term, $\rho_{12}^{(2)}$. Referring to the integral equation for the $\rho_{ij}^{(n)}$ in Eq. (B.30) we have

$$
\begin{aligned}
\rho_{12}^{(2)} &= -\frac{i}{\hbar} e^{-i(\omega_{12}-i\Gamma_{12})t} \int_{-\infty}^{t} e^{i(\omega_{12}-i\Gamma_{12})t'} \left[V,\rho^{(1)}\right]_{12}(t') dt' \qquad (\text{B.44}) \\
&= -\frac{i}{\hbar} e^{-i(\omega_{12}-i\Gamma_{12})t} \int_{-\infty}^{t} e^{i(\omega_{12}-i\Gamma_{12})t'} (-V_{32}\rho_{31}^{(1)}) dt'
\end{aligned}
$$

$$= -\frac{i}{\hbar}e^{-i(\omega_{12}-i\Gamma_{12})t}\int_{-\infty}^{t}e^{i(\omega_{12}-i\Gamma_{12})t'}\Theta(t)\,dt'$$

$$= -\frac{\bar{\rho}_{11}^{(0)}}{\hbar^2}\sum_{\alpha,\beta,j,k}\frac{(\mu_\alpha)_{32}(\mu_\beta)_{13}E_j^{(\alpha)}E_k^{(\beta)}e^{i(\omega_j+\omega_k)t}}{(\omega_{12}+\omega_j+\omega_k-i\Gamma_{12})(\omega_{31}+\omega_j-i\Gamma_{31})},$$

where

$$\Theta(t) = \bar{\rho}_{11}^{(0)}\sum_{j,k,\alpha,\beta}\frac{(\mu_\alpha)_{32}(\mu_\beta)_{13}E_j^{(\alpha)}E_k^{(\beta)}e^{i(\omega_j+\omega_k)t}}{(\omega_{31}+\omega_j-i\Gamma_{31})}. \tag{B.45}$$

Similar operations yield for the remaining second order terms

$$\rho_{13}^{(2)} = \frac{\bar{\rho}_{11}^{(0)}}{\hbar^2}\sum_{\alpha,\beta,j,k}\frac{(\mu_\alpha)_{12}(\mu_\beta)_{23}E_j^{(\alpha)}E_k^{(\beta)}e^{i(\omega_j+\omega_k)t}}{(\omega_{13}+\omega_j+\omega_k-i\Gamma_{13})(\omega_{12}+\omega_j-i\Gamma_{12})}, \tag{B.46}$$

and

$$\rho_{23}^{(2)} = -\frac{\bar{\rho}_{11}^{(0)}}{\hbar^2}\sum_{\alpha,\beta,j,k}\frac{(\mu_\alpha)_{12}(\mu_\beta)_{13}E_j^{(\alpha)}E_k^{(\beta)}[\omega_{21}+\omega_{13}+2\omega_j-i(\Gamma_{13}+\Gamma_{21})]e^{i(\omega_j+\omega_k)t}}{(\omega_{23}+\omega_j+\omega_k-i\Gamma_{23})(\omega_{13}+\omega_j-i\Gamma_{13})(\omega_{21}+\omega_j-i\Gamma_{21})}. \tag{B.47}$$

Similar operations give for the third order terms

$$\rho_{12}^{(3)} = -\frac{\bar{\rho}_{11}^{(0)}}{\hbar^3}\sum_{\alpha,\beta,\gamma,j,k,l}\frac{(\mu_\gamma)_{12}E_j^{(\alpha)}E_k^{(\beta)}E_l^{(\gamma)}}{(\omega_{12}+\omega_j+\omega_k+\omega_l-i\Gamma_{12})} \times \tag{B.48}$$

$$\left[\frac{2(\mu_\alpha)_{12}(\mu_\beta)_{12}(\omega_j-i\Gamma_{12})}{(\omega_j+\omega_k-iK_2)[\omega_{12}^2-i(\omega_j-i\Gamma_{12})^2]}\right.$$

$$-\frac{(\mu_\alpha)_{13}(\mu_\beta)_{13}[\omega_{12}+\omega_{13}+2\omega_j-i(\Gamma_{13}+\Gamma_{12})]}{(\omega_{32}+\omega_j+\omega_k-i\Gamma_{32})(\omega_{12}+\omega_j-i\Gamma_{12})(\omega_{31}+\omega_j-i\Gamma_{13})}$$

$$-\frac{(\mu_\alpha)_{23}(\mu_\beta)_{23}}{(\omega_{13}+\omega_j+\omega_k-i\Gamma_{13})(\omega_{12}+\omega_j-i\Gamma_{12})}$$

$$\left.+\frac{2(\mu_\alpha)_{12}(\mu_\beta)_{12}(\omega_j-i\Gamma_{12})}{(\omega_j+\omega_k-iK_1)[\omega_{12}^2-(\omega_j-i\Gamma_{12})^2]}\right]e^{i(\omega_j+\omega_k+\omega_l)t},$$

$$\rho_{13}^{(3)} = -\frac{\bar{\rho}_{11}^{(0)}}{\hbar^3}\sum_{\alpha,\beta,\gamma,j,k,l}\frac{(\mu_\gamma)_{13}E_j^{(\alpha)}E_k^{(\beta)}E_l^{(\gamma)}}{(\omega_{13}+\omega_j+\omega_k+\omega_l-i\Gamma_{13})} \times \tag{B.49}$$

$$\left[\frac{2(\mu_\alpha)_{13}(\mu_\beta)_{13}(\omega_j-i\Gamma_{13})}{(\omega_j+\omega_k-iK_3)[\omega_{13}^2-i(\omega_j-i\Gamma_{13})^2]}\right.$$

$$-\frac{(\mu_\alpha)_{12}(\mu_\beta)_{12}[\omega_{21} + \omega_{13} + 2\omega_j - i(\Gamma_{13} + \Gamma_{12})]}{(\omega_{23} + \omega_j + \omega_k - i\Gamma_{23})(\omega_{13} + \omega_j - i\Gamma_{13})(\omega_{21} + \omega_j - i\Gamma_{21})}$$

$$+\frac{(\mu_\alpha)_{32}(\mu_\beta)_{32}}{(\omega_{12} + \omega_j + \omega_k - i\Gamma_{12})(\omega_{31} + \omega_j - i\Gamma_{31})}$$

$$\left. +\frac{2(\mu_\alpha)_{12}(\mu_\beta)_{12}(\omega_j - i\Gamma_{12})}{(\omega_j + \omega_k - iK_1)[\omega_{12}^2 - (\omega_j - i\Gamma_{12})^2]} \right] e^{i(\omega_j + \omega_k + \omega_l)t},$$

and

$$\rho_{13}^{(3)} = \frac{\bar\rho_{11}^{(0)}}{\hbar^3} \sum_{\alpha,\beta,\gamma,j,k,l} \frac{(\mu_\gamma)_{32} E_j^{(\alpha)} E_k^{(\beta)} E_l^{(\gamma)}}{(\omega_{32} + \omega_j + \omega_k + \omega_l - i\Gamma_{32})} \times \tag{B.50}$$

$$\left[\frac{(\mu_\alpha)_{31}(\mu_\beta)_{31}}{(\omega_{12} + \omega_j + \omega_k - i\Gamma_{12})(\omega_{31} + \omega_j - i\Gamma_{31})} \right.$$

$$-\frac{2(\mu_\alpha)_{12}(\mu_\beta)_{12}(\omega_j - i\Gamma_{12})}{(\omega_j + \omega_k - iK_2)[\omega_{12}^2 - (\omega_j - i\Gamma_{12})^2]}$$

$$+\frac{(\mu_\alpha)_{12}(\mu_\beta)_{12}}{(\omega_{31} + \omega_j + \omega_k - i\Gamma_{31})(\omega_{21} + \omega_j - i\Gamma_{21})}$$

$$\left. +\frac{2(\mu_\alpha)_{13}(\mu_\beta)_{13}(\omega_j - i\Gamma_{13})}{(\omega_j + \omega_k - iK_3)[\omega_{13}^2 - (\omega_j - i\Gamma_{13})^2]} \right] e^{i(\omega_j + \omega_k + \omega_l)t},$$

where K_i is the decay rate of level i.

To illustrate how one might extract the elements of the second order nonlinear susceptibility tensor for a given process let us consider the second order effect of difference frequency mixing. Assume that the input optical field has two Fourier frequency components, ω_2 and ω_3, which are nearly in resonance with levels 2 and 3, respectively, and that $\omega_3 - \omega_2 \approx \omega_{32}$. Keeping only those terms oscillating at $\omega = \omega_3 - \omega_2$, we find for $\rho_{12}^{(2)}$ of Eq. (B.44)

$$\rho_{12}^{(2)}(\omega) = -\frac{\bar\rho_{11}^{(0)}}{\hbar^2} \sum_{\alpha,\beta} \frac{(\mu_\alpha)_{32}(\mu_\beta)_{13}}{(\omega_{12} + \omega - i\Gamma_{12})} \times \tag{B.51}$$

$$\left[\frac{E_3^{(\alpha)} E_{-2}^{(\beta)}}{(\omega_{31} + \omega_3 - i\Gamma_{31})} + \frac{E_{-2}^{(\alpha)} E_3^{(\beta)}}{(\omega_{31} - \omega_2 - i\Gamma_{31})} \right] e^{i\omega t}.$$

A similar procedure yields for the $\rho_{13}^{(2)}$ term

$$\rho_{13}^{(2)}(\omega) = \frac{\bar\rho_{11}^{(0)}}{\hbar^2} \sum_{\alpha,\beta} \frac{(\mu_\alpha)_{12}(\mu_\beta)_{23}}{(\omega_{13} + \omega - i\Gamma_{13})} \times \tag{B.52}$$

$$\left[\frac{E_3^{(\alpha)} E_{-2}^{(\beta)}}{(\omega_{12} + \omega_3 - i\Gamma_{12})} + \frac{E_{-2}^{(\alpha)} E_3^{(\beta)}}{(\omega_{12} - \omega_2 - i\Gamma_{12})} \right] e^{i\omega t}.$$

Finally, for the $\rho_{23}^{(2)}$ term we have

$$\rho_{23}^{(2)}(\omega) \approx -\frac{\bar{\rho}_{11}^{(0)}}{\hbar^2} \sum_{\alpha,\beta} \frac{(\mu_\alpha)_{12}(\mu_\beta)_{13}}{(\omega_{23} + \omega - i\Gamma_{23})} \times \tag{B.53}$$

$$\left[\frac{E_3^{(\alpha)} E_{-2}^{(\beta)}}{(\omega_{13} + \omega_3 - i\Gamma_{13})} + \frac{E_{-2}^{(\alpha)} E_3^{(\beta)}}{(\omega_{21} - \omega_2 - i\Gamma_{21})} \right] e^{i\omega t},$$

where we retain only near-resonant denominators in the square brackets.

Let us now make two additional simplifying assumptions. First, let the optical fields be linearly polarized, and second, apply the fields such that $E_3^{(y)} = E_3^{(z)} = E_{-2}^{(x)} = E_{-2}^{(z)} = 0$. Carrying out the sums over α and β for these three terms we find

$$\rho_{12}^{(2)}(\omega) = -\frac{\bar{\rho}_{11}^{(0)}}{\hbar^2(\omega_{12} + \omega - i\Gamma_{12})} \times \tag{B.54}$$

$$\left[\frac{(\mu_x)_{32}(\mu_y)_{13}}{(\omega_{31} + \omega_3 - i\Gamma_{31})} + \frac{(\mu_x)_{13}(\mu_y)_{32}}{(\omega_{31} - \omega_2 - i\Gamma_{31})} \right] E_3^{(x)} E_{-2}^{(y)} e^{i\omega t},$$

$$\rho_{13}^{(2)}(\omega) = -\frac{\bar{\rho}_{11}^{(0)}}{\hbar^2(\omega_{13} + \omega - i\Gamma_{13})} \times \tag{B.55}$$

$$\left[\frac{(\mu_x)_{12}(\mu_y)_{23}}{(\omega_{12} + \omega_3 - i\Gamma_{12})} + \frac{(\mu_x)_{23}(\mu_y)_{12}}{(\omega_{12} - \omega_2 - i\Gamma_{12})} \right] E_3^{(x)} E_{-2}^{(y)} e^{i\omega t},$$

and

$$\rho_{23}^{(2)}(\omega) \approx -\frac{\bar{\rho}_{11}^{(0)}}{\hbar^2(\omega_{23} + \omega - i\Gamma_{23})} \times \tag{B.56}$$

$$\left[\frac{(\mu_x)_{12}(\mu_y)_{13}}{(\omega_{13} + \omega_3 - i\Gamma_{13})} + \frac{(\mu_x)_{13}(\mu_y)_{12}}{(\omega_{21} - \omega_2 - i\Gamma_{21})} \right] E_3^{(x)} E_{-2}^{(y)} e^{i\omega t}.$$

Suppose that we are now interested in the induced polarization oscillating at ω along, say, the x direction. From the expression for the polarization in Eq. (B.36) we have

$$P_x^{(2)}(\omega) = N[\rho_{12}^{(2)}(\mu_x)_{21} + \rho_{13}^{(2)}(\mu_x)_{31} + \rho_{23}^{(2)}(\mu_x)_{32}] + c.c. \tag{B.57}$$

$$= -\frac{N\bar{\rho}_{11}^{(0)}}{\hbar^2}\left\{\frac{(\mu_x)_{21}}{\omega_{12}+\omega-i\Gamma_{12}}\left[\frac{(\mu_x)_{32}(\mu_y)_{13}}{\omega_{31}+\omega_3-i\Gamma_{31}} + \frac{(\mu_x)_{13}(\mu_y)_{32}}{\omega_{31}-\omega_2-i\Gamma_{31}}\right]\right.$$
$$+\frac{(\mu_x)_{31}}{\omega_{13}+\omega-i\Gamma_{13}}\left[\frac{(\mu_x)_{12}(\mu_y)_{23}}{\omega_{12}+\omega_3-i\Gamma_{12}} + \frac{(\mu_x)_{23}(\mu_y)_{12}}{\omega_{12}-\omega_2-i\Gamma_{12}}\right]$$
$$\left.+\frac{(\mu_x)_{32}}{\omega_{23}+\omega-i\Gamma_{23}}\left[\frac{(\mu_x)_{12}(\mu_y)_{13}}{\omega_{13}+\omega_3-i\Gamma_{13}} + \frac{(\mu_x)_{13}(\mu_y)_{12}}{\omega_{21}-\omega_2-i\Gamma_{21}}\right]\right\}E_3^{(x)}E_{-2}^{(y)}e^{i\omega t}$$
$$+ c.c.$$

Using $P_x^{(2)} = \sum_{j,k}\chi_{xjk}^{(2)}E^{(j)}E^{(k)}$, we proceed to make the identification

$$\chi_{xxy}^{(2)} = \chi_{xyx}^{(2)} \tag{B.58}$$

$$= -\frac{N\bar{\rho}_{11}^{(0)}}{\hbar^2}\left\{\frac{(\mu_x)_{21}}{\omega_{12}+\omega-i\Gamma_{12}}\left[\frac{(\mu_x)_{32}(\mu_y)_{13}}{\omega_{31}+\omega_3-i\Gamma_{31}} + \frac{(\mu_x)_{13}(\mu_y)_{32}}{\omega_{31}-\omega_2-i\Gamma_{31}}\right]\right.$$
$$+\frac{(\mu_x)_{31}}{\omega_{13}+\omega-i\Gamma_{13}}\left[\frac{(\mu_x)_{12}(\mu_y)_{23}}{\omega_{12}+\omega_3-i\Gamma_{12}} + \frac{(\mu_x)_{23}(\mu_y)_{12}}{\omega_{12}-\omega_2-i\Gamma_{12}}\right]$$
$$\left.+\frac{(\mu_x)_{32}}{\omega_{23}+\omega-i\Gamma_{23}}\left[\frac{(\mu_x)_{12}(\mu_y)_{13}}{\omega_{13}+\omega_3-i\Gamma_{13}} + \frac{(\mu_x)_{13}(\mu_y)_{12}}{\omega_{21}-\omega_2-i\Gamma_{21}}\right]\right\} + c.c.$$

The permuting of the last xy on $\chi^{(2)}$ is permissible since it makes no physical sense to hold that field $E^{(x)}$ could be applied before (or after) field $E^{(y)}$.

Let us now take as an example third harmonic generation to show how to extract the elements of the third order nonlinear susceptibility tensor for this particular process. We will assume an input optical field with only one Fourier component ω_p, and, as with our discussion of difference frequency mixing, we shall focus only on those terms in $P^{(3)}$ of interest, namely those oscillating at $3\omega_p$. Let us also assume that as in the previous case the optical electric field is linearly polarized and contains only an x component. That is, $E^{(y)} = E^{(z)} = 0$. From Eq. (B.48) for $\rho_{12}^{(3)}$ we have for the terms oscillating at $3\omega_p$

$$\rho_{12}^{(3)}(3\omega_p) = -\frac{\bar{\rho}_{11}^{(0)}}{\hbar^3(\omega_{12}+3\omega_p-i\Gamma_{12})} \times \tag{B.59}$$

$$\left\{ \frac{2(\mu_x)_{12}(\mu_x)_{12}(\mu_x)_{12}(\omega_p - i\Gamma_{12})}{(2\omega_p - iK_2)[\omega_{12}^2 - (\omega_p - i\Gamma_{12})^2]} \right.$$

$$- \frac{(\mu_x)_{12}(\mu_x)_{13}(\mu_x)_{13}[\omega_{12} + \omega_{13} + 2\omega_p - i(\Gamma_{13} + \Gamma_{12})]}{(\omega_{32} + 2\omega_p - i\Gamma_{32})(\omega_{12} + \omega_p - i\Gamma_{12})(\omega_{31} + \omega_p - i\Gamma_{31})}$$

$$- \frac{(\mu_x)_{12}(\mu_x)_{32}(\mu_x)_{32}}{(\omega_{12} + \omega_p - i\Gamma_{12})(\omega_{13} + 2\omega_p - i\Gamma_{13})}$$

$$\left. - \frac{2(\mu_x)_{12}(\mu_x)_{12}(\mu_x)_{12}(\omega_p - i\Gamma_{12})}{(2\omega_p - iK_1)[\omega_{12}^2 - (\omega_p - i\Gamma_{12})^2]} \right\} E^{(x)} E^{(x)} E^{(x)} e^{3i\omega_p t}.$$

For the corresponding terms in $\rho_{13}^{(3)}$ we have

$$\rho_{13}^{(3)}(3\omega_p) = -\frac{\bar{\rho}_{11}^{(0)}}{\hbar^3(\omega_{13} + 3\omega_p - i\Gamma_{13})} \times \tag{B.60}$$

$$\left\{ \frac{2(\mu_x)_{13}(\mu_x)_{13}(\mu_x)_{13}(\omega_p - i\Gamma_{13})}{(2\omega_p - iK_3)[\omega_{13}^2 - (\omega_p - i\Gamma_{13})^2]} \right.$$

$$- \frac{(\mu_x)_{13}(\mu_x)_{12}(\mu_x)_{12}[\omega_{21} + \omega_{13} + 2\omega_p - i(\Gamma_{13} + \Gamma_{21})]}{(\omega_{23} + 2\omega_p - i\Gamma_{23})(\omega_{13} + \omega_p - i\Gamma_{13})(\omega_{21} + \omega_p - i\Gamma_{21})}$$

$$+ \frac{(\mu_x)_{13}(\mu_x)_{32}(\mu_x)_{32}}{(\omega_{31} + \omega_p - i\Gamma_{31})(\omega_{12} + 2\omega_p - i\Gamma_{12})}$$

$$\left. + \frac{2(\mu_x)_{13}(\mu_x)_{12}(\mu_x)_{12}(\omega_p - i\Gamma_{12})}{(2\omega_p - iK_1)[\omega_{12}^2 - (\omega_p - i\Gamma_{12})^2]} \right\} E^{(x)} E^{(x)} E^{(x)} e^{3i\omega_p t}.$$

Finally, for the third harmonic term originating in $\rho_{23}^{(3)}$ we have

$$\rho_{32}^{(3)}(3\omega_p) = -\frac{\bar{\rho}_{11}^{(0)}}{\hbar^3(\omega_{32} + 3\omega_p - i\Gamma_{32})} \times \tag{B.61}$$

$$\left\{ -\frac{(\mu_x)_{32}(\mu_x)_{31}(\mu_x)_{31}}{(\omega_{31} + \omega - i\Gamma_{31})(\omega_{12} + 2\omega_p - i\Gamma_{12})} \right.$$

$$+ \frac{(\mu_x)_{32}(\mu_x)_{12}(\mu_x)_{12}(2\omega_p - i\Gamma_{12})}{(2\omega_p - iK_2)[\omega_{12}^2 - (\omega_p - i\Gamma_{12})^2]}$$

$$- \frac{(\mu_x)_{32}(\mu_x)_{12}(\mu_x)_{12}}{(\omega_{31} + 2\omega_p - i\Gamma_{31})(\omega_{21} + \omega_p - i\Gamma_{21})}$$

$$\left. - \frac{2(\mu_x)_{32}(\mu_x)_{13}(\mu_x)_{13}(\omega_p - i\Gamma_{13})}{(2\omega_p - iK_3)[\omega_{13}^2 - (\omega_p - i\Gamma_{13})^2]} \right\} E^{(x)} E^{(x)} E^{(x)} e^{3i\omega_p t}.$$

If we are interested in, for example, the x component of the polarization P oscillating at $3\omega_p$, we have

$$P_x^{(3)}(3\omega_p) = N[\rho_{12}^{(3)}(\mu_x)_{21} + \rho_{13}^{(3)}(\mu_x)_{31} + \rho_{32}^{(3)}(\mu_x)_{23}] + c.c. \tag{B.62}$$

Using the results just obtained for the third harmonic terms in $\rho_{ij}^{(3)}$ above we can write for the polarization

$$
\begin{aligned}
P_x^{(3)}(3\omega_p) = \frac{-N\bar{\rho}_{11}^{(0)}}{\hbar^3} \Bigg\{ & \frac{(\mu_x)_{21}}{(\omega_{12} + 3\omega_p - i\Gamma_{12})} \times \\
& \left[\frac{2(\mu_x)_{12}(\mu_x)_{12}(\mu_x)_{12}(\omega_p - i\Gamma_{12})}{(2\omega_p - iK_2)[\omega_{12}^2 - (\omega_p - i\Gamma_{12})^2]} \right. \\
& - \frac{(\mu_x)_{12}(\mu_x)_{13}(\mu_x)_{13}[\omega_{12} + \omega_{13} + 2\omega_p - i(\Gamma_{13} + \Gamma_{12})]}{(\omega_{32} + 2\omega_p - i\Gamma_{32})(\omega_{12} + \omega_p - i\Gamma_{12})(\omega_{31} + \omega_p - i\Gamma_{31})} \\
& - \frac{(\mu_x)_{12}(\mu_x)_{32}(\mu_x)_{32}}{(\omega_{12} + \omega_p - i\Gamma_{12})(\omega_{13} + 2\omega_p - i\Gamma_{13})} \\
& \left. - \frac{2(\mu_x)_{12}(\mu_x)_{12}(\mu_x)_{12}(\omega_p - i\Gamma_{12})}{(2\omega_p - iK_1)[\omega_{12}^2 - (\omega_p - i\Gamma_{12})^2]} \right] \\
& + \frac{(\mu_x)_{31}}{(\omega_{13} + 3\omega_p - i\Gamma_{13})} \left[\frac{2(\mu_x)_{13}(\mu_x)_{13}(\mu_x)_{13}(\omega_p - i\Gamma_{13})}{(2\omega_p - iK_3)[\omega_{13}^2 - (\omega_p - i\Gamma_{13})^2]} \right. \\
& - \frac{(\mu_x)_{13}(\mu_x)_{12}(\mu_x)_{12}[\omega_{21} + \omega_{13} + 2\omega_p - i(\Gamma_{13} + \Gamma_{21})]}{(\omega_{23} + 2\omega_p - i\Gamma_{23})(\omega_{13} + \omega_p - i\Gamma_{13})(\omega_{21} + \omega_p - i\Gamma_{21})} \\
& + \frac{(\mu_x)_{13}(\mu_x)_{32}(\mu_x)_{32}}{(\omega_{31} + \omega_p - i\Gamma_{31})(\omega_{12} + 2\omega_p - i\Gamma_{12})} \\
& \left. + \frac{2(\mu_x)_{13}(\mu_x)_{12}(\mu_x)_{12}(\omega_p - i\Gamma_{12})}{(2\omega_p - iK_1)[\omega_{12}^2 - (\omega_p - i\Gamma_{12})^2]} \right] \\
& + \frac{(\mu_x)_{32}}{(\omega_{32} + 3\omega_p - i\Gamma_{32})} \left[-\frac{(\mu_x)_{32}(\mu_x)_{31}(\mu_x)_{31}}{(\omega_{31} + \omega - i\Gamma_{31})(\omega_{12} + 2\omega_p - i\Gamma_{12})} \right. \\
& + \frac{(\mu_x)_{32}(\mu_x)_{12}(\mu_x)_{12}(2\omega_p - i\Gamma_{12})}{(2\omega_p - iK_2)[\omega_{12}^2 - (\omega_p - i\Gamma_{12})^2]} \\
& - \frac{(\mu_x)_{32}(\mu_x)_{12}(\mu_x)_{12}}{(\omega_{31} + 2\omega_p - i\Gamma_{31})(\omega_{21} + \omega_p - i\Gamma_{21})} \\
& \left. \left. - \frac{2(\mu_x)_{32}(\mu_x)_{13}(\mu_x)_{13}(\omega_p - i\Gamma_{13})}{(2\omega_p - iK_3)[\omega_{13}^2 - (\omega_p - i\Gamma_{13})^2]} \right] \right\} E^{(x)}E^{(x)}E^{(x)}e^{3i\omega_p t} \\
& + c.c.,
\end{aligned}
$$

$(B.63)$

from which we can make the identification

$$
\chi_{xxxx}^{(3)}(3\omega_p) = \frac{-N\bar{\rho}_{11}^{(0)}}{\hbar^3} \left\{ \frac{(\mu_x)_{21}}{(\omega_{12} + 3\omega_p - i\Gamma_{12})} \times \right.
$$

$$
\left[\frac{2(\mu_x)_{12}(\mu_x)_{12}(\mu_x)_{12}(\omega_p - i\Gamma_{12})}{(2\omega_p - iK_2)[\omega_{12}^2 - (\omega_p - i\Gamma_{12})^2]} \right.
$$

$$
- \frac{(\mu_x)_{12}(\mu_x)_{13}(\mu_x)_{13}[\omega_{12} + \omega_{13} + 2\omega_p - i(\Gamma_{13} + \Gamma_{12})]}{(\omega_{32} + 2\omega_p - i\Gamma_{32})(\omega_{12} + \omega_p - i\Gamma_{12})(\omega_{31} + \omega_p - i\Gamma_{31})}
$$

$$
- \frac{(\mu_x)_{12}(\mu_x)_{32}(\mu_x)_{32}}{(\omega_{12} + \omega_p - i\Gamma_{12})(\omega_{13} + 2\omega_p - i\Gamma_{13})}
$$

$$
\left. - \frac{2(\mu_x)_{12}(\mu_x)_{12}(\mu_x)_{12}(\omega_p - i\Gamma_{12})}{(2\omega_p - iK_1)[\omega_{12}^2 - (\omega_p - i\Gamma_{12})^2]} \right]
$$

$$
+ \frac{(\mu_x)_{31}}{(\omega_{13} + 3\omega_p - i\Gamma_{13})} \left[\frac{2(\mu_x)_{13}(\mu_x)_{13}(\mu_x)_{13}(\omega_p - i\Gamma_{13})}{(2\omega_p - iK_3)[\omega_{13}^2 - (\omega_p - i\Gamma_{13})^2]} \right.
$$

$$
- \frac{(\mu_x)_{13}(\mu_x)_{12}(\mu_x)_{12}[\omega_{21} + \omega_{13} + 2\omega_p - i(\Gamma_{13} + \Gamma_{21})]}{(\omega_{23} + 2\omega_p - i\Gamma_{23})(\omega_{13} + \omega_p - i\Gamma_{13})(\omega_{21} + \omega_p - i\Gamma_{21})}
$$

$$
+ \frac{(\mu_x)_{13}(\mu_x)_{32}(\mu_x)_{32}}{(\omega_{31} + \omega_p - i\Gamma_{31})(\omega_{12} + 2\omega_p - i\Gamma_{12})}
$$

$$
\left. + \frac{2(\mu_x)_{13}(\mu_x)_{12}(\mu_x)_{12}(\omega_p - i\Gamma_{12})}{(2\omega_p - iK_1)[\omega_{12}^2 - (\omega_p - i\Gamma_{12})^2]} \right]
$$

$$
+ \frac{(\mu_x)_{32}}{(\omega_{32} + 3\omega_p - i\Gamma_{32})} \left[-\frac{(\mu_x)_{32}(\mu_x)_{31}(\mu_x)_{31}}{(\omega_{31} + \omega - i\Gamma_{31})(\omega_{12} + 2\omega_p - i\Gamma_{12})} \right.
$$

$$
+ \frac{(\mu_x)_{32}(\mu_x)_{12}(\mu_x)_{12}(2\omega_p - i\Gamma_{12})}{(2\omega_p - iK_2)[\omega_{12}^2 - (\omega_p - i\Gamma_{12})^2]}
$$

$$
- \frac{(\mu_x)_{32}(\mu_x)_{12}(\mu_x)_{12}}{(\omega_{31} + 2\omega_p - i\Gamma_{31})(\omega_{21} + \omega_p - i\Gamma_{21})}
$$

$$
\left. \left. - \frac{2(\mu_x)_{32}(\mu_x)_{13}(\mu_x)_{13}(\omega_p - i\Gamma_{13})}{(2\omega_p - iK_3)[\omega_{13}^2 - (\omega_p - i\Gamma_{13})^2]} \right] \right\}
$$

$$
+ \text{c.c.}
$$

APPENDIX C

MAXWELL'S EQUATIONS

MAXWELL'S EQUATIONS

In this section we will briefly review Maxwell's equations, using MKS units throughout. They are

$$\vec{\nabla} \times \vec{E} = -\frac{\partial \vec{B}}{\partial t} \qquad \text{(Faraday's law)} \qquad \text{(C.1)}$$

$$\vec{\nabla} \times \vec{H} = \frac{\partial \vec{D}}{\partial t} + \vec{j} \qquad \text{(Ampere's law)} \qquad \text{(C.2)}$$

$$\vec{\nabla} \cdot \vec{D} = \rho \qquad \text{(Poisson's equation)} \qquad \text{(C.3)}$$

$$\vec{\nabla} \cdot \vec{B} = 0. \qquad \text{(no name)} \qquad \text{(C.4)}$$

for electric field E, magnetic induction $\vec{B} = \mu\vec{H} = \mu_0(\vec{H} + \vec{M})$, magnetization $\vec{M}$ (density of magnetic dipoles), polarization P (density of electric dipoles), $\vec{D} = \epsilon_0\vec{E} + \vec{P}$ is the electric displacement, and ρ and $\vec{j}$ are the charge and current densities, respectively. ρ and $\vec{j}$ are related by the continuity equation

$$\vec{\nabla} \cdot \vec{j} = -\frac{\partial \rho}{\partial t}. \qquad \text{(C.5)}$$

The linear polarization $\vec{P}_L$ is related to the electric field by

$$\vec{P}_L = \epsilon_0 \chi^{(1)} \vec{E}, \qquad \text{(C.6)}$$

where $\chi^{(1)}$ is the linear susceptibility and the dielectric constant is given by

$$\epsilon = \epsilon_0(1 + \chi^{(1)}). \qquad \text{(C.7)}$$

The nonlinear polarization is made up of terms such as

$$\vec{P}_{NL} = \chi^{(2)} \vec{E}\vec{E} + \chi^{(3)} \vec{E}\vec{E}\vec{E} + \ldots, \qquad (C.8)$$

where the $\chi^{(n)}$ are the nonlinear susceptibility tensors.

Taking the curl of both sides of Faraday's Law in Eq. (C.1), we get, assuming a nonmagnetic material ($\vec{M} = 0$),

$$\vec{\nabla} \times \vec{\nabla} \times \vec{E} = -\vec{\nabla} \times \mu_0 \frac{\partial \vec{H}}{\partial t}. \qquad (C.9)$$

Using the vector identity

$$\vec{\nabla} \times \vec{\nabla} \times \vec{E} = \vec{\nabla}(\vec{\nabla} \cdot \vec{E}) - \vec{\nabla}^2 \vec{E}, \qquad (C.10)$$

we get for a charge-free region of space ($\vec{\nabla} \cdot \vec{E} = 0$)

$$\vec{\nabla}^2 \vec{E} = \mu_0 \frac{\partial}{\partial t}\left(\vec{\nabla} \times \vec{H}\right). \qquad (C.11)$$

Ampere's law in Eq. (C.2) may be recast as

$$\vec{\nabla} \times \vec{H} = \sigma \vec{E} + \frac{\partial \epsilon \vec{E}}{\partial t} + \frac{\partial \vec{P}_{NL}}{\partial t}, \qquad (C.12)$$

where we have used Eqs. (C.6) and (C.7), and assumed an ohmic conductor ($\vec{j} = \sigma \vec{E}$). Substituting this last equation for curl H into Eq. (C.11) we find

$$\vec{\nabla}^2 \vec{E} = \mu_0 \sigma \frac{\partial \vec{E}}{\partial t} + \mu_0 \epsilon \frac{\partial^2 \vec{E}}{\partial t^2} + \mu_0 \frac{\partial^2 \vec{P}_{NL}}{\partial t^2} \qquad (C.13)$$

which shows how a nonlinear polarization $\vec{P}_{NL}$ can act as a driving term for the wave equation in $\vec{E}$.

On a slightly different note, the electric field $\vec{E}$ is related to the electrostatic scalar potential ϕ by

$$\vec{E} = -\vec{\nabla}\phi. \qquad (C.14)$$

Since the divergence of $\vec{B}$ is zero we can define a vector potential $\vec{A}$ such that

$$\vec{B} = \vec{\nabla} \times \vec{A}, \tag{C.15}$$

where we note that $\vec{\nabla} \cdot \vec{\nabla} \times \vec{G} = 0$ for any vector function $\vec{G}$. Substituting this expression for $\vec{B}$ from Eq. (C.15) into the expression for the curl of $\vec{E}$ in Eq. (C.1) we have

$$\begin{aligned} \vec{\nabla} \times \vec{E} &= -\frac{\partial}{\partial t}(\vec{\nabla} \times \vec{A}) \\ &= -\vec{\nabla} \times \left(\frac{\partial A}{\partial t}\right) \end{aligned} \tag{C.16}$$

or

$$\vec{\nabla} \times \left(\vec{E} + \frac{\partial A}{\partial t}\right) = 0, \tag{C.17}$$

from which follows

$$\vec{E} = -\frac{\partial A}{\partial t} \tag{C.18}$$

Finally, we might note that the first of Maxwell's equations involving the curl of $\vec{E}$ is satisfied by an electric field to which has been added the gradient of an arbitrary scalar function ψ, since we always have $\vec{\nabla} \times \vec{\nabla}\psi = 0$. Thus, for generality, we let the new $\vec{E}$ be

$$\vec{E} = -\frac{\partial A}{\partial t} - \vec{\nabla}\psi \tag{C.19}$$

APPENDIX D

ELECTRIC DIPOLE APPROXIMATION

ELECTRIC DIPOLE APPROXIMATION

In this section we will derive the electric dipole interaction Hamiltonian. Throughout this discussion, the charge on the electron is taken to be $-e$, where e is a positive number. We begin by writing the Lorentz force on an electron in an electromagnetic field

$$\vec{F} = -e\left[\vec{E} + (\vec{v} \times \vec{B})\right] \tag{D.1}$$

where $\vec{v}$ is the electron velocity. Referring to Appendix C on Maxwell's equations, let us substitute into the equation for the Lorentz force the expressions for $\vec{E}$ and $\vec{B}$ from Eqs. (C.19) and (C.15), respectively. This gives for $\vec{F}$

$$\vec{F} = -e\left[-\frac{\partial A}{\partial t} - \vec{\nabla}\psi + \vec{v} \times (\vec{\nabla} \times \vec{A})\right] \tag{D.2}$$

Using the vector identity

$$\vec{\nabla}(\vec{A} \cdot \vec{B}) = \vec{A} \times (\vec{\nabla} \times \vec{B}) + \vec{B} \times (\vec{\nabla} \times \vec{A}) + (\vec{A} \cdot \vec{\nabla})\vec{B} + (\vec{B} \cdot \vec{\nabla})\vec{A} \tag{D.3}$$

and noting that the velocity is a function of *time* but not *position*, we can recast the third term in the Lorentz force in Eq. (D.2) as

$$\vec{v} \times \vec{\nabla} \times \vec{A} = \vec{\nabla}(\vec{v} \cdot \vec{A}) - (\vec{v} \cdot \vec{\nabla})\vec{A}, \tag{D.4}$$

from which follows

$$\vec{F} = e\left[\frac{\partial A}{\partial t} + (\vec{v} \cdot \vec{\nabla})\vec{A} - \vec{\nabla}(\vec{v} \cdot \vec{A}) + \vec{\nabla}\psi\right] \tag{D.5}$$

The first two terms inside the square brackets evaluate to $d\vec{A}/dt$, and are collectively called the *convective derivative* of $\vec{A}$. To see this consider the time rate of change of $\vec{A}$ at the location of the moving particle. Suppose that at time t the particle is at point $\vec{r}$ where the potential is $\vec{A}(\vec{r},t)$, and a moment later it is at $(\vec{r}+\vec{v}\,dt)$, where the potential is $\vec{A}(\vec{r}+\vec{v}\,dt,t+dt)$. The change in $\vec{A}$, then, is

$$
\begin{aligned}
d\vec{A} &= \vec{A}(\vec{r}+\vec{v}\,dt,t+dt) - \vec{A}(\vec{r},t) && \text{(D.6)}\\
&= \left(\frac{\partial\vec{A}}{\partial x}\right)(v_x dt) + \left(\frac{\partial\vec{A}}{\partial y}\right)(v_y dt) + \left(\frac{\partial\vec{A}}{\partial z}\right)(v_z dt) + \left(\frac{\partial\vec{A}}{\partial t}\right)dt,
\end{aligned}
$$

or,

$$
\frac{d\vec{A}}{dt} = \frac{\partial\vec{A}}{\partial t} + (\vec{v}\cdot\vec{\nabla})\vec{A}. \tag{D.7}
$$

The Lorentz force equation then becomes

$$
\vec{F} = e\left[-\vec{\nabla}\left(\vec{v}\cdot\vec{A}-\psi\right) + \frac{d\vec{A}}{dt}\right]. \tag{D.8}
$$

We now associate the quantity

$$
U = e\left(\vec{v}\cdot\vec{A}-\psi\right) \tag{D.9}
$$

with the generalized potential We may then write the Lagrangian for this system as

$$
\begin{aligned}
L &= T - U && \text{(D.10)}\\
&= \frac{1}{2}m\vec{v}^{\,2} + e\psi - e\vec{v}\cdot\vec{A},
\end{aligned}
$$

for kinetic energy T. Recalling that the generalized momentum p_x is

$$
p_x = \frac{\partial L}{\partial \dot{q}_x}, \tag{D.11}
$$

where $\dot{q}_x = v_x$, we find

$$p_x = mv_x - eA_x \qquad (D.12)$$

and similarly for y and z. From the definition of the Hamiltonian

$$
\begin{aligned}
H &= \sum_i p_i \dot{q}_i - L \qquad (D.13)\\
&= \left(m\vec{v}^2 - e\vec{v} \cdot \vec{A} \right) - \left(\frac{m\vec{v}^2}{2} + e\psi - e\vec{v} \cdot \vec{A} \right)\\
&= \frac{m\vec{v}^2}{2} - e\psi.
\end{aligned}
$$

Using Eq. (D.12) for $\vec{v}$, we obtain

$$H = \frac{m}{2} \left(\vec{p} + e\vec{A} \right)^2 - e\psi, \qquad (D.14)$$

The vector potential seen by an electron varies, in general, from point to point in space. Given the relatively small size of the atom, however, the spatial variation of $\vec{A}$ over the dimensions of the atom is slight for the externally applied fields that will be of interest to us. We therefore expand the vector potential $\vec{A}$ about the nuclear position $\vec{R}$.

$$\vec{A}(\vec{R} + \vec{r}, t) = \vec{A}(\vec{R}, t) + (\vec{r} \cdot \vec{\nabla}_R)\vec{A}(\vec{R}, t) + \dots, \qquad (D.15)$$

where

$$\vec{\nabla}_R = \hat{i}\frac{\partial}{\partial R_x} + \hat{j}\frac{\partial}{\partial R_y} + \hat{k}\frac{\partial}{\partial R_z} \qquad (D.16)$$

and $\partial/\partial R_x$ denotes partial differentiation with respect to x evaluated at the nuclear position. The first term in the expansion when substituted into the Lagrangian of Eq. (D.10) yields

$$L = \frac{m\vec{v}^2}{2} + e\psi - e\dot{\vec{r}} \cdot \vec{A}(\vec{R}, t), \qquad (D.17)$$

noting that this approximation amounts to neglecting the spatial variation of $\vec{A}$ over atomic dimensions. Since a total time derivative can be added to the

Lagrangian without changing the equations of motion of the system *, a term of the form

$$e\frac{d}{dt}\left[\vec{r}\cdot\vec{A}(\vec{R},t)\right] \tag{D.18}$$

is added to L to give

$$L = \frac{m\vec{v}^{\,2}}{2} - V + e\psi + e\vec{r}\cdot\frac{d\vec{A}(\vec{R},t)}{dt}. \tag{D.19}$$

The corresponding Hamiltonian can be obtained from Eq. (D.13)

$$H = \frac{\vec{p}^{\,2}}{2m} + V - e\psi - e\vec{r}\cdot\frac{d\vec{A}(R,t)}{dt}, \tag{D.20}$$

where we have added a term $V(\vec{r})$ to account for the effective potential of the electron about the nucleus. With the appropriate choice of gauge transformations it is possible to choose the potential function so that the scalar ψ vanishes. We then refer back to the expression given by Eq. (C.18) relating the electric field $\vec{E}$ to the vector potential $\vec{A}$ to yield

$$H = \frac{\vec{p}^{2}}{2m} + V - \vec{\mu}\cdot\vec{E}(\vec{R},t), \tag{D.21}$$

where we have introduced the *dipole moment* $\vec{\mu} = -e\vec{r}$.

Therefore, the dipole moment term represents the interaction of the electromagnetic field with the atomic system when terms dependent on $\vec{r}$ in the multipole expansion of $\vec{A}$ in Eq. (D.15) can be neglected. This limiting case is referred to as the *electric dipole approximation.*

---

*See Appendix E.

APPENDIX E

HAMILTON'S PRINCIPLE

HAMILTON'S PRINCIPLE

We will show here that it is possible to add to the Lagrangian of a system a total derivative with respect to time without changing the equations of motion of the system.

The most general formulation of the law governing the motion of mechanical systems is taken to be *Hamilton's principle*, or the *principle of least action*, according to which every mechanical system is characterized by a definite function $L(q, \dot{q})$ and that the motion of the system is such that a certain condition is satisfied.

Let the system occupy, at the instants t_1 and t_2, positions defined by two set of values of the coordinates, $q^{(1)}$ and $q^{(2)}$. Then the condition is that the system moves between these positions in such a way that the integral

$$S = \int_{t_1}^{t^2} L(q, \dot{q}) \, dt \tag{E.1}$$

takes the least possible value. The function L is called the Lagrangian, and the integral is called the *action*. $q = q(t)$ and $\dot{q} = \dot{q}(t)$, are the generalized coordinate and velocity, respectively, at time t. Hamilton's principle states that the variation, which we denote by δ, of S is zero

$$\delta S = \delta \int_{t_1}^{t^2} L(q, \dot{q}) \, dt = 0, \tag{E.2}$$

where the function $q(t)$ is assumed to minimize S. We will first show that Lagrange's equations can be obtained from the variation of S, and then proceed to demonstrate that the addition of a total time derivative to L leaves those same equations unchanged.

Since S is minimized by the function $q(t)$, S is increased when q is replaced by any function of the form

$$q(t) + \delta q(t), \tag{E.3}$$

where $\delta q(t)$ is a function which is small everywhere in the interval of time from t_1 to t_2; $\delta q(t)$ is called the *variation* of the function $q(t)$. Since, for $t = t_1$ and $t = t_2$, the function in Eq. (E.3) must take the values $q^{(1)}$ and $q^{(2)}$, respectively, it follows that

$$\delta q(t_1) = \delta q(t_2) = 0. \tag{E.4}$$

Effecting the variation of S, we have

$$\begin{aligned}
\delta S &= \delta \int_{t_1}^{t_2} L(q, \dot{q})\, dt \\
&= \int_{t_1}^{t_2} \left(\frac{\partial L}{\partial q} \delta q + \frac{\partial L}{\partial \dot{q}} \delta \dot{q} \right) dt.
\end{aligned} \tag{E.5}$$

Noting that $\delta \dot{q} = (d/dt)\delta q$, we may integrate the second term in the integrand by parts as follows

$$\int_{t_1}^{t_2} \frac{\partial L}{\partial \dot{q}} \delta \dot{q}\, dt = \left[\frac{\partial L}{\partial \dot{q}} \delta q \right]_{t1}^{t_2} - \int_{t_1}^{t_2} \frac{d}{dt}\frac{\partial L}{\partial \dot{q}} \delta q\, dt. \tag{E.6}$$

From the equation for the variations of $q(t)$ in Eq. (E.4) we see that the integrated term on the right hand side vanishes. Combining the remaining integral with the first term in Eq. (E.5) for δS we have

$$\delta S = \int_{t_1}^{t_2} \left(\frac{\partial L}{\partial q} - \frac{d}{dt}\frac{\partial L}{\partial \dot{q}} \right) \delta q\, dt = 0. \tag{E.7}$$

Since this equation must be true for all δq, the integrand itself must vanish, and we have the familiar Lagrange's equations

$$\frac{\partial L}{\partial q} - \frac{d}{dt}\frac{\partial L}{\partial \dot{q}} = 0, \tag{E.8}$$

from which the equations of motion can be had.

We have now shown that the equations of motion can be obtained from the action S. What we now show is that the addition of a total derivative to the Lagrangian has no effect on the variation of S and therefore no effect on the equations of motion. We first transform L to the form

$$L \to L + \frac{dF(q, \dot{q})}{dt}, \tag{E.9}$$

for an arbitrary function $F(q, \dot{q})$. In terms of the variation of S, we postulate that

$$\delta \int_{t_1}^{t_2} L(q, \dot{q}) \, dt = \delta \int_{t_1}^{t_2} \left[L(q, \dot{q}) + \frac{dF(q, \dot{q})}{dt} \right] dt \tag{E.10}$$

Omitting the treatment of the original portion of the variation of S, we obtain for that part concerning dF/dt

$$
\begin{aligned}
\delta \int_{t_1}^{t_2} \frac{dF(q, \dot{q})}{dt} \, dt &= \delta \left\{ F[q(t_2), \dot{q}(t_2)] - F[(q(t_1), \dot{q}(t_1)] \right\} \tag{E.11} \\
&= F[q(t_2) + \delta q(t_2), \dot{q}(t_2) + \delta \dot{q}(t_2)] - F[q(t_2), \dot{q}(t_2)] \\
&\quad - F[q(t_1) + \delta q(t_1), \dot{q}(t_1) + \delta \dot{q}(t_1)] + F[q(t_1), \dot{q}(t_1)] \\
&= F[q(t_2), \dot{q}(t_2)] - F[q(t_2), \dot{q}(t_2)] \\
&\quad - F[q(t_1), \dot{q}(t_1)] + F[q(t_1), \dot{q}(t_1)] \\
&= 0, \tag{E.12}
\end{aligned}
$$

where we have proceeded from the second of these equations to the third by way of Eq. (E.4). This proves the proposition stated in Eq. (E.10).

APPENDIX F

THE CLOSURE RELATION

THE CLOSURE RELATION

A discrete set, $|u_n\rangle$, or a continuous one, $|w_\alpha\rangle$, constitutes a basis if every ket $|\psi\rangle$ has a unique expansion on the $|u_n\rangle$ or the $|w_\alpha\rangle$. Considering the discrete basis, $|u_n\rangle$, we have

$$|\psi\rangle = \sum_i c_i \, |u_i\rangle \qquad \text{(F.1)}$$

Let us also assume that the basis is orthonormal. Then performing the scalar multiplication on both sides of Eq. (F.1) with $\langle u_j |$ gives us

$$
\begin{aligned}
\langle u_j \,|\, \psi\rangle &= \langle u_j \,|\, \sum_i c_i \,|\, u_i\rangle \qquad \text{(F.2)} \\
&= \sum_i c_i \langle u_j \,|\, u_i\rangle \\
&= \sum_i c_i \delta_{ij} \\
&= c_j
\end{aligned}
$$

Now substitute $\langle u_i \,|\, \psi\rangle$ for the c_i in the expression for ψ in Eq. (F.1) to give

$$
\begin{aligned}
|\psi\rangle &= \sum_i c_i \,|\, u_i\rangle \qquad \text{(F.3)} \\
&= \sum_i \langle u_i \,|\, \psi\rangle \,|\, u_i\rangle \\
&= \sum_i |\, u_i\rangle\langle u_i \,|\, \psi\rangle \\
&= \left(\sum_i |\, u_i\rangle\langle u_i \,| \right) |\, \psi\rangle
\end{aligned}
$$

Since $|\psi\rangle$ is arbitrary, we must have

$$\sum_i |u_i\rangle\langle u_i| = 1 \qquad\qquad (F.4)$$

The result given by Eq. (F.4) is called the *closure relation.*

ζ

VITA

MARK STEFAN PETROVIC

Candidate for the Degree of

Doctor of Philosophy

Thesis: PICOSECOND NONLINEAR OPTICAL PROPERTIES OF UN-
DOPED CADMIUM TELLURIDE

Major Field: Physics

Biographical:

Personal Data: Born in Independence, Missouri, December 6, 1960, the son
of Alexander M. and Frances M. Petrovic. Wed Velina Elaine Fristoe,
December 30, 1983.

Education: Graduated from Saint Mary High School, Independence, Mis-
souri, May, 1979; received Bachelor of Science Degree in physics from
the Oklahoma State University, Stillwater, Oklahoma, December,
1983; completed the requirements for the Doctor of Philosophy De-
gree at the Oklahoma State University, Stillwater, Oklahoma, May,
1991.